Dissertation zur Erlangung des Doktorgrades
der Fakultät für Chemie und Pharmazie
der Ludwig-Maximilians-Universität München

Lipo-Xenopeptide Nanoparticles for CRISPR/Cas9 Based Gene Editing at Ultra-Low Dose

Janin Germer
aus Freiburg im Breisgau, Deutschland

2024

Erklärung

Diese Dissertation wurde im Sinne von § 7 der Promotionsordnung vom 28. November 2011 von Herrn Prof. Dr. Ernst Wagner betreut.

Eidesstattliche Versicherung

Diese Dissertation wurde eigenständig und ohne unerlaubte Hilfe erarbeitet.

München, 22.05.24

……..

Janin Germer

Dissertation eingereicht am	22.05.24
1. Gutachter:	Prof. Dr. Ernst Wagner
2. Gutachter:	Ass.-Prof. Dr. Ulrich Lächelt
Mündliche Prüfung am	27.06.24

To my Grand Father

To my Siblings

TABLE OF CONTENTS

1. Introduction

This chapter provides a brief introduction into the research field of molecular gene therapeutics and associated delivery strategies. It is not considered to be a complete review of the whole scientific area.

1.1. Overview of Gene Therapy

Gene therapy stands as a revolutionary approach in modern medicine, offering potential cures for a range of genetic disorders [1]. Its conceptual roots trace back to the early 20th century [2], but it wasn't until the latter half of the century that the field began to take shape [3]. The emerge of recombinant DNA technology in the 1970s laid the groundwork, providing tools to modify genetic material [3]. The first official gene therapy trial was conducted in 1990 on a four-year-old girl suffering from adenosine deaminase deficiency (ADA-SCID), a rare genetic disorder [4]. This landmark trial opened the door for further exploration and development in the field leading to the approval of currently > 32 gene therapies and > 28 RNA therapies as medical drugs [5].

Over the decades, gene therapy has evolved significantly, driven by advancements in understanding genetic diseases, the human genome, and the development of sophisticated delivery systems [6-8]. Initially, the focus was on monogenic diseases – disorders caused by a defect in a single gene [9]. However, as knowledge expanded, the scope of gene therapy extended to more complex conditions, including cancer, cardiovascular diseases, and neurodegenerative disorders [1, 9, 10].

Two key methodologies have emerged in gene therapy: gene addition and gene editing. Gene addition involves inserting a functional gene into a patient's cells to compensate for a non-functional or missing gene [11]. This method gained early traction and continues to be widely used. However, new gene editing technologies, such as the clustered regularly interspaced short palindromic repeats (CRISPR/Cas9) system, have revolutionized the field [12]. Unlike gene addition, gene editing allows for direct modification of the patient's genetic material, offering more precision and potentially permanent solutions to genetic disorders [13].

Despite these advances, intracellular delivery of the therapeutic cargo for gene therapy remains a challenge. Viral vectors, which use viruses to deliver therapeutic genes, have been the mainstay due to their efficiency in gene transfer [14]. However, they pose risks such as immune reactions and insertional mutagenesis [14-16]. Non-viral methods, while safer, have struggled with issues of efficiency and targeted delivery. This dilemma has driven research and innovation to develop safer and more effective delivery systems [10, 16-19].

The turn of the century saw gene therapy gaining momentum with several landmark approvals. In 2012, Glybera became the first gene therapy approved in the European Union for the treatment of lipoprotein lipase deficiency [20]. This was followed by a wave of approvals across the globe, including Luxturna for inherited retinal disease [21], Zolgensma for spinal muscular atrophy [22], and several CAR-T cell therapies for cancer [23]. These successes confirmed gene therapy as a viable treatment option and opened up ways to cure previously untreatable diseases.

In recent years, gene therapy has entered a prolific phase, characterized by rapid advancements in technology and a growing pipeline of therapies in clinical trials [5]. The emergence of novel platforms, such as mRNA vaccines, has further expanded the potential applications of gene therapy [19, 24]. As we move forward, ethical considerations, regulatory frameworks, and access to these therapies remain key areas of focus[25-27].

The field of gene therapy stands on the brink of a new era, where once incurable genetic diseases could become a thing of the past. With continuous research, refinement of techniques, and collaboration across scientific disciplines, gene therapy promises to be a cornerstone in the future of personalized medicine.

1.2. Importance and Potential of Gene Therapy

At current >32 gene therapies and >28 RNA therapies have been approved as medical drugs [5]. Gene therapy represents a paradigm shift from symptomatic treatment to addressing the root cause of diseases at the molecular level [28]. This approach has profound implications for a wide range of genetic disorders, many of which were previously considered untreatable.

1.2.1. Therapeutic Potential

Gene therapy's primary advantage lies in its potential to provide lasting cures. Unlike traditional treatments that manage symptoms or slow disease progression, gene therapy aims to correct the underlying genetic defect causing the disease [28]. This therapeutic approach is particularly significant for monogenic disorders, where a single gene anomaly can lead to severe health issues [9]. By correcting or compensating for these genetic defects, gene therapy can potentially offer a one-time, enduring solution.

1.2.2. Diseases Targeted

The spectrum of diseases targeted by gene therapy is expansive and continually growing. Initially focused on hereditary diseases like cystic fibrosis, hemophilia, and sickle cell anemia, the scope has broadened to include cancers, cardiovascular diseases, and neurodegenerative

disorders like Alzheimer's and Parkinson's disease [9, 29, 30]. In cancer treatment, for example, gene therapy is used to modify patients' immune cells to attack malignant cells – a technique central to CAR-T cell therapies [23]. For genetic disorders, the ability to directly modify or replace faulty genes offers hope for diseases that were once deemed incurable [12, 13].

1.2.3. Impact on Modern Medicine

The impact of gene therapy on modern medicine is multi-faceted. It is driving the shift towards personalized medicine, where treatments are tailored to the individual's genetic makeup, enhancing efficacy and minimizing side effects [31, 32]. This approach is a significant departure from the one-size-fits-all strategy of conventional medicine [33]. Furthermore, gene therapy's success in rare genetic disorders has provided a blueprint for tackling common diseases with genetic components. Its integration into clinical practice is also prompting advancements in diagnostics and genetic screening, enabling earlier intervention and more precise treatments [6, 32].

1.2.4. Future Perspectives

The future of gene therapy is incredibly promising. As research continues and technologies like CRISPR/Cas9 advance, the precision, safety, and efficiency of gene therapies are expected to improve [34]. This progress will likely expand the range of treatable diseases and make gene therapies more accessible and cost-effective. Moreover, the successful application of mRNA vaccine technology in combating the COVID-19 pandemic has underlined the potential of gene-based therapies, potentially accelerating their development and approval [24, 35].

In summary, gene therapy holds transformative potential for modern medicine. Its ability to directly address genetic anomalies offers a new horizon in treating a wide array of diseases, fundamentally changing our approach to healthcare and disease management. As research and clinical trials continue to advance, gene therapy bares the potential to become an integral part of medical treatment, offering hope to millions affected by genetic disorders.

1.3. Delivery Systems for Different Nucleic Acid and Gene Therapeutics

A major obstacle in the implementation of gene therapeutics is the insufficient delivery to the intracellular site of action. Among other factors, poor biodistribution, rapid degradation of the macromolecular drug in the body, suboptimal pharmacokinetics, toxicity, and insufficient specificity for the targeted tissue impeded their widespread clinical application [36]. Hence, the development of efficient delivery systems are crucial for guaranteeing the effectiveness of the therapeutic payload, reducing undesired side effects, and improving patient adherence [37]. The delivery system must be capable of navigating through both external and internal cellular barriers, protect its cargo from nuclease in the bloodstream, improve and facilitate its cellular uptake, and ensure its release from endosomes after entering the cell [10, 16, 38].

Amongst other methods, nanocarriers, an enormous and diverse group of nanoparticles, have been employed to transport therapeutic agents to specific targets [16, 39]. Those nanocarriers can be categorized into viral and non-viral vectors [16, 40]. Each type has its advantages and drawbacks [41]. By biological evolution, viruses have optimized their strategies to meet dynamic and bioresponsive requirements for successful nucleic acid delivery into the host cell. Due to their superior *in vivo* potency, viral vectors such as AAV pioneered the development of novel in *vivo* gene therapies [42]. Viruses known for their effective DNA transfection capabilities, including lentiviruses, retroviruses, adenoviruses, parvoviruses, and adeno-associated viruses, have been utilized in the treatment of conditions like HIV, cancer, and muscular dystrophy [14]. However, despite achieving high transfection efficiencies, viral vectors face limitations such as rapid clearance due to generation of neutralizing antibodies or pre-existing antibodies against the vector, limited vector size capacity (usually below 7 kb), challenges in large-scale production and possible side effects like severe immune responses or insertional mutagenesis [16, 40]. Despite these issues, viral vectors are frequently used in research, as well as in vaccine development and gene therapy trials, due to their high transfection efficiency and known cell targeting abilities [14, 35, 43, 44]. Nevertheless, the use of viral delivery systems presents a significant risk of severe adverse reactions, including treatment-induced leukemia and deaths caused by the treatment [45, 46]. In contrast to viral vectors, non-viral carriers exhibit lower immunogenicity, have the potential to deliver larger genetic payloads, can be produced at large scale and in precise form allowing flexible optimization for different cargo properties [42]. Therefore, in the following section non-viral delivery systems are described in more detail.

1.3.1. Non-Viral Delivery Systems for Nucleic Acid and Gene Therapeutics

Inspired by their viral counterparts, a range of strategies for creating virus-like synthetic carriers has been explored in the field of non-viral nanocarriers. These carriers incorporate various domains designed to mimic the efficient and dynamic delivery process characteristic of viral infections [47-50]. The exploration has included a diverse array of materials, ranging from biodegradable polymers like dendrimers [51], polylactic acid (PLA) [52], polyethyleneimine (PEI) [52, 53], and chitosan (CS) [54], to various nanoparticles including liposomes [55], gold [56], mesoporous silica [57], lipid nanoparticle (LNP) [18, 58], and carbon nanotubes [59, 60]. Continuously developing synthetic, non-viral nucleic acid delivery for over five decades finally resulted in the recent global medical impact of lipid nanoparticles (LNPs) in SARSCoV2 mRNA vaccines [24]. Additionally, LNPs as hepatocyte-targeted siRNA drug Onpattro for treatment of hereditary transthyretin amyloidosis were approved [61].

Cationic transfection reagents have been explored for over the past decades offering a promising route in search of a safer alternative for viral gene delivery systems. Several breakthrough developments were triggered by the identification of distinct biological extra- and intracellular delivery barriers and the rapid progress in macromolecular chemistry as much as our continuously increasing understanding interactions of cationic lipid as well as cationic polymer with negatively charged nucleic acids [17, 38, 62-66]. Polyplexes are based on the condensation of negatively charged nucleic acids by electrostatic attraction with polycationic condensing compounds [38, 67, 68]. Formation of lipid nanoparticles (LNP) however, is only partly contributed to electrostatic interactions. Hydrophobic lipid-lipid associations, co-assembly of cationic or ionizable lipids into polycationic lipid micelles and liposomal structure, result in incorporation and encapsulation of the nucleic acid cargo. Therefore, the size of nucleic acid cargo is less influential [17]. The resulting compact particles protect the nucleic acid and also improve the uptake into the cells. Numerous cationic compounds have been used for formulating nucleic acids into complexes. Ideally, the cationic carrier will carry out multiple tasks (**Figure 1**) which include compacting nucleic acids into particles that can migrate to the target tissue, shielding the particles against degradation and undesired interactions, and enhancing cell binding and intracellular delivery into cytoplasm and the nucleus.

An array of novel nucleic acid entities initially focusing on plasmid DNA (pDNA)-based gene therapy, a series of novel therapeutic nucleic acid entities such as stabilized messenger RNA (mRNA), chemically modified small interfering RNA (siRNA) and micro RNA (miRNA), splice-modifying oligonucleotides, or CRISPR/Cas9 and single guide RNA (sgRNA) for

genome modification have entered research and clinical evaluation [69]. Recent experience indicates that different macromolecular cargos may require different tailor-made carriers based on their different biophysical characteristics, distinct intracellular target sites and mode of action (**Figure 1**) [17, 70-72]. In practical terms, a classical polymer itself is unable to carry out all these tasks [73].

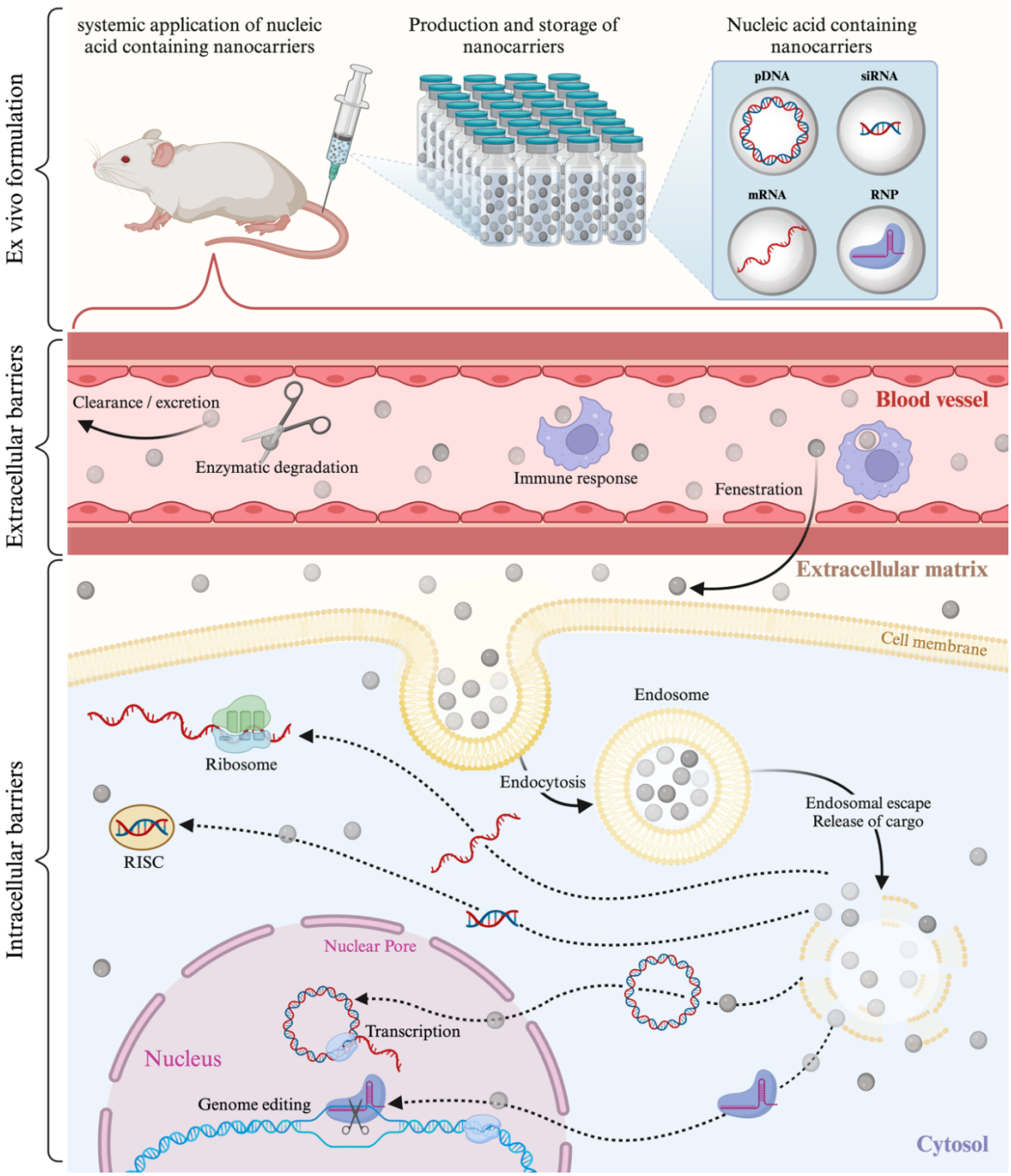

Figure 1. Barriers for *in vivo* delivery of nonviral, nanocarrier-based nucleic acid therapeutics. After successful formulation of nucleic acid cargo into nanoparticles e.g. polyplexes or LNPs, stability during transport and storage until their administration must be ensured. Once in the bloodstream, nanoparticles need to withstand nonspecific biodistribution, rapid excretion, enzymatic degradation, and clearance by immune cells. Optimally, nanocarriers shield their cargo against degradation and undesired interactions, enabling migration to the target tissue, enhancing cell binding and uptake to the cytoplasm. After reaching the cell, endosomal escape needs to be facilitated followed by release of the cargo from the formulation at its respected target site. Different intracellular pathways for productive delivery of pDNA, mRNA, siRNA, and Cas9 RNP are represented. Figure was created using BioRender.com.

Additional functional domains must be integrated into the formulation. Advantageously, polymers can be chemically linked to molecules such as cell targeting ligands, including proteins (antibodies, growth factors) and small molecules (carbohydrates, peptides, vitamins). Various polymer-ligand gene delivery systems have been demonstrated to facilitate receptor-cell mediated delivery into cultured cells. Targeted delivery to the lung, the liver, or tumors has been achieved in experimental trials, either by localized or systemic application. pH dependent polycations such as polyethylene imine (PEI) and its derivates have shown great potential in both *in vitro* and *in vivo* applications [53, 74-76]. To further finetune the advantageous properties of PEI, our working group led by Prof. Dr. Ernst Wagner (Chair of Pharmaceutical Biotechnology; LMU, Munich) utilized artificial oligoamino acids such as succinoyl tetraethylene pentamine (Stp) in solid-phase assisted peptide synthesis (SPPS). Small libraries of sequence-defined artificial oligoaminoamide (OAA) peptides were created and assessed [77]. These libraries of sequence defined xenopeptides also encompassed supplementary hydrophilic or lipophilic elements and residues, along with diverse topologies derived from branching points [77, 78]. Different tailor-made carriers were designed distinct for distinct nucleic acid cargos and their respective intracellular target sites and mode of action [17, 70, 71, 79, 80]. Whilst purely hydrophilic cationizable domains with optional polyethylene glycol (PEG) shielding and receptor targeting segments were proven effective for plasmid DNA (pDNA) polyplexes [81, 82] the incorporation of lipidic residues and additional stabilization measures were found crucial for stable polyplex formation with much smaller double stranded siRNA (small-interfering RNA) [83, 84]. Lipid-containing T-shaped oligoaminoamides (lipo-OAAs) were identified as efficacious carriers for intracellular Cas9 protein/sgRNA RNP delivery and gene disruption wherein the type of contained fatty acid, exhibited a crucial effect on the knock out efficiency [85-87]. The challenge of balancing stability and cargo release in mRNA polyplexes was effectively addressed by incorporating a bioreducible disulfide bond between the cationizable hydrophilic polycationic backbone and the hydrophobic domain for dynamic mRNA release upon the reductive removal of the fatty acids in the cytosol [79].

In our recent work we combined our established cationizable synthetic amino acid units i.e. succinoyl tetraethylene pentamine (Stp) with new novel cationizable apolar residues. These lipo amino fatty acids (LAF) exhibit a pH dependent switch of polarity allowing a dynamic and reversible cationization, applied to both hydrophilic and lipophilic regions. This facilitates the dynamic binding, protection, and release of the cargo nucleic acid and induces host/endosomal membrane destabilization using both cationic and lipidic mechanisms. Even at a fraction of

previously tested doses, these new carriers for pDNA, mRNA, and siRNA delivery surpassed the efficiencies of preceding carrier generations several hundred times. Notably, these new carriers demonstrated exceptional *in vivo* performance delivering mRNA with fast kinetics, whether used as polyplexes or as ionizable compounds in LNP formulations [88, 89].

In this thesis these novel LAF lipo-xenopeptides were evaluated for formulation of Cas9 mRNA/sgRNA polyplexes or LNPs and their application for genome editing *in vitro* and *in vivo*.

1.4. Different Nucleic Acid and Gene Therapeutic Cargos

Continuous advancements are being made in identifying novel delivery systems and therapeutic agents. Initially, gene transfer research primarily utilized DNA viruses like adenovirus, adenovirus-associated virus, and herpes simplex virus, each carrying its specific type of genetic material, in gene therapy trials [14].

1.4.1. Plasmid DNA (pDNA)

As small, circular, double-stranded DNA molecules, plasmids are naturally occurring elements in bacterial cells, but their application extends far beyond their biological origins [90]. The properties of pDNA – including its size, structural configuration, easy and cheap production, and modifiability – make it a valuable tool in gene therapy [91].

It can be engineered to include various regulatory elements that control the expression of the therapeutic gene. Typically ranging from 1-1000 kilobase pairs (kbp), these molecules are large enough to carry significant genetic payloads, including not only therapeutic genes but also necessary regulatory sequences [90-92]. Plasmids usually consist of a multiple cloning site, where the foreign gene is inserted, a polyadenylation site, regulating gene transcription and time of gene expression, a promotor sequence and origin of replication site [93]. Additional antibiotic resistence genes enable positive selection of clones, hence facilitates the production of pDNA. Since several studies revealed improved transfection efficiencies when decreasing the plasmid size, resistance markers are removed in so-called miniplasmids [91, 94]. The circular nature of pDNA contributes to its stability within host cells, aiding the persistence of the therapeutic gene.

Despite these advantageous properties, pDNA's relatively large size compared to other nucleic acid therapies poses difficulties in cellular uptake and nuclear entry. Nuclear import of the pDNA must occur for transcription before translation into desired proteins. Therefore, delivery

of the pDNA into the cytosol doesn't result in protein expression in non-dividing cells [95]. Overcoming these barriers requires innovative delivery systems capable of protecting the pDNA from degradation, facilitating its entry into the cell, and ensuring its transport to the nucleus where gene expression is initiated [10, 17]. Furthermore, insertional mutagenesis can lead to integration of the pDNA into the host's genome. This integration may cause malfunction of genes by changing the transcription, regulation, or coding sequences. Such alterations can be carcinogenic, particularly if they result in the deactivation of tumor suppressor genes or the activation of oncogenes [96]. Additionally, recognition of unmethylated cytosine-phosphate-guanine (CpG) dinucleotides in bacterial DNA by mammalian Toll-like-receptor 9 (TLR9) can cause transgene silencing but also immune response [91, 97].

1.4.2. Messenger RNA (mRNA)

All genetic information originates from genomic DNA. Serving as template for all proteins expressed in a eukaryotic organism, DNA is transcribed into RNA, which then undergoes translation to form proteins [98]. RNA-polymerase II transcribes DNA into precursor messenger RNA (pre-mRNA), a process governed by transcription factors, promoters, enhancers, and silencers. Concurrent with the production of pre-mRNA, it is subjected to three primary processing stages resulting in mature messenger RNA (mature mRNA) [99]. First, 5' capping with methylated guanosine (m^7G) provides protection from exonuclease degradation, facilitates transport to the cytosol and assists in the recognition and binding of eukaryotic initiation factor 4E (eIF4E) during the process of translation [99-101]. Secondly, splicing by precise excision of the introns interspersing the exons of the pre-mRNA, a vital step in diversifying the proteome of eukaryotic organisms [102]. The mature mRNA consists of joined exons only. The endonucleolytic cleavage approximately 10-30 nucleotides downstream a specific signal sequence followed by polyadenylation of the 3' end of the RNA is the last step finalizing the RNA processing [101]. The long chain of adenine nucleotides (poly-A tail) at the 3' end increases enzymatic stability of the mRNA, regulates translation efficiency and defines the half-life of mature mRNA [103].

The advancement of *in vitro* transcription (IVT) techniques has led to the rise of synthetic mRNA as a new category in gene therapy. Successful intracellular delivery of mRNA enables the cytosolic expression of essentially any desired therapeutic protein (e.g., restoration of function for monogenic diseases, growth factors, therapeutic antibodies, antigens in vaccines), preserving the post-translational modifications of the encoded proteins innate to the host cell. Custom designed IVT mRNA presents an alternative for the challenging formulation and

delivery of protein-based drugs. In contrast to pDNA-based approaches, the delivery into the nucleus is not required, thus avoiding the hazard of insertional mutagenesis and reducing the cellular barriers for delivery. Nevertheless, the hydroxyl group in 2' position of the pentose ring in RNA makes it less stable and more reactive as deoxyribose containing DNA [104]. Integration of a 5' cap and 3' poly-A tail in in vitro transcribed (IVT) mRNA mimics natural eukaryotic mRNA, increasing its enzymatic stability, regulating translation efficiency, and enhancing protein expression [103, 105]. Further stabilization of the mRNA was achieved by the introduction of phosphorothioate modifications especially into the 5' untranslated mRNA sequence demonstrating increased protein translation and up to 22-fold higher protein expression [106].

Recognition of endocytosed IVT mRNA by various endosomal innate immune receptors, including TLR3, TLR7, and TLR8, as well as cytoplasmic proteins like melanoma differentiation-associated protein 5 (MDA5) and retinoic acid inducible gene I protein (RIG-I) can trigger immune responses and potentially hinder the functionality of the mRNA [19, 107, 108]. Immunogenicity might be beneficial for immunotherapeutic vaccination, however, for non-immunotherapy related applications, it is disadvantageous since the induced immune responses can slow down the translation of mRNA, promote RNA degradation, and impede repeated application, as in RNA-mediated protein replacement therapy [19, 107, 109]. Nucleotide modifications such as 2-thiouridine (s2U), 5-methyluridine (m5U), pseudouridine (Ψ), N1-methylpseudouridine (m1Ψ), 5-methylcytidine (m5C), 5-hydroxymethylcytosine (5hmC), and N6-methyladenosine (N6mA) can be incorporated to obtain a reduced immunogenicity and prolonged stability of the mRNA (**Figure 2**) [19, 110, 111]. Additionally, immunogenicity could be reduced by sequence-engineered unmodified mRNA and mRNA purification by denaturing high-performance liquid chromatography (dHPLC) [112, 113]. Thus, depending on the application, production of encoded protein may be transient or also persistent for a prolonged period of time.

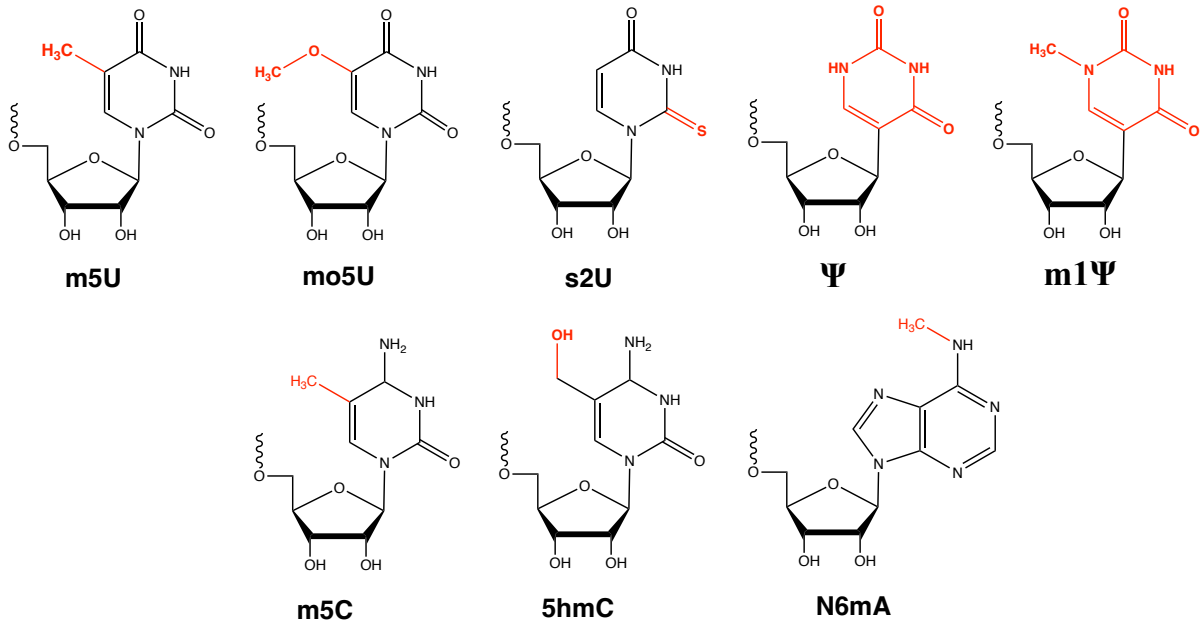

Figure 2. Nucleotide modifications in IVT mRNA. m5U: 5-methyluridine; mo5U: 5-methoxyuridine; s2U: 2-thiouridine; Ψ: pseudouridine; m1 Ψ: N1-methylpseudouridine; m5C: 5-methycytidine; 5hmC: 5-hydroxymethylcytosine; N6mA: N6-methyladenosine

Up to now, both in clinical and early-stage trials, mRNA vaccines have shown a promising safety profile and the ability to stimulate an immune response against various diseases, including rabies [114], respiratory syncytial virus (RSV) [115], prostate cancer [116], and non-small cell lung cancer [117]. A phase 3 study is underway, combining cancer immunotherapy with the humanized antibody pembrolizumab and a novel personalized mRNA cancer vaccine that encodes up to 34 patient-specific tumor neoantigens. This study is testing the combination as an adjuvant therapy for patients with resected high-risk melanoma [31, 118]. A new use of mRNA technology has been identified in transforming various human cell types into RNA-induced pluripotent stem cells (RiPSCs). Additionally, this approach has been utilized in tissue engineering to direct differentiation of RiPSCs into fully developed muscle cells. [111].

A great breakthrough in mRNA therapeutics was achieved when two SARSCoV2 mRNA vaccines using lipid nanoparticles (LNPs) obtained their conditional marketing authorization as a result of the COVID-19 pandemic [24, 119].

1.4.3. Other RNA Cargos

The above-mentioned cargos serve to substitute absent or faulty proteins, either by direct replacement or by introducing their templates in the form of mRNA or pDNA. In numerous diseases, including cancers, various genetic disorders, and viral infections, the expression of certain genes can actually cause the disease. By influencing the genomic template or the subsequent processes through various adjustments at the mRNA biosynthesis level and the following translation stage these diseases can be directly addressed and treated. Therefore, in medical treatments, genome editing via nucleases like the RNA-guided CRISPR/Cas9 system, natural microRNA (miRNA), artificially created short interfering RNA (siRNA), or antisense oligonucleotides (ASOs) are used [16, 38].

siRNA and miRNA both operate by the RNA interference (RNAi) mechanism. Forming an RNA-induced silencing complex (RISC) with nucleotide sequences complementary to the target mRNA, they prevent the expression of targeted genes by cleavage of the mRNA (for siRNA) or repression of translation (for miRNA). Consequently, specific inhibition of gene expression at the posttranscriptional level without risk of insertional mutagenesis to the host genome can be achieved, presenting a safe alternative for gene therapeutic approaches.

Additionally, antisense oligonucleotides (ASOs) can be employed to precisely target the splicing process in mRNA processing. Utilizing ASOs alters the splicing pattern, thereby reinstating the expression of a functional gene. Given that numerous acquired and inherited diseases result from genomic mutations that cause splicing irregularities, modulating splicing represents a hopeful strategy for treating such diseases [120-122].

Advancements in siRNA and antisense oligonucleotides (ASO) therapeutics have resulted in the discovery of several chemical alterations to RNA. These modifications include carbohydrate modifications like 2′ O-methyl RNA (2′OMe RNA) and 2′-deoxy-2′-fluoro-RNA (2′F RNA) as much as chemical modification of the phosphate backbone reduce susceptibility to nucleases in blood and cells, hence, significantly enhance the effectiveness of gene suppression after in vivo administration [123-125].

The CRISPR/Cas9 system, a complex of the RNA-guided endonuclease Cas9 and a single guide RNA (sgRNA) enables precision genome editing [126]. If not introduced by pDNA encoding for the whole CRISPR/Cas9 system, the Cas9 nuclease is either introduced directly as protein of as its approximately 4,500 nucleotide (nt) long mRNA blueprint. As the other key component of the system, the considerably smaller sgRNA, approximately 100 nucleotides in size, can be

generated by IVT or solid-phase synthesis. In vitro transcription (IVT) is a popular method for synthesizing single-guide RNA (sgRNA) due to its affordability, high yield, and easy implementation. However, sgRNA produced through IVT encounters challenges similar to those seen with IVT-generated mRNA products like poor stability and immune responses making it unfavorable for in vivo usage [127-129]. Despite being more cost intensive, chemically synthesized sgRNA allows site-specific incorporation of modified nucleotides enabling effective *in vivo* application [125].

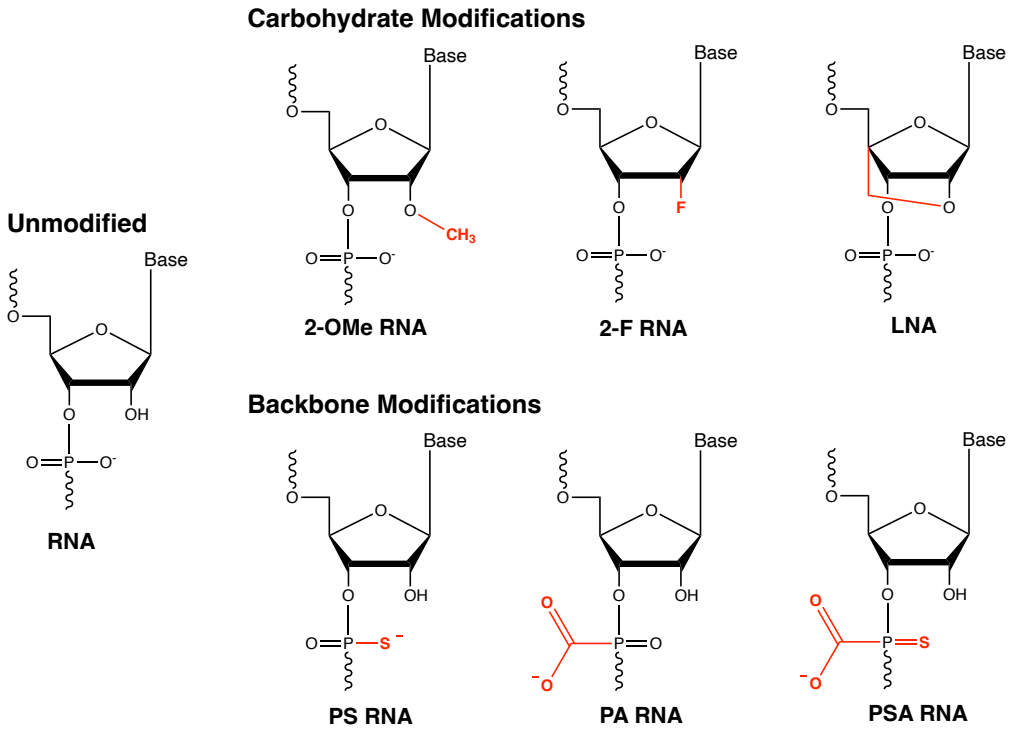

Figure 3. Schematic structures of different oligonucleotide analogues. RNA: Ribonucleic acid; 2-OMe RNA:2-O-methyl RNA; 2-F RNA: 2-fluoro RNA; LNA: locked nucleic acid;PS RNA: phosphorothioate RNA; PA RNA: phosphonoacetate RNA; PSA RNA: thiophosphonoacetate RNA

Building on the finding in siRNA and ASO modifications, various chemically modified nucleotides including have been identified to enhance the enzymatic stability, specificity, editing efficiency as much as to minimize off-target effects and immunogenicity could be reduced [125, 130-133] (**Figure 3**). Nevertheless, chemical modifications can also hamper the biological activity of therapeutic RNAs e.g. by inhibiting interaction of Cas9 with sgRNA making a sequence specific modification crucial for their effectiveness [125, 133].

Optimization of the RNA chemistry for enhanced stability was the basis for the design and finally the approval of five siRNA [5, 134], eleven ASO [5, 135, 136] and in late 2023 the first approval of the first *ex vivo* CRISPR/Cas9 application for treatment of sickle cell anemia [137, 138].

1.4.4. Protein

Proteins are incredibly diverse and essential macromolecules in our bodies as they serve as catalysts, form part of membrane structures like receptors and channels, provide structural support both inside and outside cells, and are crucial for transporting molecules within cells and across different organs [139]. Any malfunction in proteins, whether due to errors in translation, post-translational modifications, damage, or altered with expression levels, often results in various diseases [140-142]. Starting with the first approval of a recombinant protein, Humulin (Insulin) [143], by the FDA in 1982, numerous therapeutic peptides and proteins have received drug approval [144, 145]. However, like nucleic acids, these therapeutic proteins and peptides face challenges in entering cells and depend on receptor-mediated uptake. Many recombinant proteins, like monoclonal antibodies and growth factors, do have external receptors, enabling them to target molecules inside cells would expand their therapeutic potential [146].

As an alternative to pDNA and mRNA methods that modify or substitute proteins within target cells, directly introducing proteins into cells is the most straight forward approach. Protein delivery bypasses the steps of transcription and translation, offering faster action due to skipping these processes. This approach also allows for more precise control over the duration and intensity of protein expression, enhancing the therapy's effectiveness [147]. However, delivering proteins directly is challenging because of their large size, varied surface charge distribution, and complex tertiary and quaternary structures. These factors make proteins unstable and susceptible to denaturation, degradation, and aggregation. Therefore, development of appropriate carriers that effectively handle these issues is a crucial yet very complex task [86, 147].

1.5. The CRISPR/Cas9 System as a Genome Editing Tool

Revolutionary advances in precise genome modifying nucleases such as zinc finger nucleases (ZFN), transcription activator-like effector nucleases (TALEN), or CRISPR-associated protein 9 (Cas9) have initiated new era for gene editing [73, 148]. The CRISPR/Cas9 system, in particular, is seen as an exceptionally promising method for gene editing due to its straightforward and efficient design. The CRISPR/Cas9 system consisting of the RNA-guided endonuclease Cas9 and a single guide RNA (sgRNA), recognizes the targeted DNA sequence adjacent to a protospacer-adjacent motif (PAM) through Watson–Crick base pairing [12, 126, 149]. This interaction leads to the creation of double-stranded DNA breaks (DSBs). These breaks are then repaired by the cell's natural mechanisms, including homology-directed repair (HDR) and nonhomologous end-joining (NHEJ) (**Figure 4)** [12, 150, 151].

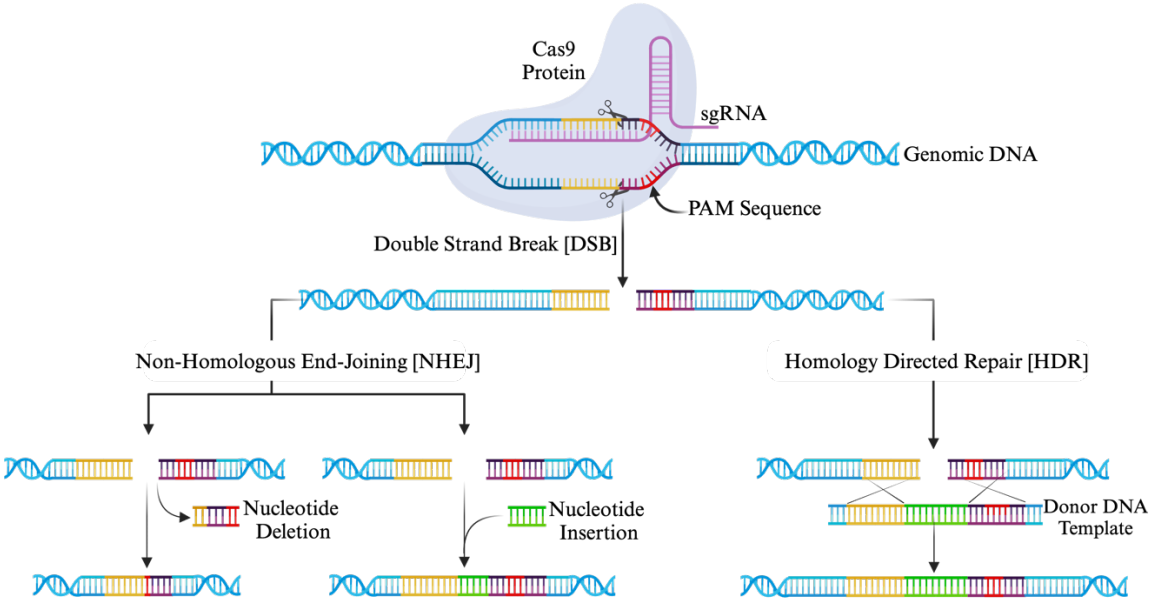

Figure 4. Mechanisms of CRISPR/Cas9 genome editing. Two main repair mechanisms after Cas9-induced double strand break of genomic DNA: Error prone non-homologous end-joining (NHEJ) can cause random deletion or insertion of nucleotide. In the presence of an donor DNA template with homologous arms a defined sequence can be inserted to the gene by homologous directed repair (HDR).Figure was created with BioRender.com.

Direct re-ligation of the cleavage site by NHEJ is an error prone mechanism leading to random insertions and deletions of nucleotides (indels), which result in disruption of the translational reading frame and target gene knock out. In the presence of a single or double stranded DNA template with homologous flanks to the target sequence, homology-directed repair (HDR) facilitates precise repair and integration of a specific DNA sequence, which is placed between homology arms at the site of cleavage [151]. The absence of secure and effective delivery systems has impeded the widespread adoption of CRISPR technology and its successful

implementation. Therefore, it is of major priority to develop efficient and safe CRISPR/Cas9 delivery technologies to enable efficient genome engineering [12, 17, 149].

Unlike conventional gene therapy for genetic diseases, which necessitates lifelong expression of therapeutic genes, the short-term and transient expression of genome-modifying nucleases is advantageous. Off-target effects and insertional mutagenesis can result from prolonged expression of the CRISPR components after viral delivery [34]. Additionally, immune response towards the viral vector can lead to significantly reduced CRISPR efficacy and potential immunotoxicity, eliminating the possibility of repeated dosing[34, 152]. Therefore, nonviral delivery systems provide a safer alternative to viral delivery systems, avoiding undesired complications caused by prolonged expression of the nucleases [153].

1.5.1. Delivery formats of CRISPR/Cas9

Constructs encoding the nuclease and sgRNA in a single DNA plasmid, mRNA encoding Cas9 nuclease plus additional sgRNA, or direct delivery of the recombinant Cas9 protein with sgRNA as RNP formulation have been utilized [34, 153]. Understanding the distinct physical and physiological characteristics of each format is essential to evaluate their impact on the Cas9 mechanism and choosing the most suitable format for practical use. A key difference among these formats is their stability. Consisting of circular and double stranded DNA, Cas9 plasmid DNA (Cas9 pDNA) has a lower reactivity than RNA based formats, is not susceptible to exonucleases and is not prone to denaturation as protein. Therefore, it is the most stable of the three formats. While Cas9 mRNA is less stable than Cas9 pDNA, its stability can be enhanced through chemical modifications to the nucleotides, as previously mentioned.

While Cas9 pDNA and mRNA formats contain only one type of biomolecule, Cas9 RNPs consist of the complex of both Cas9 protein and sgRNA. This composition makes Cas9 RNPs vulnerable to degradation by both proteases and RNases, potentially rendering them the most unstable format. Additionally, the Cas9 protein might lack resistance to organic solvents or low pH and can be easily denatured. An instance of this is seen when Cas9 RNP undergoes denaturation in acidic citrate buffer at pH 4.0, a condition commonly used for formulating nucleic acid-loaded LNPs [34].

Another clear distinction lies in different intracellular target sites. As previously mentioned, the nuclear entry of pDNA is necessary. On the other hand, Cas9 mRNA only needs to be transported to the cytoplasm, where it can start being translated right away. Nevertheless, in both scenarios, the RNP complex must be formed with sgRNA once the Cas9 protein is

synthesized, leading to an inherent delay between intracellular availability of the protein and RNA components. Therefore, delivering pre-formed functional RNPs represents the most straightforward approach to cellular genome editing, and is widely regarded as the most effective method [153].

The period that intracellular components persist depends on how stable the genetic 'blueprints' are and how quickly the encoded protein breaks down. In genome editing, CRISPR/Cas elements are only briefly needed to make the desired genomic changes. Keeping them in the cell longer than necessary is not ideal, as it can increase the chances of unintended genetic alterations. Therefore, it's important to precisely manage the CRISPR/Cas system's availability and ensure its degradation or inactivation once the target modification is achieved. Cas9 RNP and mRNA, known for their faster degradation in target cells, offer a transient exposure of the cell's genome to active Cas9 proteins, thus lowering the likelihood of off-target editing events. However, longer gene expression after application of pDNA constructs, may increase off-target effects [153, 154].

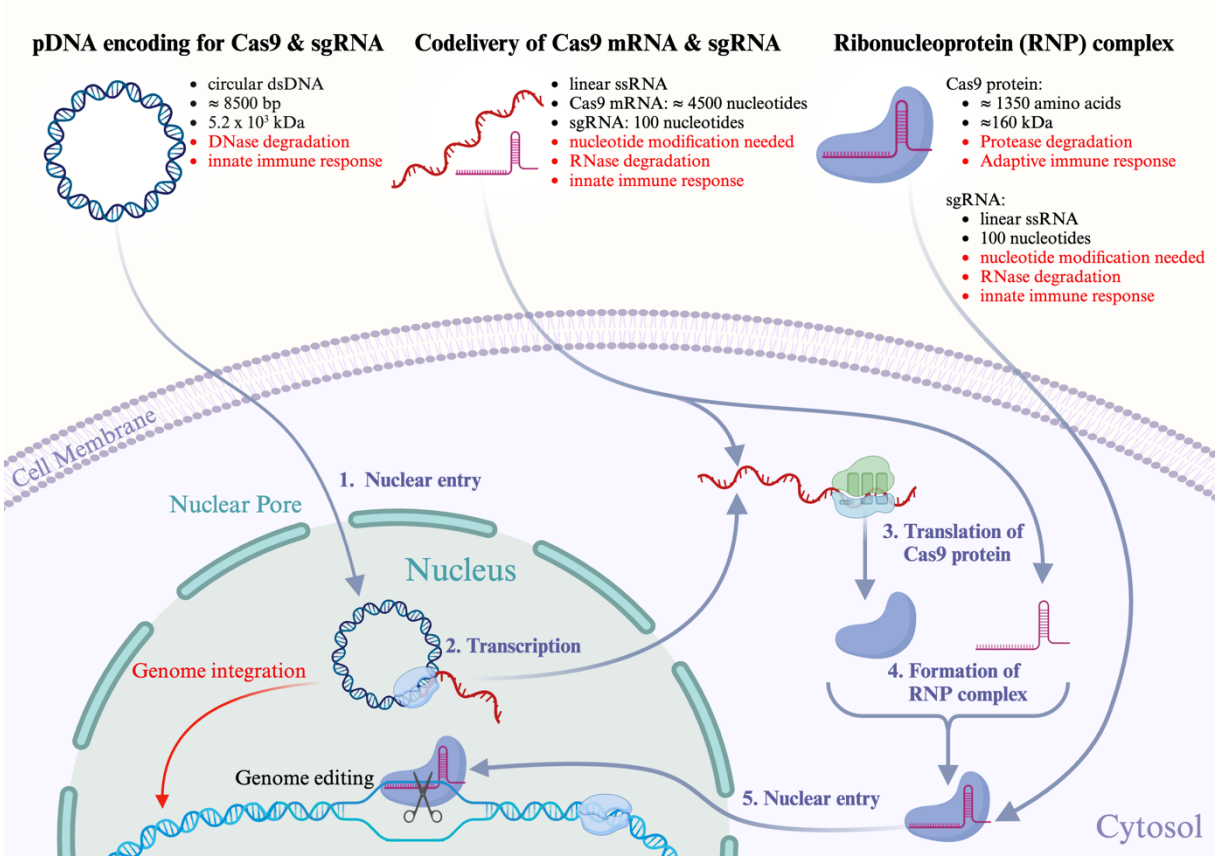

Figure 5. Comparison of different delivery formats for the CRISPR/Cas9 system. Drawbacks of each format are pointed out in red. Figure was created with BioRender.com

In addition to their stability and functionality, safety is a primary concern, particularly for potential in vivo applications. As previously mentioned, the spontaneous integration of Cas9 plasmid DNA into the host genome could result in dangerous insertional mutagenesis. Moreover, continuous expression of Cas9 might cause unintended off-target effects and trigger immune responses via the major histocompatibility complex (MHC) class I pathway [155]. Additionally, the primary form of immune response generated by these three formats varies. Cas9 plasmid DNA (pDNA) and mRNA primarily initiate innate immune responses through the activation of Toll-like receptors (TLRs), whereas Cas9 ribonucleoprotein (RNP) can induce adaptive immune reactions. Recent research has shown that antibodies and T cells against Cas9 already exist, likely as a result of previous bacterial infections [153, 155, 156]. IgG antibodies against Cas9 could be detected in 58 % and anti-Cas9 T cells were found in 68 % of human adults [155].

While Cas9 mRNA and RNP offer benefits in editing efficiency and safety, their production is more expensive compared to pDNA. As mentioned before simple design, production, and scaling of pDNA makes it more cost effective. Producing pure active Cas9 proteins, however, involves a lengthy and intricate process. Among other critical steps, this includes isolation the protein from bacterial cultures, its purification, and ensuring proper storage of this labile protein product [153]. In conclusion, each of the respective CRISPR/Cas9 systems has unique characteristics in terms of its physical and chemical properties, stability, mechanisms of action, safety, and manufacturing processes. **Figure 5** summarized differences and individual characteristics of each delivery format.

The clinical application of nucleic acid-based therapeutics is currently more advanced than the intracellular delivery of proteins. This is clearly evidenced by the recent achievements in siRNA-based drugs and mRNA vaccines [24, 61, 136]. Therefore, this thesis focuses on the development of nanoparticles for non-viral delivery for mRNA based CRISPR/Cas9 gene editing.

1.6. Aim of the Thesis

The CRISPR/Cas9 technology has revolutionized the field of gene editing, offering a powerful tool for precisely modifying the genome. Its simple design presents a highly promising approach to genome editing [12, 34]. Different delivery formats comprising viral and non-viral vectors, as well as different CRISPR/Cas9 formats such as Cas9 plasmid DNA, Cas9 mRNA/sgRNA and Cas9/sgRNA ribonucleoprotein (RNP) can be selected. Unlike conventional gene therapy for genetic diseases, which often requires lifelong expression of therapeutic genes, the short-term and transient expression of genome-modifying nucleases presents an advantage. Therefore, non-viral RNA-based delivery of the nuclease minimizes the risk of insertional mutagenesis and off-target effects. The absence of safe and effective delivery systems, however, has impeded the widespread adoption of CRISPR technology and its successful implementation. Additionally, effectively delivering the CRISPR components to extrahepatic tissue remains a challenge.

The aim of this thesis was to develop and evaluate novel non-viral delivery systems for the delivery of CRISPR/Cas9 gene editing components, focusing on the codelivery of Cas9 mRNA and sgRNA. At the core of this endeavor were our previously described pH-responsive lipo amino fatty acid (LAF) containing succinoyl tetraethylene pentamine (Stp) carriers. This thesis had to explore the biophysical and functional aspects of Cas9 nanoparticles. To identify the most potent carrier topologies, a variety of LAF-Stp carriers with different topologies, variations of LAF/Stp ratios, and LAF types were screened for their ability to compact and deliver Cas9 mRNA and sgRNA in form of polyplexes or LNP. The thesis also delves into the complexities of cell type dependent responses to these carriers. A series of *in vitro* experiments employing various cell types provided insights into how different cellular environments impact the nanocarriers efficacy. This aspect of the study is crucial for understanding the broader applicability of the developed carriers in treating a variety of genetic disorders. A subsequent aim was the evaluation of Cas9 polyplexes in different reporter and disease models *in vitro*, including GFP knockout and HDR mediated conversion, *Pcsk9* knockouts and dystrophin gene editing that trigger splicing modulation.

The last aim was the comparative *in vivo* assessment of the lipo-xenopeptide carriers and a current state-of-the-art lipid nanoparticle (LNP) formulation after local and systemic administration.

2. Materials

This chapter has been adapted from:

Germer J, Lessl AL, Pöhmerer J, Grau M, Weidinger E, Höhn M, Yazdi M, Cappelluti MA, Lombardo A, Lächelt U, Wagner E. Lipo-Xenopeptide Polyplexes for CRISPR/Cas9 Based Gene Editing at Ultra-Low Dose. Journal of Controlled Release

2.1. Solvents and Reagents

The following table summarizes the used solvents and reagents and the source of supply including their unique CAS number. For all experiments solvents and reagents were used in high quality.

Table 1 Chemicals and solvents in alphabetical order

Solvents and Reagents	CAS number	Supplier
Agarose	9012-36-6	Sigma-Aldrich, Munich, Germany
Ampicillin	69-53-4	Sigma-Aldrich, Munich, Germany
Adenosine 5′-triphosphate (ATP) disodium salt trihydrate	51963-61-2	Sigma-Aldrich, Munich, Germany
polyethyleneimine, branched 25 kDa	9002-98-6	Sigma-Aldrich, Munich, Germany
Cell culture lysis buffer	-	Promega, Mannheim, Germany
Coenzyme A trilithium salt	18439-24-2	Sigma-Aldrich, Munich, Germany
Collagen A	9007-34-5	Biochrom, Germany
Cholesterol	3483-12-3	Sigma-Aldrich, Munich, Germany
DAPI'(4',6-Diamidino-2-phenylindol)	28718-90-3	Sigma-Aldrich, Munich, Germany
Dimethyl sulfoxide (water free)	67-68-5	Sigma-Aldrich, Munich, Germany
Di-tert-butyl dicarbonate	24424-99-5	Sigma-Aldrich, Munich, Germany
D-luciferin sodium	103404-75-7	Promega, Mannheim, Germany
DOPE (1,2-dioleoyl-sn-glycero-3-phosphoethanolamine)	4004-05-1	Avanti Polar Lipids, Alabaster, USA
DMG-PEG (1,2-dimyristoyl-rac-glycero-3-methoxypolyethylene glycol-2000)	160743-62-4	Avanti Polar Lipids, Alabaster, USA
DSPC (1,2-Distearoyl-sn-glycero-3-phosphocholine)	816-94-4	Avanti Polar Lipids, Alabaster, USA
DTT (dithiotreitol)	3483-12-3	Sigma-Aldrich, Munich, Germany
EDTA disodium salt dihydrate	6381-92-6	Sigma-Aldrich, Munich, Germany
Ethanol absolute	64-17-5	VWR Int., Darmstadt, Germany
Fetal bovine serum	-	Sigma-Aldrich, Munich, Germany
Gelred®	-	Sigma-Aldrich, Munich, Germany
Glucose	50-99-7	Merck, Darmstadt, Germany
Heparin sodium salt 5000 I.U mL-1	9041-08-1	Braun SE, Melsungen,Germany

HEPES	7365-45-9	Biomol, Hamburg, Germany
HBTU (Hexafluorophosphate)	94790-37-1	Multisyntech, Witten, Germany
Hydrazine monohydrate	7803-57-8	Sigma-Aldrich, Munich, Germany
Hydrochloric acid solution (1 M) (1 M HCl)	7647-01-0	Bernd Kraft, Duisburg, Germany
Isopropanol	67-63-0	Merck, Darmstadt, Germany
Lipofectamine™ 3000	-	ThermoFisher Scientific, Schwerte, Germany
Lipofectamine™ MessengerMAX™		ThermoFisher Scientific, Schwerte, Germany
Millipore water	-	In-house purification
MTT (3-(4,5-dimethylthiazol-2-yl)-2,5-diphenyiltetrazolium bromide)	298-93-1	Sigma-Aldrich, Munich, Germany
Nuclease-free water	-	Sigma-Aldrich, Munich, Germany
Paraformaldehyde (PFA)	50-00-0	Sigma-Aldrich, Munich, Germany
Penicillin/Streptomycin	-	Life Technologies, Carlsbad, USA
peqGold 1KB DNA ladder	-	VWR Int., Darmstadt, Germany
Potassium chloride	7440-09-7	Sigma-Aldrich, Munich, Germany
Propidium iodide	9041-08-1	Sigma-Aldrich, Munich, Germany
Rhodamine phalloidin	219920-04-4	Life Technologies, Carlsbad, USA
RNASolv ®	R6830-02	VWR, Darmstadt Germany
RNAlater™ Stabilization Solution	AM7021	ThermoFisher Scientific, Schwerte, Germany
Sodium Acetate	S-5889	Sigma-Aldrich, Munich, Germany
Sodium chloride	7647-14-5	Sigma-Aldrich, Munich, Germany
Sodium hydroxide	1310-73-2	Sigma-Aldrich, Munich, Germany
SM-102	2089251-47-6	Biosynth Carbosynth, Berlin Germany
succinic anhydride	108-30-5	Sigma-Aldrich, Munich, Germany
Trifluoro acetic acid (TFA)	76-05-1	Iris Biotech, Marktredwitz, Germany
Triton X-100	9036-19-5	Sigma-Aldrich, Munich, Germany
Trypsin/EDTA	9002-07-7	PAN Biotech GmbH, Aidenbach, Germany

2.2. Buffers

Table 2 Buffers used for experimental procedures

Buffer	Composition
Agarose electrophoresis loading buffer	3 mL glycerine, 1.2 mL 0.5 M EDTA solution (pH 8.0), 2.8 mL H2O, 10 mg bromophenol blue
HBG	20 mM HEPES, 5 % glucose, pH 7.4
LAR buffer	20 mM glycylglycine; 1 mM MgCl2; 0.1 mM EDTA; 3.3 mM DTT; 0.55 mM ATP; 0.27 mM coenzyme A, pH 8–8.5
PBS buffer	136.9 M NaCl, 2.68 M KCl, 8.1 M Na_2HPO_4, 1.47 M KH_2PO_4
10× TBE buffer	89 mM Trizma® base, 89 mM boric acid, 2 mM EDTA-Na_2

2.3. Kits

Table 3 Commercial kits used for experimental procedures

Kit	Catalog number	Supplier
Quant-iT™ RiboGreen RNA Assay-Kit	R11490	ThermoFisher Scientific, Schwerte, Germany
Peqlab peqGOLD, total RNA Kit	13-6834-01	VWR, Darmstadt Germany
qScript cDNA SuperMIx	733-1177	Quantabio, Beverly. Massachusetts, USA
qScript cDNA Synthese Kit	95047	Quantabio, Beverly. Massachusetts, USA
QIAmp DNA Mini Kit	51306	Qiagen, Hilden, Germany
Qiagen Plasmid Maxi Prep	12163	Qiagen, Hilden, Germany
QIAquick PCR Purification Kit	28104	Qiagen, Hilden, Germany
QIAquick Gel Extraction Kit	28704	Qiagen, Hilden, Germany

2.4. Proteins

Table 4 Proteins used for experimental procedures

Protein	Catalog number	Supplier
BsaI	R3733S	New England Biolabs, Ipswich, USA
Cas9 protein	-	in house generation
GoTaq^R Hot Start polymerase	M5001	New England Biolabs, Ipswich, USA
One *Taq*^{R} DNA Polymerase	M0480X	New England Biolabs, Ipswich, USA
Taq^R DNA polymerase	M0273X	New England Biolabs, Ipswich, USA

Cas9 protein expression and purification were performed in house by Miriam Höhn (Pharmaceutical Biotechnology, LMU München) as previously described [85].

2.5. Nucleic Acids

2.5.1. sgRNA and single stranded DNA (ssDNA)

Table 5 Sequences of sgRNA and ssDNA used in this research

sgPcsk9 (Axolabs)	Target site / PAM	CCCATACCTTGGAGCAACGG / CGG [157, 158]
	full RNA sequence	5'mC*mC*mC*AUACCUUGGAGCAACGGGUUUUAGAmGmCmU mAmGmAmAmAmUmAmGmCAAGUUAAAUAAGGCUAGUCCGU UAUCAmAmCmUmUmGmAmAmAmAmAmGmUmGmGmCmAmC mCmGmAmGmUmCmGmGmUmGmCmUmU*mU*mU* 3'
sgDMD$_{Ex23}$ (IDT)	Target site / PAM	ATTTCAGGTAAGCCGAGGTT / TGG [159]
	full RNA sequence	5'mA*mU*mU*UCAGGUAAGCCGAGGUUGUUUUAGAGCUAGA AAUAGCAAGUUAAAAUAAGGCUAGUCCGUUAUCAACUUGA AAAAGUGGCACCGAGUCGGUGCmU*mU*mU*U 3'
sgGFP (IDT)	Target site / PAM	GCTGAAGCACTGCACGCCGT / AGG [86]
	full RNA sequence	5' mG*mC*mU*GAAGCACUGCACGCCGUGUUUUAGAGCUAGA AAUAGCAAGUUAAAAUAAGGCUAGUCCGUUAUCAACUUGA AAAAGUGGCACCGAGUCGGUGCmU*mU*mU*U 3'
ssDNA (IDT)	GFP to BFP	5'G*C*CACCTACGGCAAGCTGACCCTGAAGTTCATCTGCACCA CCGGCAAGCTGCCCGTGCCCTGGCCCACCCTCGTGACCACCCT GAGCCACGGCGTGCAGTGCTTCAGCCGCTACCCCGACCACAT *G*A 3'

Modification pattern: 'm_' = 2'-O-methyl RNA bases e.g. 'mA' ; '_*' = phosphorothioated RNA bases e.g. 'A*'

2.5.2. Messenger RNA (mRNA)

Table 6 mRNA used in this research

Name	**Encoding**	**Supplier**
CleanCap® Cas9 mRNA (5 moU),	Streptococcus pyogenes SF370 Cas9 protein (CRISPR Associated Protein 9)	Trilink Biotechnologies, San Diego,USA
CleanCap® FLuc mRNA (5moU)	Firefly Luciferase	Trilink Biotechnologies, San Diego,USA
CleanCap® mCherry mRNA (5moU)	mCherry	Trilink Biotechnologies, San Diego,USA

Fully substituted with 5-Methoxy-Uridine

2.5.3. Plasmid DNA (pDNA)

Table 7 pDNA used for experimental procedures

Name	**Encoding**	**Supplier**
pEGFP-N1	eGFP	Clontech Laboratories now Takara Bio, San Jose, USA
PB-CAG-mCherry-DMDEx23-eGFP	mCherry-DMDEx23 and eGFP	In-house generation by Anna-Lina Lessl (PhD student at Pharmaceutical Biotechnology, LMU, Munich)

2.5.4. PCR Primers

Primers were provided by Eurofins (Ebersberg, Germany).

Table 8 List of PCR primers used for this research

Primer name	Sequence
Pcsk9 fwd	5'-GGCCCGTTAATGTTTAATCAGA-3'
Pcsk9 rev	5'-TTTACTTCGGAGGACACGTTTT-3'
mCherry-DMDex23_SpliSwi_fwd	5'-GGAGGATAACATGGCCATCA-3'
mCherry-DMDex23_SpliSwi_rev	5'-GTCCTTCAGCTTCAGCCTCT-3'
mCherry-DMD$_{Ex23}$ SpliSwi nested_fwd	5'-GGAGTTCATGCGCTTCAAGG-3'
mCherry-DMD$_{Ex23}$ SpliSwi nested_rev	5'-GCCGTCCTCGAAGTTCATCA-3'
DMD_Ex20-26 fwd	5'-CAGAATTCTGCCAATTGCTGAG-3' [160]
DMD_Ex20- DMD_Ex24/25 rev	5'-TCACCAACTAAAAGTCTGCATTG-3' [161]
DMD_Ex20/21 fwd	5'-AAAATTTGTAAGGATGAAGTCAAC-3'
DMD_Ex20-24 rev	5'-CAGCCATCCATTTCTGTAAGG-3' [162]
DMD genomic fwd	5'-AAACTTCTGTGATGTGAGGACA-3'
DMD genomic rev	5'-ACAAATGGCCAACTATGAGAAAC-3'
DMD genomic sequencing fwd	5'-GAAACTCATCAAATATGCGTGTTAGTG-3'
DMD genomic sequencing rev	5'-GGCAAGTTGCAATCCTTTGA-3'

2.6. Cell Culture

Table 9 Reagents for cell culture

Material	Supplier
Dulbecco's Modified Eagle's Medium (DMEM)	Life Technologies, Carlsbad, USA
Fetal bovine serum (FBS)	Life Technologies, Carlsbad, USA
Penicillin/Streptomycin	Life Technologies, Carlsbad, USA
Trypsin/EDTA	PANBiotech, Aidenbach, Germany

3. Methods

This chapter has been adapted from:

Germer J, Lessl AL, Pöhmerer J, Grau M, Weidinger E, Höhn M, Yazdi M, Cappelluti MA, Lombardo A, Lächelt U, Wagner E. Lipo-Xenopeptide Polyplexes for CRISPR/Cas9 Based Gene Editing at Ultra-Low Dose. Journal of Controlled Release

3.1. Synthesis of Ionizable Nucleic Acid Carriers

The solid phase synthesis of the LAF–Stp carrier library was performed as previously described by Thalmayr et al [163]. All LAF-Stp carrier were synthesized by Melina Grau as part of her PhD study at Pharmaceutical Biotechnology, LMU, Munich. Succinylated branched PEI 25 kDa (succPEI; succinylation degree of 10 %) was synthesized and analyzed as described previously [53]. The starting material branched PEI (brPEI) 25 kDa was purchased from Sigma Aldrich (Munich, Germany).

3.2. Polyplex Formation

Either Luc mRNA or a combination of Cas9 mRNA and sgRNA at a fixed weight ratio of 1:1 was mixed and diluted in HBG (20 mM of HEPES, 5 % (w/v) glucose, pH 7.4). The calculated amounts of aminolipid carrier at indicated N/P (nitrogen/phosphate) ratio were diluted in separate tubes of HBG. All secondary amines, terminal amines and the tertiary amines of the carrier structure were considered in the N/P ratio calculations. Equal volumes of nucleic acid solution and aminolipid solution were mixed by rapid pipetting and incubated 40 min at RT in a closed Eppendorf reaction tube. The final concentration of nucleic acid in the polyplex solution was 12.5 µg mL^{-1} (6.25 µg mL^{-1} Cas9 mRNA plus 6.25 µg mL-^{1} sgRNA or 12.5µg µg mL-^{1} Luc mRNA) for *in vitro* experiments. For *in vivo* experiments polyplexes were mixed achieving a final concentration of 20 µg mL^{-1} (or 67 µg mL^{-1}) and 60 µg mL^{-1} (or 200 µg mL^{-1}) total RNA (Luc mRNA or Cas9 mRNA and sgRNA at weight ratio 1:1) for intravenous and intramuscular application, respectively.

3.3. Polyplex Formation for mRNA/pDNA Codelivery

mCherry mRNA and pEGFP-N1 at a fixed weight ratio of 1:1 were mixed and diluted in HBG. Calculated amounts of aminolipid at indicated N/P (nitrogen/phosphate) ratios (see above) were diluted in separate tubes of HBG. Equal volumes of nucleic acid solution and aminolipid solution were mixed by rapid pipetting and incubated 40 min at RT in a closed Eppendorf

reaction tube. The final concentration of nucleic acid in the polyplex solution was 5 µg mL^{-1} (2.5 µg mL^{-1} mCherry mRNA plus 2.5 µg mL^{-1} pEGFP-N1 pDNA).

3.4. Cas9 mRNA/sgGFP2/ssDNA Polyplex Formation for eGFP to BFP Conversion Study

Cas9 mRNA and sgGFP at a fixed weight ratio of 1:1 were mixed with indicated molar ratios of total sgGFP to the single stranded DNA (ssDNA) template (IDT, Coralville, IA, USA) and diluted in HBG. Calculated amounts of LAF-Stp carrier 1611 were diluted in separate tubes of HBG. Equal volumes of nucleic acid solution and 1611 solution were mixed by rapid pipetting resulting in an N/P ratio of 18 and incubated 40 min at RT in a closed Eppendorf reaction tube. The final total concentration of nucleic acid in the polyplex solution was 7.5 µg mL^{-1}.

3.5. Lipid Nanoparticle (LNP) Formation

LNPs of commercially available positive control ionizable lipid SM-102 or the LAF carrier 1621 were formulated by mixing an acidic aqueous phase containing the nucleic acid with an ethanolic phase containing helper lipids and the ionizable lipid by rapid pipetting. The aqueous phase was prepared in citrate buffer (10 mM, pH 4.0) containing either Luc mRNA or a mix of Cas9 mRNA and sgRNA at weight ratio 1:1. The ethanolic phase includes a mixture of the lipidic components at molar ratio of 38.5:10:1.5:50 mol% (Chol:DSPC:PEG-DMG:SM-102) or 47.6:23.8:4.8:23.8 mol% (Chol:DOPE:PEG-DMG:1621)[164] at the N/P ratio of 6 for SM-102 or 24 for 1621, respectively. The aqueous nucleic acid solution and ethanolic lipid mixture were mixed at a defined volumetric ratio of 3:1 (lipid mixture : nucleic acid solution) by rapid pipetting. Following 15 min incubation at RT, the solutions were dialyzed for 2 h against HBG in 1 kDa MWCO tubes at 4 °C. If needed HBG was added to obtain final concentration of 20 µg mL^{-1} and 60 µg mL^{-1} total RNA (Luc mRNA or Cas9 mRNA and sgRNA at weight ratio 1:1) for intravenous and intramuscular application, respectively.

3.6. Particle Size and Zeta-Potential Measurements

Polyplexes and LNPs were formulated in HBG as described above and if needed diluted with HBG to a concentrations of 12.5 µg mL^{-1} total RNA (Cas9 mRNA sgRNA at weight ratio 1:1 or Luc mRNA). Measurements of size and zeta potential were performed with a Zetasizer Nano ZS (Malvern Instruments, Malvern) in a folded capillary cell (DTS1070) by dynamic and electrophoretic laser-light scattering (DLS, ELS). Size and polydispersity index were measured in 80 µL of polyplex or LNP solution using the following instrument settings: equilibration time

30 sec, temperature 25 °C, refractive index 1.330, viscosity 0.8872 mPa*s. Samples were measured three times with six sub-runs per measurement. For measurement of the zeta potential, all samples were diluted to 800 µL with HBG directly before measurement. Parameters were identical to the size measurement apart from an equilibration time of 60 sec. Three measurements with 15 sub-runs lasting 10 sec each were performed, and zeta potentials were calculated by the Smuchowski equation.

3.7. Encapsulation Efficiency

The encapsulation efficiency (EE (%)) of LNPs and polyplexes was determined using the Quant - iT™ RiboGreen RNA Assay-Kit (Thermo Fisher Scientific). Polyplexes and LNPs were mixed as above and diluted with 1× TE (10 mM Tris-HCl, 1 mM EDTA, pH 7.5 in RNase-free water) to an mRNA concentration of 2 µg mL^{-1}. 50 µL of the diluted nanoparticles was either mixed with 50 µL of 1 × TE as untreated controls or added to 50 µL of 1 × TE containing 2 % (v/v) Triton X-100 as treated samples. Additional 250 I.U. mL^{-1} heparin was added for complete dissociation of polyplexes. After a 10 min incubation at 37 °C under constant shaking at 150 rpm and cooling down to RT, 100 µL of RiboGreen reagent 200-fold in 1x TE was added to each sample. Fluorescence was measured after 5 min in a Tecan microplate reader (Spectrafluor Plus, Tecan, Männedorf, Switzerland) at excitation/emission wavelength of 485/535 nm in duplicates. Background was measured with pure HBG in 1× TE, 1× TE supplemented with Triton X-100 for LNP or 1× TE supplemented with Triton X-100 and heparin for polyplexes, treated in the same manner as the respective nanoparticle samples. The following formula was used to calculate encapsulation efficiency after background subtraction of each sample:

$$EE(\%) = 100\% - \frac{mean\ emission_{untreated\ control}}{mean\ emission_{treated\ sample}}\ x\ 100\%$$

3.8. Agarose Gel Shift Assay

A 1.5 % (w/v) agarose gel for Cas9 mRNA / sgRNA polyplexes was prepared by heating up agarose (Agarose BioReagent, Sigma-Aldrich, Merck, Darmstadt) in TBE buffer (18.0 g of tris(hydroxymethyl)aminomethane, 5.5 g of boric acid, 0.002 M disodium ethylenediaminetetraacetic acid (EDTA) at pH 8, in 1 L of water). After cooling down to about 50 °C, 1× GelRed™ (Biotium, Hayward, CA, USA) was added. The agarose solution was casted into an electrophoresis unit and cooled down for gelification. Polyplexes and LNP were

formulated as described in the section 3.2 “polyplex formation” and 3.5 “LNP formation”, respectively. 3 µL of loading buffer (6×; prepared from 6 mL of glycerol, 1.2 mL of 0.5 M EDTA, 2.8 mL of H_2O, 0.02 g of bromophenol blue) was added to 15 µL of the polyplex solution. Samples were loaded to the pockets of the gel and electrophoresis was performed at 120 V for 70 min in TBE buffer. Free Luc mRNA or a combination of Cas9 mRNA and sgRNA (weight ratio 1:1) diluted in 15 µL HBG to a total RNA concentration of 12,5 g/mL were used as control. Control groups for the evaluation of nanoparticles after incubation in full fetal bovine serum (FBS) were either 15 µL pure FBS, free RNA in 15 µL FBS or free RNA in 15 µL HBG buffer.

3.9. Cell Culture

Hepa 1-6 *Pcsk9*^{tdTomato} (a Hepa 1-6 cell line stably expressing tdTomato in the 3’UTR of the *Pcsk*9 gene, generated by HDR-mediated insertion of the 2A-tdTomato-pA cassette post Cas9-induced double strand break in exon 12 of *Pcsk*9) [158, 165], HeLa mCherry-DMD_{Ex23} (stably expressing an artificial mCherry construct, interrupted by a dystrophin exon 23 sequence, derived from the murine Duchenne muscular dystrophy (DMD) *mdx* model) [166], CT26 eGFP-Luc (stably expressing the green fluorescent protein/luciferase (eGFP-Luc) fusion gene) [167], and HeLa GFPd2 (stably expressing destabilized eGFP) [86] were cultured in Dulbecco’s modified Eagles’s medium (DMEM)-low glucose (1 g L^{-1} glucose) supplemented with 10 % (v/v) fetal bovine serum (FBS), 4 mM of stable glutamine, 100 U mL^{-1} of penicillin, and 100 µg mL^{-1} of streptomycin. The cells were cultured at 37 °C and 5 % CO2 in an incubator with a relative humidity of 95 %.

3.10. Genome Editing Reporter Cell Lines

Pcsk9 knock out. For *Pcsk*9 knock out studies, sgPcsk9 [157] which binds and directs the Cas9 protein to the first exon of the *Pcsk*9 gene was used on the Hepa 1-6 *Pcsk9*^{tdTomato} cell line. Thus, the expression of the tdTomato reporter protein is inactivated by the Cas9 induced destruction of the *Pcsk*9 gene. The gene knock out of the *Pcsk9* gene can be quantified by flow cytometry as described as described in section 3.11.

mdx DMD$_{Ex23}$ splicing modification. The positive read-out reporter cell line HeLa mCherry-DMD_{Ex23} was used to test the transfection efficiency of Cas9 mRNA/sgDMD_{Ex23} polyplexes. Cas9 induced cleavage at the 3’ prime end of the artificial *mdx* exon 23 construct triggers alternative mRNA splicing with *mdx* exon 23 skipping and mediates expression of functional

mCherry protein. The transfection efficiency can be quantified by the percentage of mCherry positive cells measured by flow cytometry as described in section 3.11.

HDR mediated eGFP to BFP conversion. The homologous directed repair (HDR) efficacy was assessed by the conversion of eGFP to BFP in the HeLa GFPd2 cell line expressing destabilized eGFP. HDR-mediated repair following the Cas9-induced double strand break (DSB) of the DNA can replace the 66th amino acid tyrosine (code: TAC) in eGFP sequence with histidine (code: CAT)[168]. In flow cytometric analysis after treatment with Cas9 mRNA/sgGFP/ssDNA-template polyplexes three cell populations were expected: eGFP positive cells representing non-edited cells; eGFP and BFP negative cells indicating gene knock out by non-homologous end joining (NHEJ) of the DSB and BFP positive and eGFP negative cells suggesting HDR-mediated gene correction.

3.11. *In Vitro* Evaluation of Cellular Gene Editing Efficiency of Cas9mRNA/sgRNA containing Nanoparticles by Flow Cytometry

All transfections were performed in triplicate in 96-well plates (Corning® Costar, Sigma-Aldrich, Germany). Hepa 1-6 *Pcsk9*^{tdTomato}, CT26 eGFP-Luc, HeLa GFPd2 and HeLa mCherry-DMDEx23 cells were seeded 24 h prior to transfection (7,500 cells/well). On the next day, the medium was replaced with 80 µL of fresh pre-warmed medium containing 10 % (v/v) FBS. The nanoparticles were prepared as described in sections 2.3 and 2.4 resulting in a total RNA concentration of 12.5 µg mL-1 (6.25 µg mL-1 Cas9 mRNA and 6.25 µg mL-1 sgRNA). Required volumes of nanocarrier solutions were pipetted to the corresponding wells and if needed HBG was added to reach the final volume of 100 µl per well. For testing the efficiency of a further reduced dose nanoparticles were 1:10 (v/v) diluted with HBG right before the transfection to ensure precise volumetric dosage. The negative control was represented by 20 µl of HBG. After 24 h of incubation HeLa mCherry-DMDEx23 cells were trypsinized, expanded and incubated for an additional 2 days. All other cell lines were expanded after 48 h and incubated for an additional 3 days. For flow cytometric evaluation, cells were collected and resuspended in PBS solution containing 10 % (v/v) FBS (FACS buffer). All samples were analyzed by flow cytometry using a CytoFLEX S Flow Cytometer (Beckman Coulter, Brea, CA, USA). Shortly before the measurement, 1 ng µL-1 of 4′,6-diamidino-2-phenylindole (DAPI) was added and used to discriminate between viable and dead cells. The cellular fluorescence was assayed by excitation of DAPI at 405 nm and detection of emission at 450 nm. For eGFP to BFP conversion studies DAPI was replaced by 1 ng µL-1 propidium iodide (PI). The cellular fluorescence was assayed by excitation of PI at 561 nm and detection of emission

at 610 nm. Only isolated viable cells were evaluated. The transfection efficiency on HeLa mCherry-DMDEx23 cells was determined as the percentage of mCherry positive cells. The cellular mCherry expression was assayed by excitation at 561 nm and the detection of emission at 610 nm. The cellular tdTomato expression in Hepa 1-6 *Pcsk9*^{tdTomato} cells was assayed by excitation at 561 nm and the detection of emission at 585 nm. The *Pcsk9* knock out efficiency was determined as the percentage of tdTomato negative cells. The cellular GFP expression in CT26 eGFP-Luc and HeLa GFPd2 was assayed by excitation at 488 nm and the detection of emission at 530 nm. The GFP knock out efficiency was determined as the percentage of GFP negative cells normalized to the control measurements with HBG buffer-treated cells. In eGFP to BFP conversion study the loss of GFP indicated gene knock out mediated NHEJ; BFP expression represented conversion from the GFP reporter protein to BFP by homology-directed repair while GFP expressing cells show non-edited reporter cells. BFP expression was assayed by excitation at 405 nm and the detection of emission at 450 nm. Flow cytometry data were analyzed using FlowJoTM v10.8 flow cytometric analysis software by FlowJo, LLC (Becton, Dickinson and Company, U.S.).

3.12. Sanger Sequencing and TIDE Analysis of *Pcsk9* Gene Edits

Genomic DNA of Hepa 1-6 *Pcsk9*^{tdTomato} cells was extracted 3 days after treatment with Cas9 mRNA/sgPcsk9 containing polyplexes using a QIAMP DNA Mini Kit (Qiagen, Hilden, Germany) according to manufacturer's protocol. The target region in the first exon of the *Pcsk9* gene was PCR amplified using GoTaq^{R} Hot Start polymerase (Promega, Walldorf, Germany). Following PCR primers and conditions were applied: *Pcsk9* fwd (5'-GGCCCGTTAATGTTTAATCAGA-3'); *Pcsk9* rev (5'-TTTACTTCGGAGGACACGTTTT-3'); initial denaturation (95 °C, 2 min), 40 cycles (95 °C, 45 sec / 56 °C, 40 sec / 72 °C, 1 min), final extension (72 °C, 5 min). The PCR products were purified using the PCR purification kit (Qiagen, Germany). Sanger sequencing of the purified sequences was performed by Eurofins GATC Biotech (Konstanz, Germany) at a concentration of 20 ng μL^{-1}. Sanger sequencing data were evaluated by the TIDE web tool (https://tide.nki.nl/) applying an indel size range of 25 and default settings for decomposition and alignment windows [169, 170].

3.13. Evaluation of Codelivery Efficiency of mRNA/pDNA Polyplexes by Flow Cytometry

mRNA/pDNA polyplex treatments were performed in triplicate in 96-well plates. Hepa 1-6, HeLa, N2a and DU 145 wildtype cells were seeded 24 h prior to transfection (10,000 cells/well). On the next day, the medium was replaced with 80 µL of fresh pre-warmed medium containing 10 % (v/v) FBS. The nanoparticles were prepared as described in section 3.3, and the volumes of 10 µL and 5 µL of polyplex solution (2.5 µg mL^{-1} mCherry mRNA and 2.5 µg mL^{-1} pEGFP-N1 pDNA) were added. 20 µL HBG buffer per well was used as negative control. After 24 h of treatment, cells were collected and re-suspended in PBS solution containing 10 % (v/v) FBS (FACS buffer) for flow cytometric evaluation. All samples were analyzed by flow cytometry using a CytoFLEX S Flow Cytometer (Beckman Coulter, Brea, CA, USA). Shortly before the measurement, 1 ng $µL^{-1}$ 4′,6-diamidino-2-phenylindole (DAPI) was added and used to discriminate between viable and dead cells. The cellular fluorescence was assayed by excitation of DAPI at 405 nm and detection of emission at 450 nm. Only isolated viable cells were evaluated. Gates were set compared to control measurements with HBG buffer-treated cells. The percentage of mCherry and eGFP positive cells represented efficient mRNA and pDNA transfection, respectively. Cells shifted to the mCherry and GFP positive gate indicated successful co-delivery and expression of both, mRNA and pDNA in one cell. Flow cytometry data were analyzed using FlowJo™ v10.8 flow cytometric analysis software by FlowJo, LLC (Becton, Dickinson and Company, U.S.). The cellular fluorescence expression was assayed by excitation at 561 nm and 488 nm, the detection of emission at 610 nm and 530 nm for mCherry and eGFP, respectively.

3.14. Evaluation of Genomic Changes on the mCherry-DMD_{Ex23} Reporter

Genomic DNA of HeLa mCherry-DMD_{Ex23} cells was extracted 2 weeks after treatment with either Cas9 mRNA/sgDMD_{Ex23} (weight ratio 1:1) or Cas9 mRNA/sgPcsk9 (weight ratio 1:1) containing polyplexes using a QIAMP DNA Mini Kit (Qiagen, Hilden, Germany) according to manufacturer's protocol. A PCR employing Taq polymerase (New England Biolabs, Ipswich, Massachusetts, USA) was conducted to amplify the mCherry-DMD_{Ex23} reporter region. The PCR was carried out with the primers mCherry-DMD_{Ex23} SpliSwi nested_fwd (5' - GGAGTTCATGCGCTTCAAGG-3') and mCherry-DMD_{Ex23} SpliSwi nested_rev (5'- GCCGTCCTCGAAGTTCATCA-3') under the following conditions: initial denaturation (94 °C, 30 sec), 30 cycles (94 °C, 30 sec / 55 °C, 1 min / 68 °C, 1 min), final extension (68 °C, 5 min). The PCR product obtained from nested PCR was subjected to analysis on a GelRed®

(Biotium, Hayward, CA, USA) containing 1 % agarose gel in 1x TBE buffer. Electrophoresis was conducted for 1.5 hours at 100 V, and the gel was analyzed using the Dark Hood DH-40 (biostep, Burkhardtsdorf, Germany) along with the biostep argusX1 software. The bands of approximately 850 bp and 450 bp were excised from the gel. For sequencing, the purified DNA fragments were sequenced (Sanger) by Eurofins GATC Biotech (Konstanz, Germany) using mCherry-DMD_{Ex23} SpliSwi nested_fwd (5'-GGAGTTCATGCGCTTCAAGG-3') and mCherry-DMD_{EX23} SpliSwi nested_rev (5'-GCCGTCCTCGAAGTTCATCA-3') primers at a concentration of 10 ng μL^{-1}.

3.15. Incubation of polyplexes in high serum

All transfections were performed in triplicate in 96-well plates (Corning® Costar, Sigma-Aldrich, Germany). HeLa mCherry-DMD_{Ex23} cells were seeded 24 h prior to transfection (7,500 cells/well). On the next day, the medium was replaced with 80 µL of fresh pre-warmed medium containing 10 % (v/v) FBS. The nanoparticles were prepared as described in section 3.2 and 3.5. To assess the efficiency in high serum of LAF containing carriers, the polyplexes were 10-20-fold diluted with 100 % FBS. After incubation of the polyplexes for 2 h at 37 °C, volumes resulting in the indicated concentration were added to the corresponding wells. To reach a final volume of 100 µL per well in all experiments, either HBG buffer or FBS were added for HBG diluted and serum incubated particles, respectively. Addition of 20 µL HBG buffer was used as negative control. The cells were incubated for 24 h. Afterwards, the cells were trypsinized, expanded and incubated for additional 2 days. Flow cytometric evaluation and analysis was performed as described in section 3.11.

3.16. Assessment of the Relative Metabolic Activity of Cells Via MTT Assay

Transfections were performed as described in section 3.11. At 24 h post transfection, 10 µL dimethylthiazol (MTT) (5 mg mL^{-1}) were added to each well, reaching a final concentration of 0.5 mg mL^{-1}. The supernatant was removed after incubation at 37 °C for 2 h. The plates were stored at –80 °C for at least 1 h. Afterwards, the purple formazan product was dissolved in 100 µL DMSO. After incubation for 30 min at 37 °C under constant shaking (125 rpm), quantification was done photometrically using a Tecan microplate reader (Spectrafluor Plus, Tecan, Männedorf, Switzerland). Absorbance was measured at wavelength $\lambda = 590$ nm with background correction at $\lambda = 630$ nm. Experiments were carried out in triplicates. Relative metabolic activity related to control wells (HBG-treated cells) was calculated by the equation:

$$\frac{A_{test}}{A_{control}} x\ 100\%$$

3.17. *In Vitro* DNA Cleavage Assay

To confirm the specificity of the cleavage of the mCherry reporter gene and the genomic donor splice site downstream the physiological dystrophin exon 23 by the RNP complex formed with $sgDMD_{Ex23}$ compared to no cleavage by RNP complex formed with other sgRNAs *in vitro*, 300 ng of a linearized plasmid or PCR amplicon surrounding the physiological dystrophin exon 23 containing the $sgDMD_{EX23}$ target site was generated. The linear DNA or PCR amplicon was then incubated with the precomplexed RNPs (150 ng of Cas9 protein and 60 ng of sgRNA) for 2 h at 37 °C. The reaction mixture was analyzed by agarose gel electrophoresis (1.5 % agarose gel). Because of the asymmetric location of the $sgDMD_{EX23}$-target sequence within the amplicon, successful cleavage by the Cas9/sgRNA complex results in two bands on the agarose gel.

3.18. Splicing Modulation Assay of Cas9 Treated Hela mCherry-DMD_{Ex23} Cells

The splicing modulation assay was performed by Anna-Lina Lessl (PhD student at Pharmaceutical Biotechnology, LMU, Munich).

The reporter cell line HeLa mCherry-DMD_{Ex23} was treated with 1611 polyplexes (N/P 18) containing either Cas9 mRNA/$sgDMD_{Ex23}$ (weight ratio 1:1) or Cas9 mRNA/sgPcsk9 (weight ratio 1:1), resulting in concentrations of 10 nM sgRNA. After three days total RNA was isolated from cells using RNASolv (VWR International GmbH, Darmstadt, Germany) according to the manufacturer's protocol. The cDNA synthesis was carried out using the qScript cDNA synthesis

kit (Quantabio, Beverly. Massachusetts, USA), utilizing 400 ng of RNA following the manufacturer's protocol. For the amplification of the exon skipping region, a nested PCR was conducted with 150 ng of cDNA, employing Taq polymerase (New England Biolabs, Ipswich, Massachusetts, USA). The specific primer sequences used for the first amplification step were mCherry-DMDex23_SpliSwi_fwd (5'-GGAGGATAACATGGCCATCA-3') and mCherry-DMDex23_SpliSwi_rev (5'-GTCCTTCAGCTTCAGCCTCT-3'). The PCR conditions used were as follows: initial denaturation (94 °C, 30 sec), 30 cycles (94 °C, 30 sec / 60 °C, 1 min / 68 °C, 1 min), final extension (68 °C, 5 min). The PCR product was purified using the PCR purification kit from Qiagen (Hilden, Germany) following the manufacturer's protocol. To selectively enrich the splicing product leading to functional mCherry expression, 1 µg of the purified PCR amplicon was subjected to an overnight digestion with 2 units of Nde I. The restriction enzyme was removed by adding 1.25 µL of 10 % sodium dodecyl sulfate (SDS, w/v) (resulting in 0.2 % SDS) into the reaction solution and incubating for 10 min at 65 °C. The removal of SDS and the restriction enzyme was accomplished by purifying the digested DNA using the PCR purification kit (Qiagen, Hilden, Germany) in accordance with the manufacturer's protocol. For the subsequent second amplification of the nested PCR 300 ng of the digested and purified DNA as template were used. The PCR was carried out with the primers mCherry-DMD_{Ex23} SpliSwi nested_fwd (5'-GGAGTTCATGCGCTTCAAGG-3') and mCherry-DMD_{Ex23} SpliSwi nested_rev (5'-GCCGTCCTCGAAGTTCATCA-3') under the following conditions: initial denaturation (94 °C, 30 sec), 30 cycles (94 °C, 30 sec / 55 °C, 1 min / 68 °C, 1 min), final extension (68 °C, 5 min). The PCR product obtained from nested PCR was subjected to analysis on a GelRed® (Biotium, Hayward, CA, USA) containing 1 % agarose gel in 1x TBE buffer. Electrophoresis was conducted for 1.5 hours at 100 V, and the gel was analyzed using the Dark Hood DH-40 (biostep, Burkhardtsdorf, Germany) along with the biostep argusX1 software. The specific target band, indicating the presence of the DNA sequence with skipped dystrophin exon 23 (~280 base pairs (bp)) was excised from the gel. The isolated DNA was purified using the QIAquick® Gel Extraction Kit (Qiagen, Hilden, Germany). For sequence determination, the purified DNA fragments were sequenced (Sanger) by Eurofins GATC Biotech (Konstanz, Germany) using mCherry-DMD_{Ex23} SpliSwi nested_fwd (5'-GGAGTTCATGCGCTTCAAGG-3') and mCherry-DMD_{EX23} SpliSwi nested_rev (5'-GCCGTCCTCGAAGTTCATCA-3') primers at a concentration of 10 ng μL^{-1}.

3.19. Confocal laser scan microscopy (CLSM) of Cas9 treated HeLa mCherry-DMD_{Ex23} cells

Transfections of HeLa mCherry-DMD_{Ex23} cells were performed as described above. Cells treated with 1611 containing polyplexes containing either Cas9 mRNA and $sgDMD_{ex23}$ (weight ratio 1:1) or Cas9 mRNA and sgPcsk9 (weight ratio 1:1) resulting in a concentration of 10 nM sgRNA in 96-well plates (Corning® Costar, Sigma-Aldrich, Germany). After 48 h of treatment cells were collected and 20,000 cells were seeded into 8 well-Ibidi µ-slides (Ibidi, Planegg/Martinsried, Germany) in a total volume of 300 µL medium per well. Cells were incubated at 37 °C and 5 % CO_2 for 24 h. The next day, cells were washed twice with 300 µL pre-warmed PBS before fixation with 4 % paraformaldehyde in PBS for 40 min at RT. The wells were washed again twice with PBS. The cytoskeleton was stained overnight under light exclusion at 4 °C with rhodamin-phalloidin (4 µg/mL in 300 µL PBS). The cell nuclei were stained with DAPI (2 µg/mL in 300 µL PBS) for 20 min under light exclusion at RT. The staining solution was removed and 300 µL of PBS was added. The images were recorded by Miriam Höhn (Pharmaceutical Biotechnology, LMU München) using a Leica TCS SP8 SMD confocal laser scanning microscope (CLSM) equipped with an HC PL APO 63x 1.4 objective (Germany). DAPI and mCherry emission was recorded at 460 nm and 610 nm, respectively. All images were processed using the LAS X software from Leica.

In vivo Studies

3.20. In Vivo Performance of Polyplexes and LNPs in BALB/c Mice

All *in vivo* experiments were performed according to the guidelines of the German Animal Welfare Act and were approved by the animal experiments ethical committee of the Government of Upper Bavaria (accreditation number Gz. ROB-55.2-2532.Vet_02-19-19). The study utilized 6-weeks-old female BALB/c mice from Janvier, Le Genest-Saint-Isle, France. Mice were randomly divided into groups of four and were housed in isolated ventilated cages under specific pathogen-free conditions with a 12 h day/night interval, and food and water ad libitum. Weight and general well-being were monitored continuously. Experiments were performed by Jana Pöhmerer and Ulrich Wilk as part of their veterinary MD studies at Pharmaceutical Biotechnology, LMU.

3.21. *In Vivo* Studies Using Cas9 mRNA / sgDMDEx23 Polyplexes and LNPs

For testing the effect of Cas9 mRNA/sgDMD$_{Ex23}$ formulations *in vivo* on the physiological dystrophin gene, nanocarrier formulations were prepared as described above right before intravenous or intramuscular injection (Cas9 mRNA and sgDMD$_{Ex23}$ at weight ratio 1:1). For systemic application, 150 µL carrier solution containing either 3 µg total RNA in 1762 polyplexes, LNP 1621 and LNP SM-102 or 10 µg total RNA in 1611 polyplexes was intravenously injected into the tail vein at three timepoints (day 0, day 2, day 7). Local administration was performed after subcutaneous treatment with Carprofen at a dose of 5 mg/kg. Single or triple applications (day 0, day 3, day 14) were tested by the injection of 50 µL carrier solution containing either 3 µg total RNA in 1762 polyplexes, LNP 1621 and LNP SM-102 or 10 µg total RNA in 1611 polyplexes into the left musculus biceps femoris. Seven days after the last injection, mice were euthanized and the brain, heart, spleen and musculus biceps femoris (injected left and contralateral muscle) were harvested. For stabilization of the mRNA, the organs were incubated in RNAlater solution (Thermo Fisher Scientific, Waltham, MA) overnight at 4 °C and stored at -20 °C. Each organ was manually homogenized in liquid nitrogen using mortar and pestle. Injections and harvesting of the organs were performed by Jana Pöhmerer, Ulrich Wilk and Mina Yazdi as part of their veterinary MD studies and PhD studies at Pharmaceutical Biotechnology, LMU.

3.22. Splicing Modulation by Cas9/sgRNA *In Vivo* on mRNA Level

The mRNA was isolated for the evaluation of splicing-modulation in the physiological dystrophin gene using the peqGOLD Total RNA Kit (VWR International GmbH, Darmstadt, Germany) according to manufacturer's protocol. 400 ng of the RNA was used to generate cDNA using the total RNA Kit qScript™ cDNA SuperMix (Quanta Biosciences, Gaithersburg, MD, USA) according to manufacturer's protocol. To amplify the region of the exon 23 skipping, 1-5 µL of the cDNA solution were used to perform a PCR using *Taq*^{R} polymerase (New England Biolabs, Ipswich, Massachussets, USA) and the primers amplifying dystrophin-Ex20-26. Following PCR primers and conditions were used: DMD_Ex20-26 fwd (5'-CAGAATTCTGCCAATTGCTGAG-3') [160]; DMD_Ex24/25 rev (5'-TCACCAACTAAAAGTCTGCATTG-3') [171]; initial denaturation (94 °C, 30 sec), 30 cycles (94 °C, 30 sec / 55 °C, 1 min / 68 °C, 1 min), final extension (68 °C, 5 min). The PCR products were purified using the PCR purification kit (Qiagen, Germany). 50 ng of the purified PCR product was used to perform a second PCR with One *Taq*^{R} DNA polymerase and the primers DMD_Ex20/21 fwd (5'-AAAATTTGTAAGGATGAAGTCAAC-3'), DMD_Ex20-24 rev (5'-CAGCCATCCATTTCTGTAAGG-3'). Following PCR conditions were used: initial denaturation (94 °C, 30 sec), 30 cycles (94 °C, 30 sec / 57 °C, 1 min / 68 °C, 1 min), final extension (68 °C, 5 min).

After performing agarose gel electrophoresis (2 % agarose gel; 100 V; 2 h), the PCR products were subjected to band intensity analysis using ImageJ software. The additional bands observed were quantified and compared to the 586 bp full-length dystrophin exon 20-24 sequence. To confirm the exon 23 skipping event in Cas9 mRNA/sgDMD$_{Ex23}$ treated mice, bands of animal #1 treated with LNP 1621 were purified by gel extraction using QIAquick® Gel Extraction Kit (Qiagen, Hilden, Germany). Sanger sequencing of the purified sequences was performed by Eurofins GATC Biotech (Konstanz, Germany) with primers DMD_Ex20/21 fwd and DMD_Ex20-24 rev [162] at a concentration of 20 ng µL^{-1}.

Analysis after single injections and analysis of systemic administration of LNP SM-102 was performed by Anna-Lina Lessl and Eric Weidinger, respectively, as part of their PhD study at Pharmaceutical Biotechnology, LMU, Munich.

3.23. Genome Editing by Cas9/sgRNA *In Vivo* at Genomic Level

Genomic DNA was isolated for the evaluation of gene editing in the physiological dystrophin gene, using the QIAMP DNA Mini Kit (Qiagen, Hilden, Germany) according to manufacturer's protocol. To amplify the region surrounding the targeted sequence downstream of the exon 23, 100 ng of the DNA solution was used to perform a PCR using *Taq*^{R} polymerase (New England Biolabs, Ipswich, Massachussets, USA). Following PCR primers and conditions were used: DMD genomic fwd (5'-AAACTTCTGTGATGTGAGGACA-3'); DMD genomic rev (5'-ACAAATGGCCAACTATGAGAAAC-3'); initial denaturation (94 °C, 30 sec), 30 cycles (94 °C, 30 sec / 58 °C, 1 min / 68 °C, 1 min), final extension (68 °C, 5 min). The PCR products were purified using the PCR purification kit (Qiagen, Germany). Sanger sequencing of the purified sequences was performed by Eurofins GATC Biotech (Konstanz, Germany) with primers DMD genomic sequencing fwd (5'-GAAACTCATCAAATATGCGTGTTAGTG-3') and DMD genomic sequencing rev (5'-GGCAAGTTGCAATCCTTTGA-3') at a concentration of 20 ng μL^{-1}. Sanger sequencing data was evaluated by the TIDE web tool (https://tide.nki.nl/) applying an indel size range of 25 and default settings for decomposition and alignment windows [169, 170]. R^2 values above 0.9 assured the reliability of the model for the analysis of the *in vivo* experiments.

DNA isolation was performed by Miriam Höhn (Pharmaceutical Biotechnology, LMU, Munich). Analysis after single injections was performed by Anna-Lina Lessl as part of her PhD study at Pharmaceutical Biotechnology, LMU, Munich.

3.24. In Vivo Performance of Luc mRNA Polyplexes and LNPs in BALB/c Mice

The experiments were performed after subcutaneous treatment with Carprofen at a dose of 5 mg kg^{-1}. Nanocarrier formulations with indicated luciferase mRNA concentrations were prepared as described above and 50 µL of each formulation injected into the left musculus biceps femoris. Mice were euthanized 6 h after injection. The organs (lungs, liver, kidneys, spleen, brain, heart, injected muscle, and complementary none-injected muscle) were dissected and washed carefully with PBS, followed by analysis via ex vivo luciferase gene expression assay. The luciferase expression was determined as described in section 3.25 and presented as relative light units per gram organ after background subtraction (lysis buffer). Experiments were performed by Jana Pöhmerer and Ulrich Wilk as part of their veterinary MD studies at Pharmaceutical Biotechnology, LMU.

3.25. *Ex Vivo* Luciferase Expression Assay of Organs

Organ tissues was homogenized in Luciferase Cell Culture Lysis Reagent1×, supplemented with 1% (v/v) protease and phosphatase inhibitor cocktail using a tissue and cell homogenizer (FastPrep-24, MP Biomedicals,USA). Then, the samples were frozen overnight at −80 °C to ensure full lysis. In the next step, the samples were thawed and centrifuged for 10 min at maximum speed (≈13 000 rpm) and 4°C. Luciferase activity in 25 µL supernatant was measured in a Centro LB 960 plate reader luminometer (Berthold Technologies, Bad Wildbad, Germany) for 10 s after addition of 100 µL/well of a LAR buffer solution (20 mM glycylglycine; 1 mM MgCl2; 0.1 mM ethylenediaminetetraacetic acid; 3.3 mM dithiothreitol; 0.55 mM adenosine 5′-triphosphate; 0.27 mM coenzyme A, pH 8-8.5) supplemented with 5% (v/v) of a mixture of 10 mm luciferin and 29 mm glycylglycine. The assay was performed by Jana Pöhmerer and Ulrich Wilk as part of their veterinary MD studies at Pharmaceutical Biotechnology, LMU.

3.26. Statistical Analysis

Data were presented as arithmetic mean ± standard deviation (SD) out of at least triplicates, if not otherwise stated. Unpaired Student's two-tailed t-test with Welch's correction was performed using GraphPad Prism^{TM} 10 to analyze statistical significances. Significance levels were indicated with symbols: ns $p > 0.05$; *$p \leq 0.05$; **$p \leq 0.01$; ***$p \leq 0.001$; ****$p \leq .0001$.

4. Results and Discussion

This chapter has been adapted from:

Germer J, Lessl AL, Pöhmerer J, Grau M, Weidinger E, Höhn M, Yazdi M, Cappelluti MA, Lombardo A, Lächelt U, Wagner E. Lipo-Xenopeptide Polyplexes for CRISPR/Cas9 Based Gene Editing at Ultra-Low Dose. Journal of Controlled Release

4.1. LAF-Stp Carriers for Cas9 mRNA/sgRNA Delivery

Figure 6 displays the design of nucleic acid carriers applied in the current study. As described in [163], polar cationizable succinoyl tetraethylene pentamine (Stp) units were combined with a dynamic lipophilic domain featuring a central tertiary amine positioned between their hydrocarbon chains. Branching lysines were utilized to covalently connect the novel moieties to different positions of the polar Stp units (**Figure 6A**). These lipo amino fatty acid (LAF) units introduce a pH-dependent switch of polarity to the hydrophobic moieties. As a result of this combination, the dual pH-responsive carriers and the corresponding nucleic acid nanoparticles can behave like chameleons in their microenvironment[163]. Their water solubility and insolubility switches depending on their protonation and lipidic surrounding (**Figure 6B**). When the tertiary amines become protonated within the endosomal environment, aqueous solubility of carriers strongly increases (about 100-fold), reducing hydrophobic interactions and stability of the nanoparticles. All these factors, along with the increased ability of the amphiphilic carriers in protonated stage to disrupt membranes, is assumed to be beneficial for facilitating transmembrane transport and efficient cargo release at the intended intracellular site of action. A library of sequence defined carriers with different topologies was generated by standard Fmoc solid phase assisted peptide synthesis (SPPS). The arrangements of the LAF and Stp units resulted in U-shaped and bundle-shaped topologies with apolar LAF units on both, C- and N-terminus or only the N-terminal side of the Stp, respectively (**Figure 6C**). The LAF unit itself was synthesized by reductive amination of different amino fatty acids with fatty aldehydes of numerous lengths. By varying the chain length of both the amino fatty acid and the fatty aldehydes, the position of the tertiary amine within the LAF building block is shifted. Our previous studies revealed that the resulting different LAF types impact both the physicochemical properties and the activity of the corresponding nucleic acid nanoparticles [163, 172].

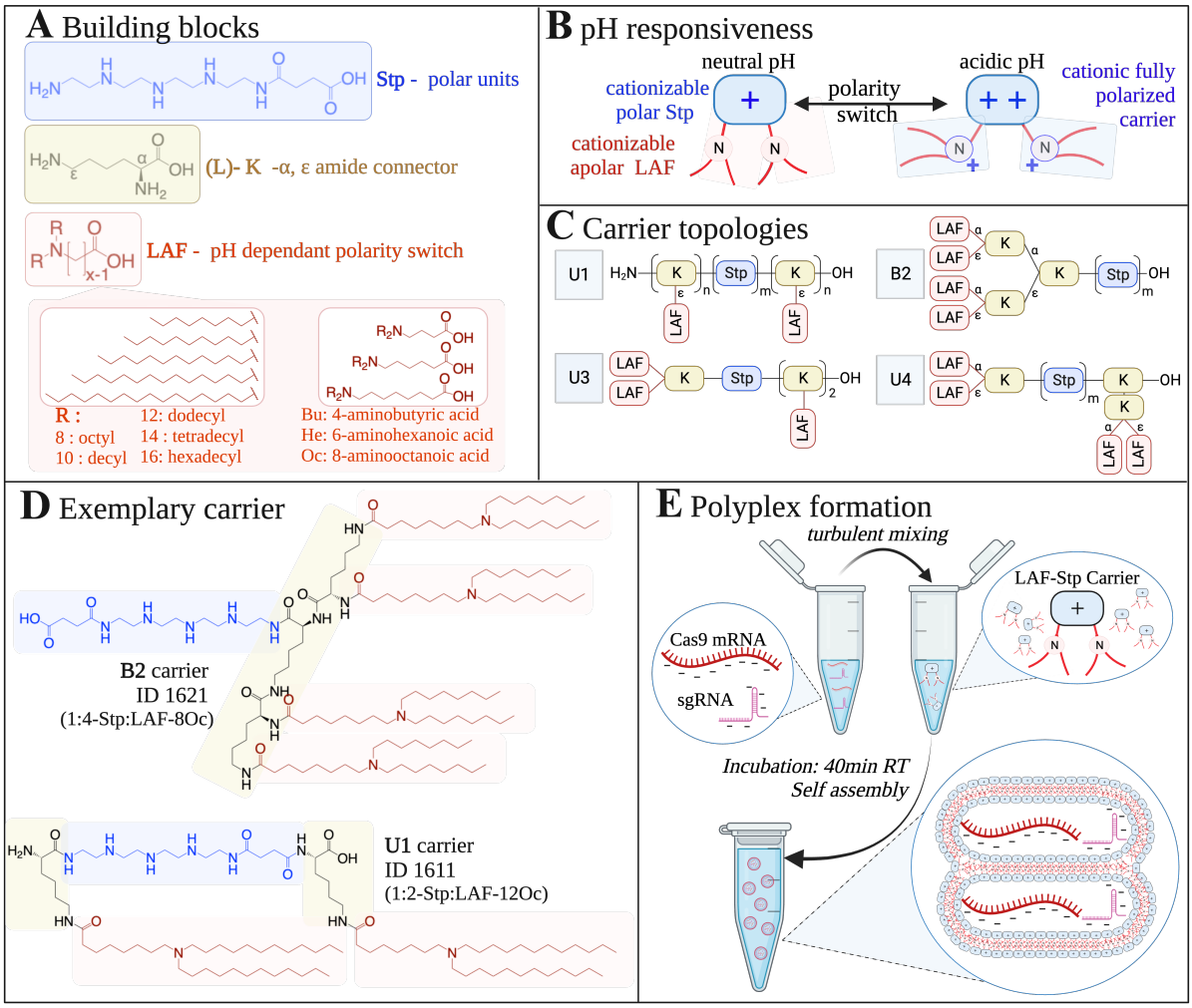

Figure 6. Lipo amino fatty acid (LAF) – succinoyl tetraethylene pentamine (Stp) carriers as cationizable carriers for polyplex formulation. (A) Building blocks used for the synthesis of LAF-Stp carriers for Cas9 mRNA/sgRNA delivery: Polar Stp (blue) units are connected via lysines (yellow) to different LAFs (red). **(B)** pH dependent polarity switch of apolar LAF unit at neutral pH to protonated polar unit at acidic pH **(C)** Chemical motif of four leading LAF-Stp carrier topologies **(D)** Exemplary chemical structures shown for B2 carrier ID# 1621 (8Oc) and U1 carrier ID# 1611 (12Oc). Stp, succinoyl tetraethylene pentaamine; (L)-K, lysine; LAF, lipo amino fatty acid. Nomenclature of LAFs: The number (8, 10, 12, 14, and 16) represents the number of C-atoms of the terminal alkyl chains, and the two letters express the ω-amino fatty acid ("Oc", 8-aminooctanoic acid; "He", 6-aminohexanoic acid; "Bu", 4-aminobutanoic acid). For bundles, m = 1, 2; for U-shapes, m = 1, 2 and n = 1, 2 (U1). Individual carriers were designated a 4-digit ID number. **(E)** Schematic illustration of polyplex preparation. LAF-Stp carrier and RNA, consisting of Cas9 mRNA and sgRNA (weight ratio, 1:1) are diluted in equal volumes HBG buffer. After combining of both solutions by turbulent mixing and incubation for 40 min at room temperature, polyplexes formed via self-assembly. Figure was created with BioRender.com.

In the LAF nomenclature provided in **Figure 6A**, the carbon chain lengths of the terminal alkyl chains are denoted by numerical values (8, 10, 12, 14, 16), and the amino fatty acids within the LAF building block are represented by two-letter abbreviations (Bu, He, Oc). Individual carriers were designated a 4-digit ID number. In total, 20 different LAF-Stp carriers were assessed in the study; **Table 10** provides an overview over the compound library. Exemplary chemical structures of lead carrier 1621 (B2-1:4-Stp:LAF-8Oc) and 1611 (U1-1:2-Stp:LAF-12Oc) are shown in **Figure 6D.**

Table 10 LAF-Stp carriers used in this research

ID	topology	sequence (N→C)	Stp:LAF ratio	LAF type	protonatable amines	Solvent
					with/without LAF	(v/v)
Bundles						**EtOH/HCl**
1613	B	K[K(12Oc)$_2$]$_2$-Stp	1:4	12Oc	7 / 3	9:1
1621	B	K[K(8Oc)$_2$]$_2$-Stp	1:4	8Oc	7 / 3	9:1
1730	B	K[K(8Oc)$_2$]$_2$-Stp$_2$	2:4	12Oc	10 / 6	9:1
1752	B	K[K(12Bu)$_2$]$_2$-Stp	1:4	12Bu	7 / 3	9:1
1753	B	K[K(16Bu)$_2$]$_2$-Stp	1:4	16Bu	7 / 3	9:1
1754	B	K[K(12He)$_2$]$_2$-Stp	1:4	12He	7 / 3	9:1
1755	B	K[K(14He)$_2$]$_2$-Stp	1:4	14He	7 / 3	9:1
1762	B	K[K(10Oc)$_2$]$_2$-Stp	1:4	10Oc	7 / 3	9:1
U-shapes						**EtOH/H$_2$O**
1611	U1	K(12Oc)-Stp-K(12Oc)	1:2	12Oc	6 / 4	1:1
1718	U1	[K(12Oc)]$_2$-Stp-[K(12Oc)]$_2$	1:4	12Oc	8 / 4	6:4
1719	U1	[K(12Oc)]$_2$-Stp$_2$-[K(12Oc)]$_2$	2:4	12Oc	11 / 6	8:2
1612	U3	K(12Oc)$_2$-Stp-K(12Oc)-K(12Oc)	1:4	12Oc	7 / 3	9:1
1722	U3	K(12Oc)$_2$-Stp$_2$-K(12Oc)-K(12Oc)	2:4	12Oc	10 / 6	7:3
1716	U4	K(12Oc)$_2$-Stp-K[K(12Oc)$_2$]	1:4	12Oc	7 / 3	9:1
1717	U4	K(12Oc)$_2$-Stp$_2$-K[K(12Oc)$_2$]	2:4	12Oc	10 / 6	7:3
1746	U1	K(8Oc)-Stp-K(8Oc)	1:2	12Oc	6 / 4	1:1
1763	U1	K(12Bu)-Stp-K(12Bu)	1:2	12Oc	6 / 4	1:1
1765	U1	K(12He)-Stp-K(12He)	1:2	12Oc	6 / 4	1:1
1766	U1	K(14He)-Stp-K(14He)	1:2	12Oc	6 / 4	1:1
1764	U1	K(16Bu)-Stp-K(16Bu)	1:2	12Oc	6 / 4	1:1

The N/P ratio represents either the molar ratio of all protonatable nitrogens (LAF +Stp + any terminal amine) of the carrier to phosphates of the mRNA, or as an alternative N/P calculation without considering the lipophilic tertiary LAF amines. Stock solutions were prepared depending on the solubility of the single LAF carriers. U shaped carriers were prepared in an EtOH/H2O at indicated ratios. B2-shaped carrier were prepared in an EtOH/HCl (0.6M) 9:1 v/v. LAF; lipoamino fatty acid; N, protonatable nitrogen; Stp, succinoyl tetraethylene pentamine.

Formulation of Cas9 mRNA and sgRNA with LAF-Stp carrier into Cas9 polyplexes (**Figure 6E**) was carried out by turbulent mixing of equal volumes of nucleic acid (Cas9 mRNA and sgRNA at fixed weight ratio 1:1) and LAF carrier solutions in HBG buffer (20 mM HEPES, 5 % glucose; pH 7.4).

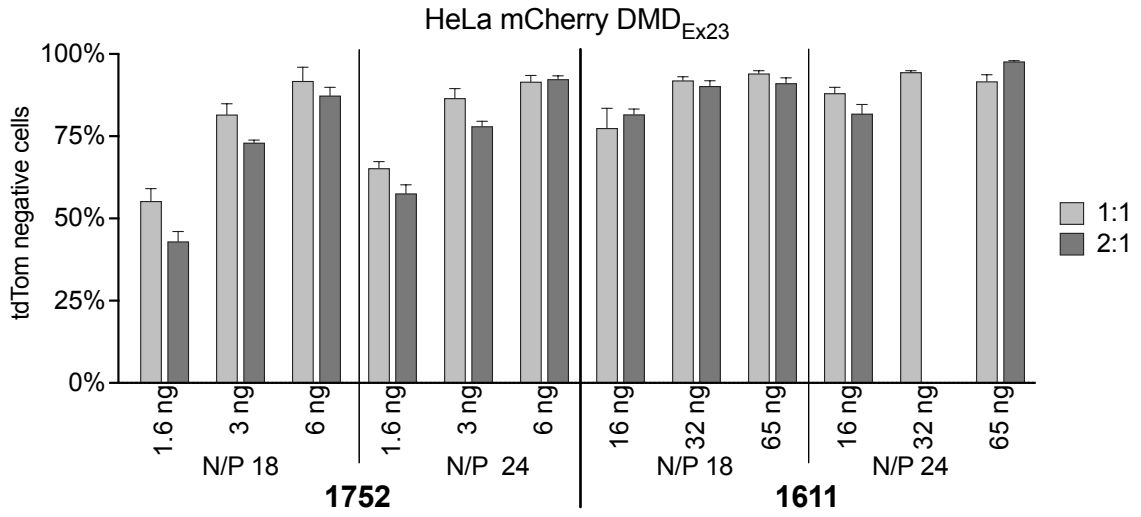

Figure 7. Weight ratio comparison of Cas9 mRNA and sgRNA in polyplexes formed with LAF-Stp carriers at N/P 18 and 24 *In vitro* gene editing efficiency by Cas9 polyplexes containing Cas9 mRNA and sgDMD$_{Ex23}$ at weight ratio 1:1 and 2:1, formed with LAF-Stp carriers 1752 (B2) and 1611 (U1) at N/P 18 and 24. HeLa mCherry-DMD$_{Ex23}$ cells were treated with Cas9 polyplexes containing indicated doses of total RNA in 96-well plates. Total RNA consisted of Cas9 mRNA and sgDMD$_{Ex23}$ at weight ratio 1:1 and 2:1 as indicated. Gene editing efficiency was determined by the percentage of mCherry positive cells, 3 days post treatment (n=3, mean ± SD). For more detailed description of the reporter model see Figure 20.

The choice of a 1:1 weight ratio for Cas9 mRNA / sgRNA which presents a high molar excess of sgRNA was based on preliminary testing (**Figure 7**) and literature precedents [130, 173], with the rational that the sgRNA needs to persist in the cytoplasm until Cas9 protein is translated and the RNP is assembled. After 40 min incubation at room temperature (RT) self-assembly of polyplexes occurred by electrostatic and hydrophobic interactions of nucleic acids and LAF carrier. The N/P ratio calculation corresponds to the molar ratio of amines to the negatively charged phosphates of the nucleic acid cargo (sum of phosphates of Cas9 mRNA and sgRNA). All protonable secondary, tertiary, and terminal amines of the LAF-Stp carrier structure (**Table 1**) were considered for the N/P calculation, irrespective of their actual far lower protonation.

In the following we evaluated the formulated Cas9 polyplexes in terms of their size, polydispersity, surface charge, and nucleic acid compaction/encapsulation (**Figure 8A,B**). According to previous findings for Luc mRNA polyplexes [163] we herein focused on four promising LAF carrier topologies, namely U1; U3; U4 with LAF-12Oc and B2 with LAF-8Oc at different Stp/LAF ratios. The physicochemical characterization of Cas9 polyplexes with N/P ratios 12, 18 and 24 was evaluated via DLS and ELS (**Figure 8A,B**; **Table S1**). Topology independent, all LAF-Stp carriers with two Stp resulted in smaller particles (≈75–125 nm) with higher zeta potential (+ 5–35 mV) than their analogs with only one Stp (exception for B2–2:4; 1730 at N/P 18 (–5.4 mV)).

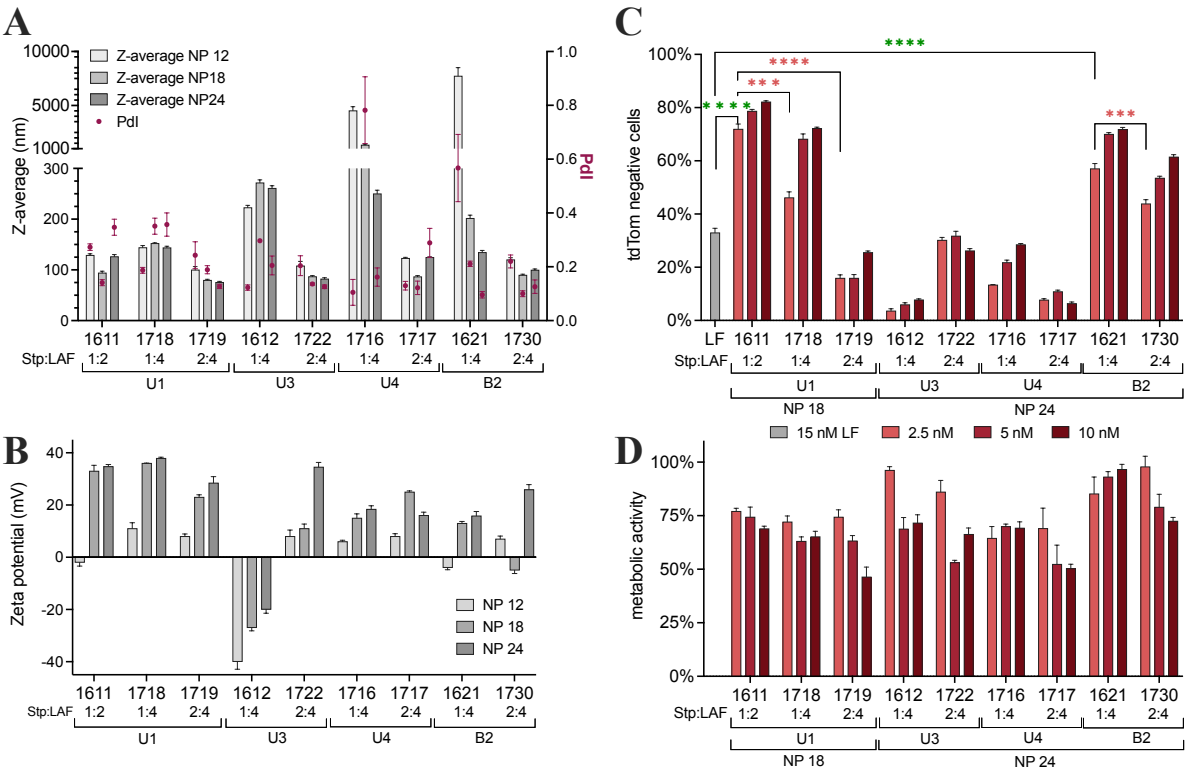

Figure 8. Physicochemical and biological evaluation of LAF-Stp polyplexes for Cas9 mRNA/sgRNA co-delivery. (A) DLS and **(B)** ELS measurements of Cas9 polyplexes containing Cas9 mRNA and sgPcsk9 at weight ratio 1:1, formed with LAF-Stp carriers (specified by carrier ID number) at indicated N/P ratios and a total RNA concentration of 12.5 µg mL^{-1} (n=3, mean ± SD). **(C)** *In vitro Pcsk9* gene knockout efficiency by Cas9 polyplexes formed with LAF-Stp carriers at optimal N/P ratios. Hepa 1-6 *Pcsk9^{tdTomato}* cells were treated with Cas9 polyplexes at concentrations of 2.5 nM sgPcsk9, 5 nM sgPcsk9 and 10 nM sgPcsk9. Lipofectamine^{TM} Messenger MAX^{TM} lipoplexes (LF) were formed with Cas9 mRNA and sgPcsk9 according to manufacturer's protocol and transfected resulting in a concentration of 15 nM sgPcsk9 in 96-well plates. Gene knockout efficiency was determined by the percentage of tdTomato negative cells 5 days post treatment (n=3, mean ± SD). **(D)** Metabolic activity of transfected Hepa 1-6 *Pcsk9^{tdTomato}* cells in relation to HBG buffer treated control cells determined via MTT assay at 24 h after transfection (n=3, mean ± SD). Statistical significance levels: ns-not significant $p > 0.05$; *$p \leq 0.05$; **$p \leq 0.01$; ***$p \leq 0.001$; ****$p \leq 0.0001$.

In general, all LAF carrier of the 1 Stp series required higher N/P ratios than those with 2 Stp units for stable polyplex formation. Probably the flexibility of two Stp units led to better electrostatic interactions between cargo and carrier and thereby providing more stability than LAF carriers with a lower Stp/LAF ratio. For the most part, a Stp/LAF ratio of 1:4 was more challenging for nanoparticle formation which might be caused by the steric bulkiness of the LAF building blocks. In U1 carriers, in contrast to the other topologies, where LAF units are linked to the alpha and epsilon amines of lysines, there is maximally one LAF linked per lysine. This seems to result in a better distribution of the sterically demanding LAF within the carrier. Hence, the carrier 1718 (U1–1:4) is the only tested carrier with a Stp/LAF ratio 1:4 able to form small and positively charged Cas9 polyplexes (144–152 nm; + 11–38 mV) at any tested N/P ratios. In the case of 8Oc bundle, B2–1:4 (1621), only Cas9 polyplexes with at N/P ratio ≥ 18 were able to form positively charged particles of acceptable size and PdI whereas, B2-2:4 carrier (1730), obtained stable particles at all tested N/P ratios. Relatively balanced Stp/LAF ratio (i.e., 1:2 or 2:4) and the additional Stp unit might be beneficial here as well. Similar tendencies were

observed for U3 and U4–shaped structures. These findings were supported by an agarose gel shift assay showing complete binding of both Cas9 mRNA and sgRNA by all carriers but the negatively charged polyplexes formed with 1612 (**Figure 9**).

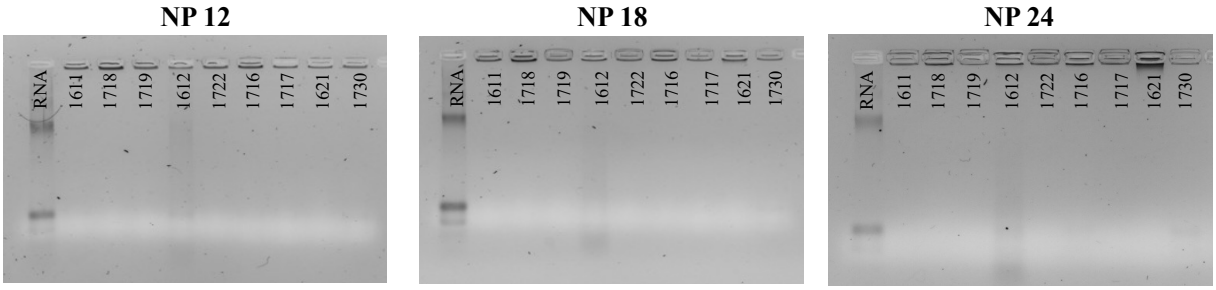

Figure 9. Gel shift assay of Cas9 polyplexes formed with LAF-Stp carriers at different N/P ratios (A) Gel shift assay of Cas9 polyplexes formed with different LAF carriers at indicated N/P ratios in comparison to free RNA.

Overall, the U1 topology seemed to be most promising in terms of polyplex formation. At any tested N/P ratio, U1 carriers resulted in small Cas9 polyplexes showing no positive effect for increasing the N/P ratio from 18 to 24. For most other LAF-Stp carriers, however, a N/P ratio of 18 resulted in increased polydispersity and a tendency to aggregation indicating to be close to the critical minimal carrier concentration needed for stable particle formation. Rising the N/P ratio to 24, however, led to a more homogenous particle formation.

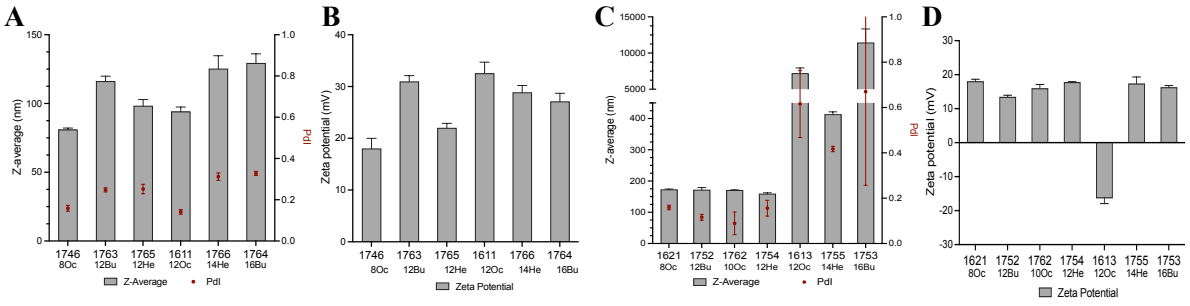

Figure 10. The effect of nitrogen catwalk on physicochemical properties of Cas9 polyplexes. U1 polyplexes with different LAF were formed at N/P 18 and B2 polyplexes with different LAF were formed at N/P 24. **(A)** DLS and **(B)** ELS measurements of Cas9 polyplexes formed with U1 LAF carriers at N/P ratio 18 and a total RNA concentration of 12.5 µg mL^{-1} (n=3, mean ± SD). **(C)** DLS and **(D)** ELS of Cas9 polyplexes formed with B2 LAF carriers at N/P ratio 24 and a total RNA concentration of 12.5 µg mL^{-1} (n=3, mean ± SD).

Furthermore, analogues of 1611 (U1-1:2) and 1621 (B2-1:4) with different LAF were evaluated (**Table S1;Figure 10**). For U1-shaped structures only a LAF with longer terminal alkyl chains (tetradecyl, hexadecyl) showed a slight increase in particle size. Nevertheless, all LAF were able to form positively charged Cas9 polyplexes with a size below 150 nm. B2-shaped carrier with longer LAF (12Oc, 14He; 16Bu) resulted in increased polydispersity and aggregation, despite the high N/P ratio 24. Shorter LAF on the other hand formed monodisperse particles with acceptable size.

The ability of LAF-Stp carriers to co-deliver Cas9 mRNA and sgRNA and induce specific *Pcsk9* gene knock out was evaluated in a Hepa 1-6 cell line, namely Hepa 1-6 *Pcsk9*^{tdTomato},stably expressing tdTomato in the 3'UTR of the *Pcsk9* gene (**Figure 8C,D**). The sgPcsk9 binds and directs the Cas9 protein to the first exon of the *Pcsk9* gene thus the expression of the tdTomato reporter protein is inactivated by the Cas9 induced destruction of the *Pcsk9* open reading frame. The gene knock out of the *Pcsk9* gene was quantified by flow cytometry. The gene knock out of the *Pcsk9* gene was quantified by flow cytometry and was also exemplarily confirmed by genomic sequence analysis using the TIDE analysis tool **(Figure 11**)[169, 170].

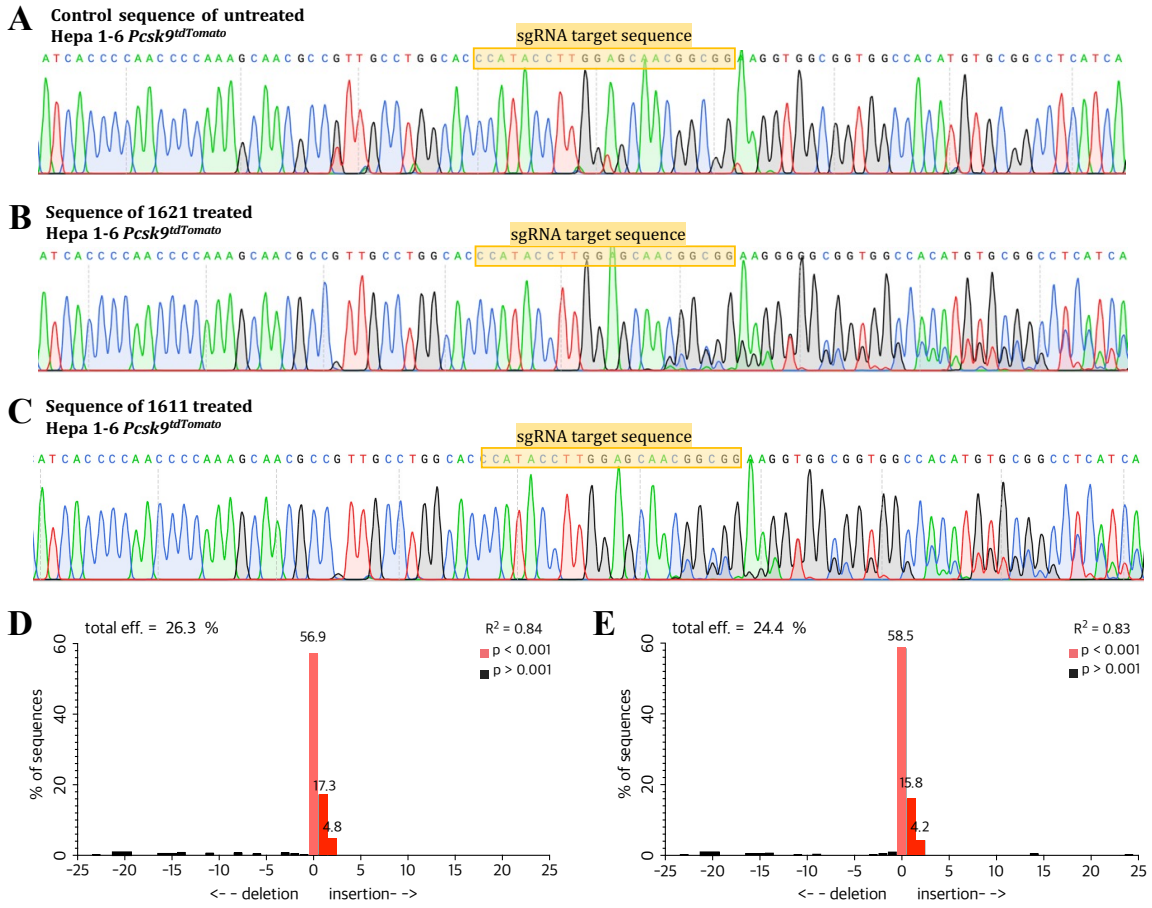

Figure 11. **Exemplary Sanger sequencing and TIDE Analysis of genomic DNA after treatment with Cas9mRNA/sgPcsk9 polyplexes formed with 1621 at N/P 24.** Total genomic DNA was extracted from untreated and treated Hepa 1-6 *Pcsk9*^{tdTomato} cells conducted to amplify the genomic region surrounding the targeted cut site in the first exon of the *Pcsk9* gene. PCR products were purified, Sanger-sequenced and evaluated by TIDE (Tracking of Indels by Decomposition) analysis. **(A)** sequence showing the section around the sgPcsk9 targeted genomic region of an untreated animal. **(B)** exemplary sequence showing the section around the sgPcsk9 targeted genomic region of Hepa 1-6 *Pcsk9*^{tdTomato} cells treated with 5 nM sgPcsk9 containing 1621 polyplexes (N/P 24). Histogram shows aberrant small peaks around and downstream the cut site. **(C)** exemplary sequence showing the section around the sgPcsk9 targeted genomic region of Hepa 1-6 *Pcsk9*^{tdTomato} cells treated with 2.5 nM sgPcsk9 containing 1611 polyplexes (N/P 18). Histogram shows aberrant small peaks around and downstream the cut site. **(D)** TIDE Analysis result of indel spectrum for the sequence shown in (B). **(E)** TIDE Analysis result of indel spectrum for the sequence shown in (C).

The metabolic activity of cells upon transfection was determined via MTT assay to assess the tolerability of the carriers. Cas9 polyplexes formed with LAF carriers at N/P ratio 12, 18, and 24 were transfected at 2.5 nM-10 nM sgPcsk9 (≈ 16 ng-66 ng total RNA, weight ratio 1:1 for Cas9 mRNA and sgPcsk9) in Hepa 1-6 *Pcsk9*^{tdTomato} and compared to gold standard lipofection of 100 ng total RNA (≈ 15 nM sgPcsk9) with Lipofectamine™ Messenger MAX™ (**Figure 8D, Figure 12B**). Overall U1 and B2 shaped carrier outperformed the other U shape topologies. At 6-fold lower dose, U1 and B2 Carriers with only one Stp showed significantly higher knock out than the Lipofectamine control. In contrast to their superiority for nucleic acid compaction and particle formation, carriers with a Stp/LAF ratio of 2:4 showed significantly reduced efficiency compared to their analogs containing only one Stp. This indicates that the right balance in between nucleic acid compaction and cargo release at its site of action is crucial for the transfection efficiency of Cas9 polyplexes. It is interesting to note that at lower N/P ratios, knock-out events showed a strong correlation with the transfected dose, whereas editing events after transfection with nanoparticles at N/P 24 were nearly dose independent (**Figure 12**).

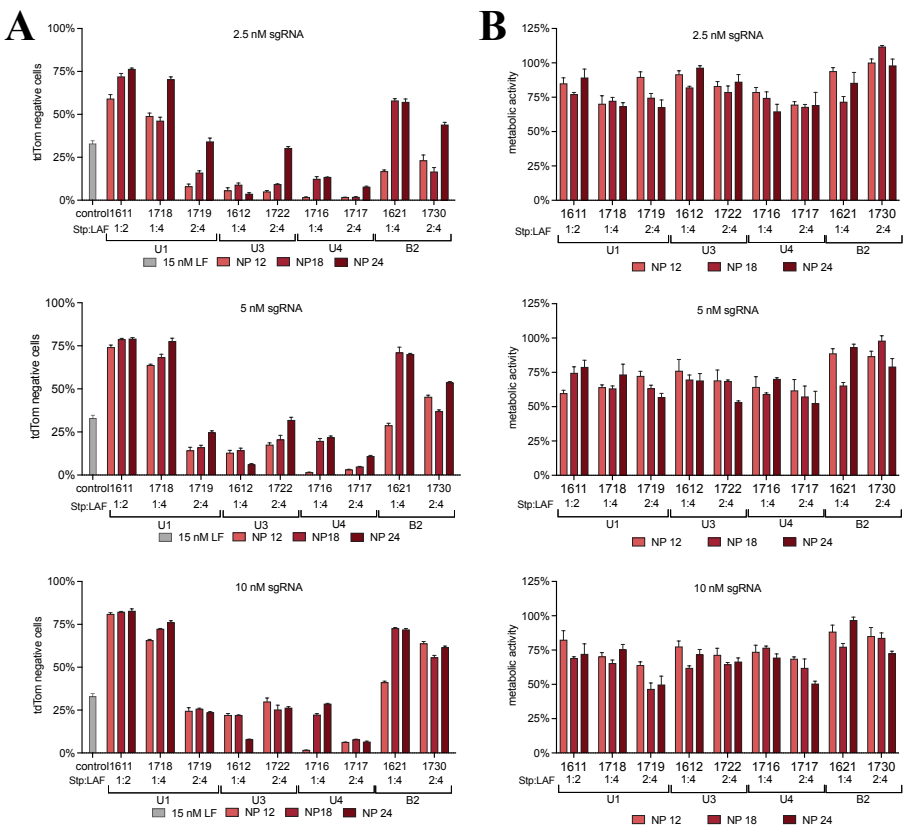

Figure 12. Evaluation of Cas9 polyplexes formed with LAF-Stp carriers at different N/P ratios (A) In vitro *Pcsk9* gene knockout efficiency by Cas9 polyplexes containing Cas9 mRNA and sgPcsk9 at weight ratio 1:1, formed with LAF carriers at optimal N/P ratios. Hepa 1-6 *Pcsk9*^{tdTomato} cells were treated with Cas9 polyplexes at concentrations of 2.5 nM sgPcsk9, 5 nM sgPcsk9 and 10 nM sgPcsk9 in graphs from top to bottom, respectively. LipofectamineTM Messenger MAXTM Lipoplexes (LF) were formed with Cas9 mRNA and sgPcsk9 according to manufacturer's protocol and transfected resulting in a concentration of 15 nM sgPcsk9 in 96-well plates. Gene knockout efficiency was determined by the percentage of tdTomato negative cells 5 days post treatment. **(C)** Metabolic activity of transfected Hepa 1-6 *Pcsk9*^{tdTomato} cells in relation to HBG buffer treated control cells determined via MTT assay at 24 h after transfection. (n=3, mean ± SD)

This demonstrates that the transfection efficiency is mainly dependent on the amount of carrier reaching each cell, rather than the cargo concentration. We assume that, upon acidification in the endosomes, a critical minimal amount of LAF units is needed to enable endosomal escape and release of the nucleic acid cargo. The pronounced effect for carriers with an Stp/LAF ratio of 2:4 supports this hypothesis. The transfection efficiency of LAF-Stp containing Cas9 polyplexes was also confirmed by GFP knock out on CT26 eGFP-Luc and HeLa GFPd2 cells (**Figure 13**), however, variations in efficacy were observed. The different transfection efficiencies across divers cell types have been frequently observed in our own and other studies for various nucleic acid cargos, based on differing cell entry routes, intracellular trafficking, and endosomal escape [174, 175].

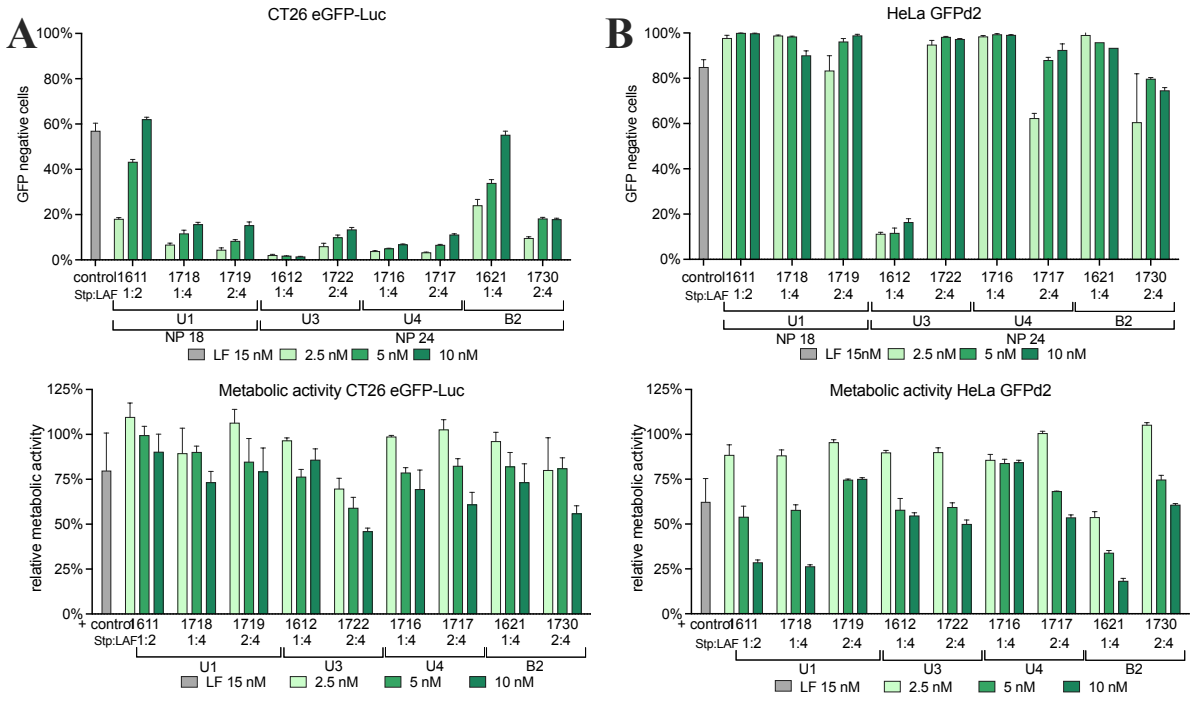

Figure 13. In vitro eGFP knockout efficiency and metabolic activity of different reporter cell lines after treatment with Cas9 polyplexes containing Cas9 mRNA and sgGFP at weight ratio 1:1, formed with LAF-Stp carriers at optimal N/P ratios. Lipofectamine™ Messenger MAX™ lipoplexes (LF) were formed with Cas9 mRNA and sgGFP according to manufacturer's protocol and transfected resulting in a concentration of 15 nM sgGFP in 96-well plates. Gene knockout efficiency was determined by the percentage of GFP cells normalized to HBG treated cells, 5 days post treatment. (n=3, mean ± SD) **(A)** top: CT26 eGFP-Luc cells were treated with Cas9 polyplexes at concentrations of 2.5 nM sgGFP, 5 nM sgGFP and 10 nM sgGFP. bottom: Metabolic activity of transfected CT26 eGFP-Luc cells in relation to HBG buffer treated control cells determined via MTT assay at 24 h after transfection **(B)** top: HeLa GFPd2 cells were treated with Cas9 polyplexes at concentrations of 2.5 nM sgGFP, 5 nM sgGFP and 10 nM sgGFP. bottom: Metabolic activity of transfected HeLa GFPd2 cells in relation to HBG buffer treated control cells determined via MTT assay at 24 h after transfection.

Furthermore, effects of LAF side chain variations (Nitrogen Catwalk) in the best performing topologies (U1–1:2; B2–1:4) on gene editing efficiencies in different cell types were assessed (**Figure 14, Figure 15**). Gene editing efficiency upon transfection of Cas9 polyplexes was assessed at further reduced dose (0.5 nM-5 nM sgRNA) and compared to gold standard transfections with 100 ng total RNA (≈ 15 nM sgRNA) Lipofectamine™ Messenger MAX™ ,

or 250 ng total RNA (≈ 38 nM sgRNA) as polyplexes formed with succinylated PEI (succPEI) at weight ratio 4:1, succPEI: total RNA [79]. Longer terminal carbon chains (tetradecyl; hexadecyl) which have already demonstrated negative effects on particle properties, showed almost no gene editing events on any tested cell line. Among the various LAF chain lengths, the initially tested LAF-Stp 1611 (12Oc) demonstrated the highest gene editing events compared to its analogs (**Figure 14**). Gene editing events were scarce in all cell lines following the transfection with 1746, an U1 analog with LAF 8Oc.

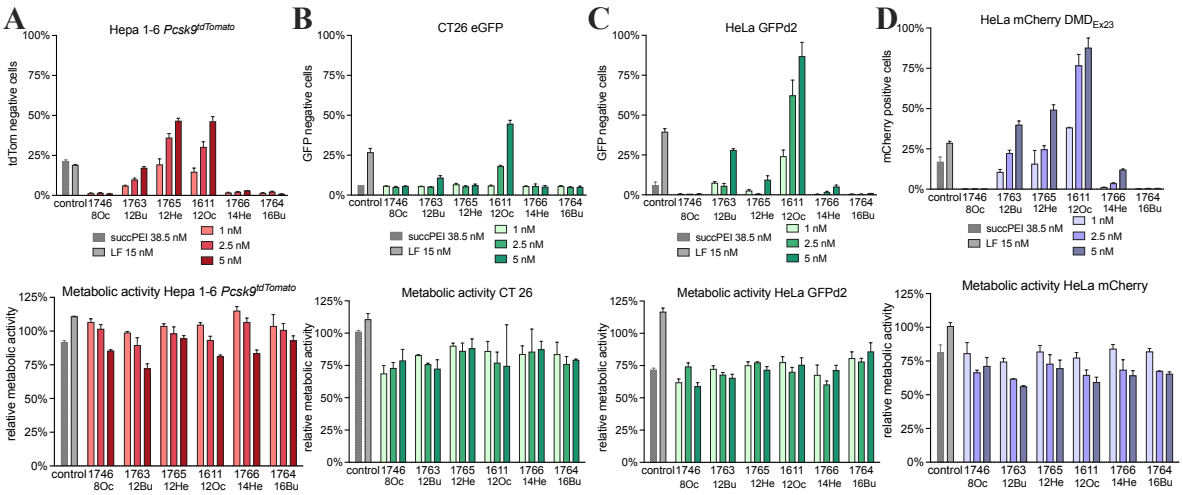

Figure 14. Nitrogen Catwalk of LAF-Stp carriers with U1 Topology. In vitro knockout efficiency and metabolic activity was tested on different reporter cell lines after treatment with Cas9 polyplexes containing Cas9 mRNA and sgRNA at weight ratio 1:1, formed with LAF-Stp carriers at N/P 18. All cell lines were treated with Cas9 polyplexes at concentrations of 1 nM sgRNA, 2.5 nM sgRNA and 5 nM sgRNA in 96-well plates. Positive controls are presented by Lipofectamine™ Messenger MAX™ lipoplexes (LF) formed with Cas9 mRNA and sgRNA according to manufacturer's protocol and transfected resulting in a concentration of 15 nM sgRNA and succPEI polyplexes at weight ratio 4:1, succPEI: total RNA (Cas9 mRNA:sgRNA; weight ratio 1:1) resulting in a concentration of 38.5 nM sgRNA (250 ng total RNA). Gene knockout efficiency was determined by the percentage of tdTomato negative for Hepa 1-6 *Pcsk9*^{tdTomato} or GFP negative cells for CT26 eGFP-Luc and Hela GFPd2 normalized to HBG treated cells, 5 days post treatment (n=3, mean ± SD). **(A)** top: Hepa$^{tdT:PCSK9}$ cells were treated with Cas9 polyplexes containing Cas9 mRNA and sgPcsk9 at weight ratio 1:1 in 96-well plates. bottom: Metabolic activity of transfected Hepa 1-6 *Pcsk9*^{tdTomato} cells in relation to HBG buffer treated control cells determined via MTT assay at 24 h after transfection **(B)** top: CT26 eGFP-Luc cells were treated with Cas9 polyplexes containing Cas9 mRNA and sgGFP at weight ratio 1:1 in 96-well plates. bottom: Metabolic activity of transfected CT26 eGFP-Luc cells in relation to HBG buffer treated control cells determined via MTT assay at 24 h after transfection **(C)** top: HeLa GFPd2 cells were treated with Cas9 polyplexes containing Cas9 mRNA and sgGFP at weight ratio 1:1 in 96-well plates. bottom: Metabolic activity of transfected HeLa GFPd2 cells in relation to HBG buffer treated control cells determined via MTT assay at 24 h after transfection. **(D)** top: HeLa mCherry-DMD$_{Ex23}$ cells were treated with Cas9 polyplexes containing Cas9 mRNA and sgDMD$_{Ex23}$ at weight ratio 1:1 in 96-well plates. Gene editing efficiency was determined by the percentage of mCherry positive cells, 3 days post treatment (n=3, mean ± SD). For more detailed description of the reporter model see Figure 3 of the main manuscript. bottom: Metabolic activity of transfected HeLa mCherry-DMD$_{Ex23}$ cells in relation to HBG buffer treated control cells determined via MTT assay at 24 h after transfection.

On the other hand, for B2 carriers, LAF 12Oc revealed counterproductive effects on both gene editing and polyplex formation, whereas the four shorter LAFs (8Oc, 12Bu, 10Oc, 12He), formed small Cas9 polyplexes demonstrating gene editing efficiency on all tested cell lines (**Figure 15**). Cell line dependent effects where more pronounced for B2 carriers. Transfection of Hepa and CT26 with B2 carriers containing 8Oc or 10Oc did not hamper the metabolic activity of the cells. Concentrations of only 2.5 nM sgRNA yielded equal to or higher knock out results than those of both positive control groups, despite the manifold higher concentration. In HeLa cells, all B2 carrier containing one of the four shorter LAF (8Oc, 12Bu, 10Oc, 12He)

exhibited a very high gene editing efficiency over 50 %. Even at lowest tested concentrations of 0.5 nM sgRNA, both positive control groups were outperformed. It is worth noting that structures exhibiting greater transfection effectiveness often display higher toxicity, compared with structures of lower efficiency. It is likely that the mechanisms responsible for effective delivery, such as destabilizing lipid membranes, initiate certain levels of cytotoxicity. Nonetheless, this toxicity can be managed by reducing the concentration.

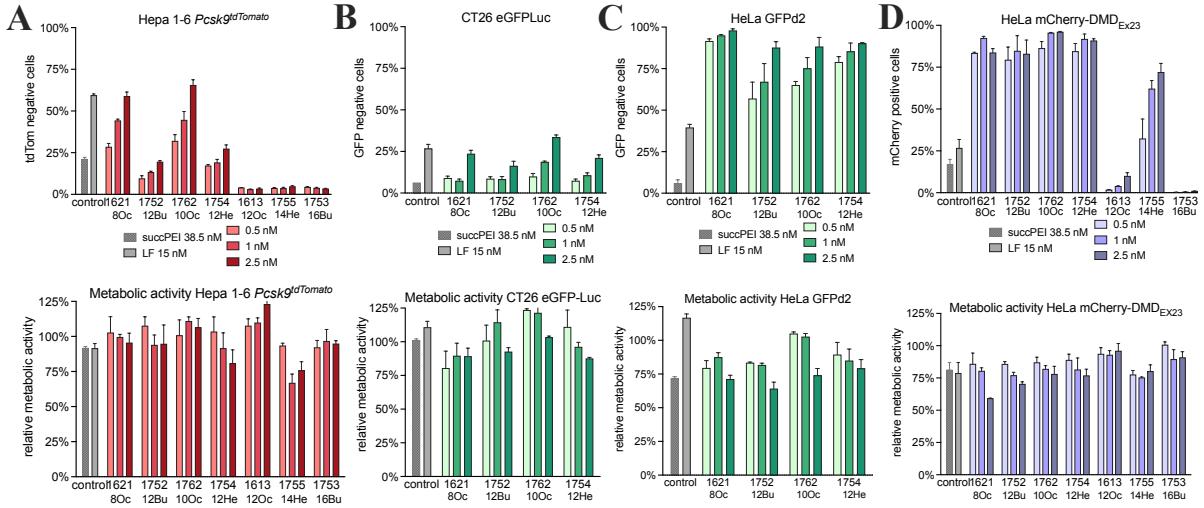

Figure 15. Nitrogen Catwalk of LAF-Stp carriers with B2 Topology. In vitro knockout efficiency and metabolic activity was tested on different reporter cell lines after treatment with Cas9 polyplexes containing Cas9 mRNA and sgRNA at weight ratio 1:1, formed with LAF-Stp carriers at N/P 24. All cell lines were treated with Cas9 polyplexes at concentrations of 0.5 nM sgRNA, 1 nM sgRNA and 2.5 nM sgRNA in 96-well plates. Positive controls are presented by Lipofectamine™ Messenger MAX™ lipoplexes (LF) formed with Cas9 mRNA and sgRNA according to manufacturer's protocol and transfected resulting in a concentration of 15 nM sgRNA and succPEI polyplexes at weight ratio 4:1, succPEI: total RNA (Cas9 mRNA:sgRNA; weight ratio 1:1) resulting in a concentration of 38.5 nM sgRNA (250 ng total RNA). Gene knockout efficiency was determined by the percentage of tdTomato negative for Hepa$^{tdT:PCSK9}$ or GFP negative cells for CT26 eGFP-Luc and Hela GFPd2 normalized to HBG treated cells, 5 days post treatment (n=3, mean ± SD). **(A)** top: Hepa 1-6 *Pcsk9*^{tdTomato} cells were treated with Cas9 polyplexes containing Cas9 mRNA and sgPcsk9 at weight ratio 1:1 in 96-well plates. bottom: Metabolic activity of transfected Hepa 1-6 *Pcsk9*^{tdTomato} cells in relation to HBG buffer treated control cells determined via MTT assay at 24 h after transfection (n=3, mean ± SD). **(B)** top: CT26 eGFP-Luc cells were treated with Cas9 polyplexes containing Cas9 mRNA and sgGFP at weight ratio 1:1 in 96-well plates. Only B2 LAF-Stp carriers forming stable particle <200 nm were transfected on these cells. bottom: Metabolic activity of transfected CT26 eGFP-Luc cells in relation to HBG buffer treated control cells determined via MTT assay at 24 h after transfection (n=3, mean ± SD). **(C)** top: HeLa GFPd2 cells were treated with Cas9 polyplexes containing Cas9 mRNA and sgGFP at weight ratio 1:1 in 96-well plates. Only B2 LAF-Stp carriers forming stable particle <200 nm were transfected on these cells. bottom: Metabolic activity of transfected HeLa GFPd2 cells in relation to HBG buffer treated control cells determined via MTT assay at 24 h after transfection (n=3, mean ± SD). **(D)** top: HeLa mCherry-DMD$_{Ex23}$ cells were treated with Cas9 polyplexes containing Cas9 mRNA and sgDMD$_{Ex23}$ at weight ratio 1:1 in 96-well plates. Gene editing efficiency was determined by the percentage of mCherry positive cells, 3 days post treatment (n=3, mean ± SD). For more detailed description of the reporter model see **Figure 20**. bottom: Metabolic activity of transfected HeLa mCherry-DMD$_{Ex23}$ cells in relation to HBG buffer treated control cells determined via MTT assay at 24 h after transfection (n=3, mean ± SD).

Overall, variations of the LAFs influenced polyplex formation and physicochemical properties (**Table S1,Figure 10**), transfection potency and toxicity (**Figure 14. Figure 15**) of corresponding Cas9 polyplexes. Consistent with Thalmayr et al. [163], 12Oc containing 1611 emerged as the most promising among U1-shaped carriers, while for bundles, a shorter LAF not only enhanced nanoparticle formation but also yielded superior results in gene editing. Carrier-1762, which contains the intermediate length LAF (10Oc), demonstrated an improved metabolic activity profile among those tested, without compromising the carrier's effectiveness.

4.2. LAF-Stp Carrier 1611 for HDR Mediated eGFP to BFP Conversion

Having demonstrated that LAF-Stp carriers form potent polyplexes for Cas9 mRNA and sgRNA delivery, enabling gene knockouts through non-homologous end joining (NHEJ), we aimed to broaden its utility by exploring the co-delivery of Cas9 components and a single-stranded DNA (ssDNA) template for facilitating gene knock-ins via homology-directed repair (HDR). Firstly, we evaluated whether LAF-Stp carriers could form stable polyplexes containing both RNA and DNA compounds. Therefore, a small selection of 1-Stp U1 and B2 carriers were tested as polyplexes with mCherry mRNA and GFP pDNA at weight ratio 1:1. The nanoparticles were transfected in different cell lines and mCherry and GFP expression was assessed by flow cytometry (**Figure 16 A-I**). For the physicochemical evaluation DLS and ELS measurement as well as an agarose gel shift assay were performed (**Figure 16J, K**). Although the binding of pDNA was incomplete, the carriers, which exhibited robust transfection capabilities for Cas9 mRNA/sgRNA, were also able to effectively co-deliver both mRNA and pDNA into cells yet demonstrating a stronger transfection profile for mRNA. The carrier 1611 was found to be highly effective in co-delivering mRNA and pDNA across all tested cell lines, leading to its selection for the gene knock-in studies through HDR. For this research, a HeLa cell line that expresses a less stable variant of green fluorescent protein (HeLa GFPd2) was utilized [86]. Through HDR-mediated DNA repair, the eGFP sequence, can potentially be transformed into blue fluorescent protein (BFP), and therefore, be evaluated by flow cytometry (**Figure 17A,B**). All 1611 polyplexes at N/P ratio 18, with Cas9 mRNA plus sgGFP (weight ratio 1:1), with and without a single-stranded DNA template (ssDNA) at three different ratios to the sgRNA, formed small homogeneous particles with positive zeta potential (**Table S5**). These polyplexes were transfected at different concentrations in HeLa GFPd2 cells. As expected, gene knock out efficiency after transfection with Cas9 polyplexes without additional ssDNA template was in line with previous results of transfections in this cell line (**Figure 14C**) and no BFP positive cells could be detected. Within the tested ratios of sgRNA to ssDNA, ranging from 1:05 to 1:2, we observed that the HDR efficiency increased with higher ratios of ssDNA template, resulting in up to 38 % BFP converted cells (**Figure 17C**). Interestingly, the overall gene editing efficiency defined by the sum of GFP knock out and BFP converted cells decreased at higher ssDNA ratios. The highest transfected concentrations reached 86 %, 82 %, 72 % and 58 % gene edited cells for sgRNA to ssDNA ratios from 1:0 to 1:2, respectively.

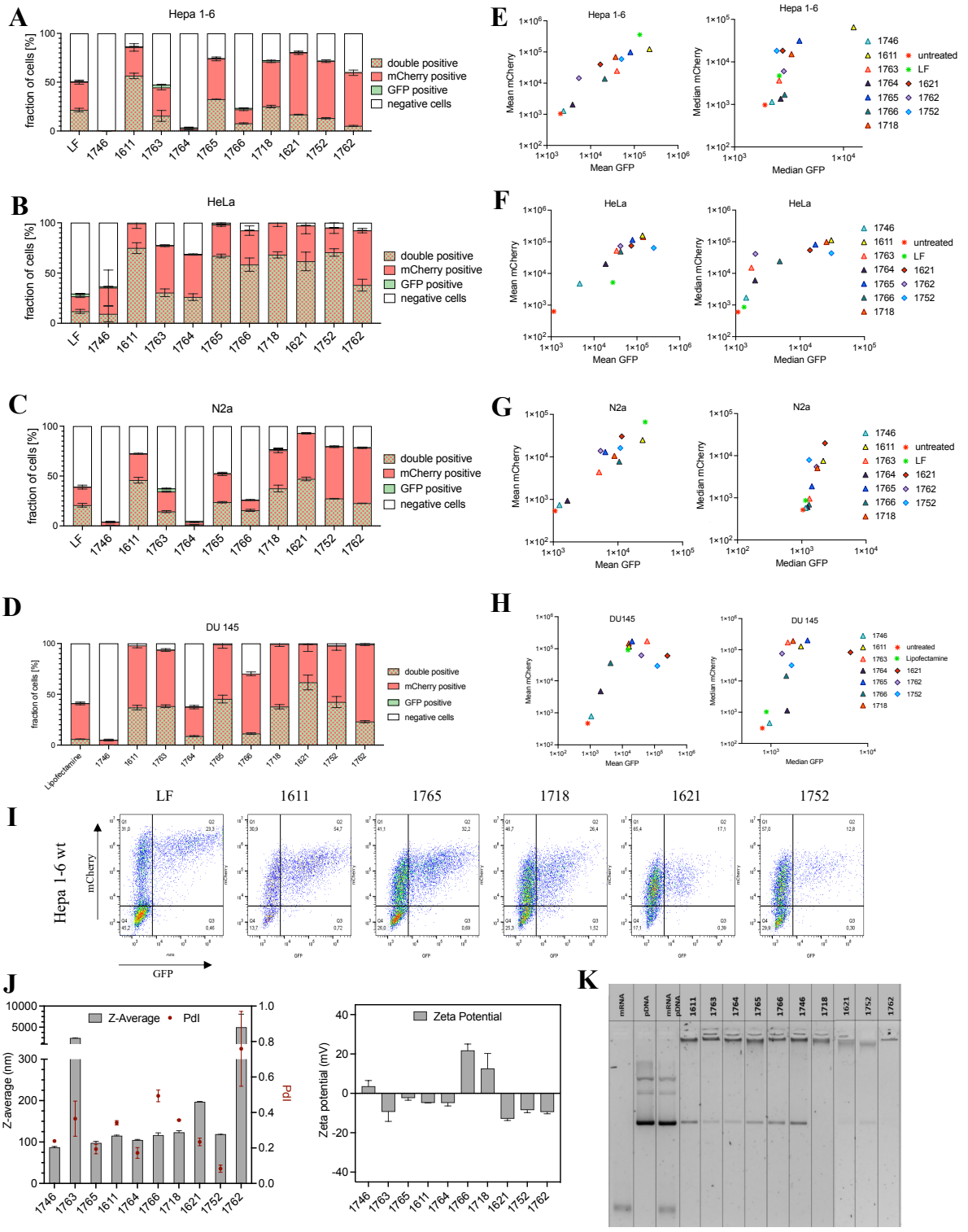

Figure 16. LAF-Stp polyplexes for the codelivery of mRNA and pDNA. U1 and B2 polyplexes with different LAF were formed at N/P 18. mCherry and GFP expression was evaluated 24 h post transfection of polyplexes containing 50 ng total nucleic acid (mCherry mRNA:GFP pDNA; weight: weight; 1:1). Percentage of cells showing mCherry, GFP or double positive shift in flow cytometric evaluation is shown for **(A)** Hepa 1-6 wildtype, **(B)** HeLa wildtype cells, **(C)** N2a wildtype cells and **(D)** DU 145 wildtype cells. **(E)** fluorescent protein expression on Hepa 1-6. Left: Mean mCherry and mean GFP intensity are plotted on the y- and x-axis, respectively. right: Median mCherry and median GFP intensity are plotted on the y- and x-axis, respectively. **(F)** fluorescent protein expression on HeLa. Left: Mean mCherry versus mean GFP intensity. right: Median mCherry versus median GFP intensity. **(G)** fluorescent protein expression on N2a. Left: Mean mCherry versus mean GFP intensity. right: Median mCherry versus median GFP intensity. **(H)** fluorescent protein expression on DU 145. Left: Mean mCherry versus mean GFP intensity. right: Median mCherry versus median GFP intensity. **(I)** exemplary flow cytometry plots and gating of Hepa 1-6 24 h after treatment. **(J)** DLS and ELS of mRNA/pDNA polyplexes formed with indicated LAF-Stp carriers. **(K)** Gel-shift assay of mRNA/pDNA polyplexes formed with LAF-Stp carriers at N/P 18.

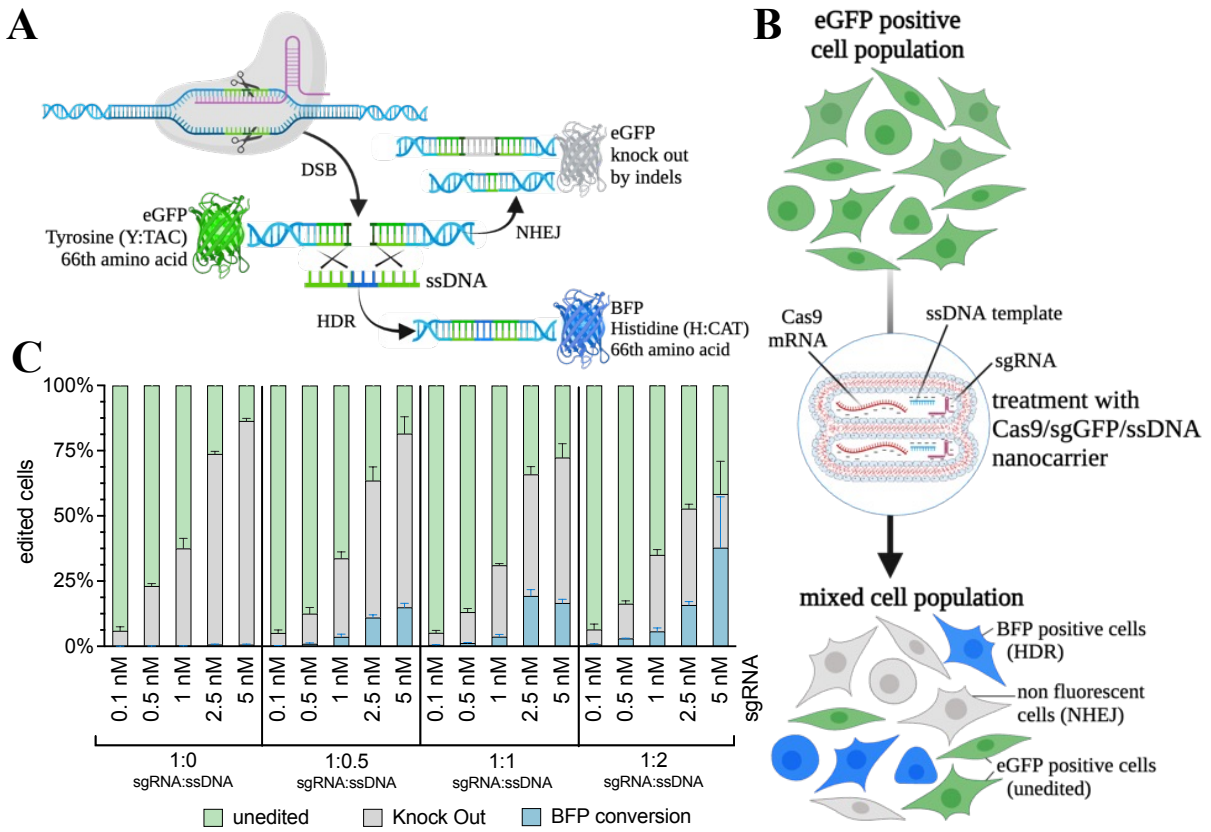

Figure 17. HDR mediated eGFP to BFP conversion. (A) Schematic illustration of cellular eGFP to BFP conversion after Cas9 induced double strand break (DSB) in the presence of a ssDNA template. Insertion or deletion of bases mediated by non-homologous end joining (NHEJ) pathways lead to eGFP knock out. HDR-mediated DNA repair leads to substitution of tyrosine (TAC), the 66th amino acid, in the eGFP sequence by histidine (CAT). Hereby, eGFP is converted into blue fluorescent protein (BFP). **(B)** schematic illustration of a population of HeLa GFPd2 cells treated with 1611 polyplexes formed at N/P ratio 18 with Cas9 mRNA and sgGFP and a single stranded DNA template (ssDNA). The efficiency of the carriers for gene knock out and HDR mediated conversion to BFP can be evaluated by flow cytometry. **(C)** Editing percentages were evaluated by flow cytometry 5 days after transfection with 1611 polyplexes formed at N/P ratio 18 with Cas9 mRNA and sgGFP (weight ratio 1:1) and a single stranded DNA template (ssDNA) at indicated molar ratios to the sgRNA. Concentrations are indicated in nanomolar sgRNA. (n=3, mean ± SD). Part A and B of this figure were created with BioRender.com

This suggests that while the RNP's ability to induce double-strand breaks (DSB) is hindered when there are elevated single-stranded DNA (ssDNA) concentrations, the chances of achieving homology-directed repair (HDR) integration are higher when the ssDNA template is in close proximity. To exclude that lower editing efficiencies are triggered by increased carrier concentrations, we tested different sgRNA to ssDNA ratios while keeping the total transfected nucleic acid amount constant (**Figure 18**). Once more, a decline in general editing effectiveness can be noted with increased template ratios. Instances where 3.9 nM sgRNA were applied with polyplexes lacking ssDNA triggered over 85 % GFP knock out, whereas utilizing polyplexes at sgRNA to ssDNA ratios of 1:2 and 1:6 with the same sgRNA concentration yielded total edited cell percentages of only 40 % and 21 %, respectively (**Figure 18**). The HDR percentage of total edited cells, however, increased with higher template ratios even though the overall efficiency was reduced (**Figure 19**).

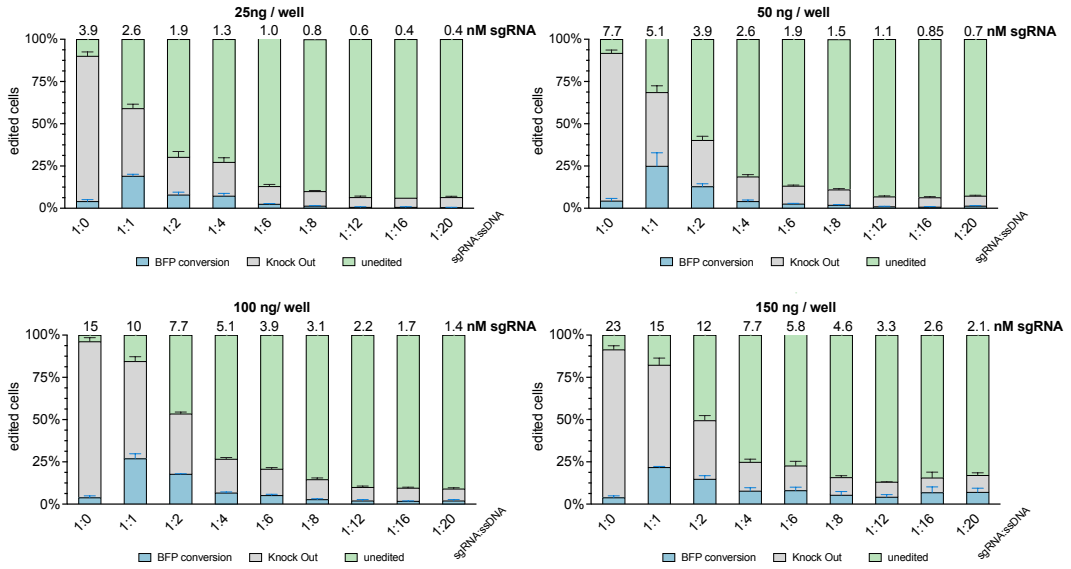

Figure 18. HDR mediated eGFP to BFP conversion. Editing percentages of NHEJ and HDR in HeLa GFPd2 cells treated with 1611 polyplexes formed with Cas9 mRNA and sgGFP at weight ratio 1:1 and the single stranded DNA template (ssDNA) at various of sgRNA:ssDNA. To evaluate editing efficiencies independent of the carrier concentration, cells were exposed to total nucleic acid amounts fixed at 25 ng, 50 ng, 100 ng, and 150 ng at different internal ratios of sgRNA to ssDNA. Resulting sgRNA concentrations are indicated on top of the bars.

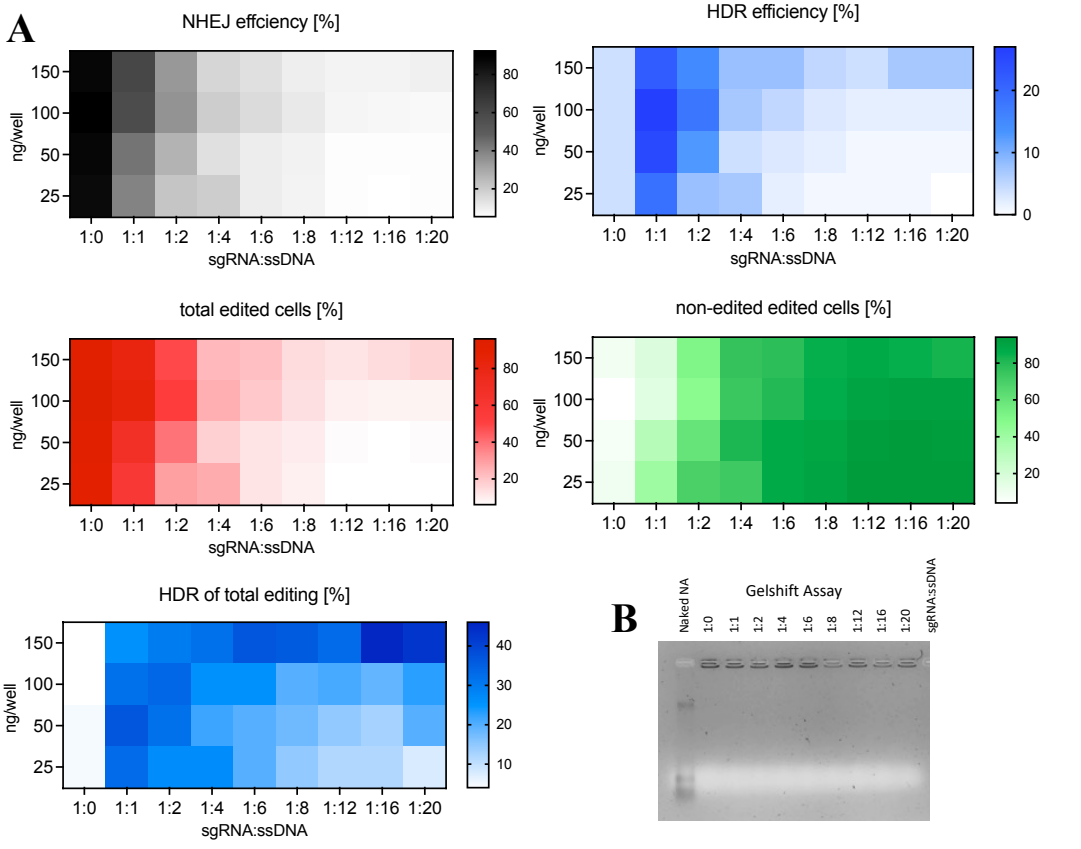

Figure 19. HDR mediated eGFP to BFP conversion. (A) Heat map of NHEJ, HDR, total edited, non-edited, and HDR of total edited percentages in HeLa GFPd2 cells treated with 1611 polyplexes formed with Cas9 mRNA and sgGFP at weight ratio 1:1 and the single stranded DNA template (ssDNA) at various ratios of sgRNA:ssDNA. To evaluate editing efficiencies independent of the carrier concentration, cells were exposed to total nucleic acid amounts fixed at 25 ng, 50 ng, 100 ng, and 150 ng at different internal ratios of sgRNA to ssDNA. **(B)** Agarose gel shift assay of 1611 polyplexes containing Cas9 mRNA, sgRNA and ssDNA at various ratios.

4.3. Positive Read Out Reporter Model for Genome Editing Triggering Exon Skipping

A reporter cell line HeLa mCherry-DMD$_{Ex23}$, expressing mCherry interrupted by a Duchenne muscular dystrophy (DMD) *dystrophin* exon 23 with nonsense mutation, was recently designed by Lessl et al. [166] (see **Figure 20A**).

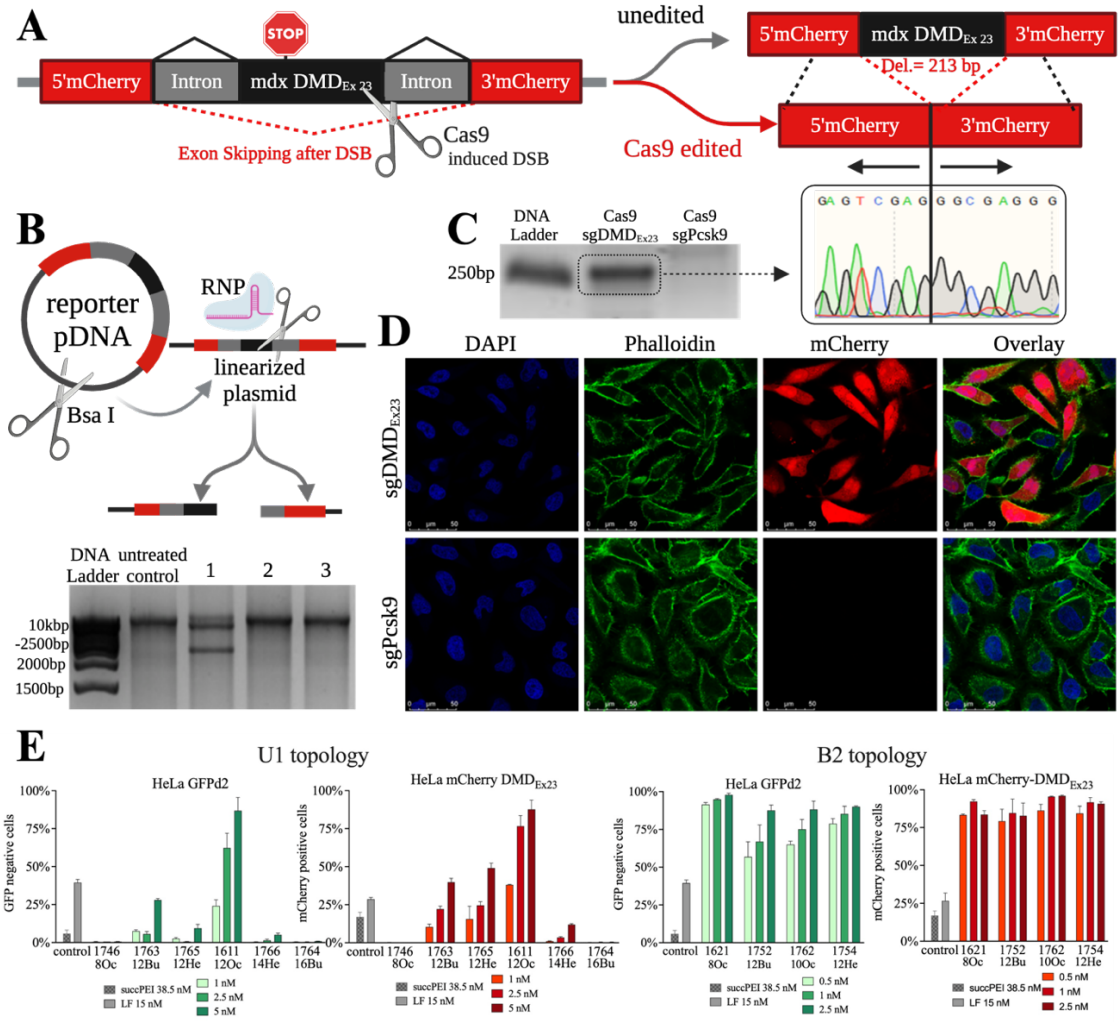

Figure 20. Positive read-out reporter model for genome editing. Functional mCherry expression is induced in HeLa mCherry-DMDex23 reporter cell line after Cas9 induced DSB. **(A)** Schematic illustration showing the structure of mCherry-DMD$_{Ex23}$ construct and its mechanism in presence or absence of Cas9 induced DSB at the donor splice site downstream the *mdx* exon 23. **(B)** *In vitro* cleavage of the plasmid DNA which was used for the generation of the HeLa mCherry-DMD$_{Ex23}$ cell line after overnight digestion of the plasmid DNA with the restriction enzyme BsaI to linearize the DNA. The linearized DNA was incubated with RNP for 2 h at 37 °C and subsequently analyzed on a 1.5 % agarose gel. Untreated linearized plasmid was used as control group; 1: linearized plasmid treated with RNP containing sgDMD$_{Ex23}$; 2: linearized plasmid treated with RNP containing sgGFP; 3: linearized plasmid treated with RNP containing sgPcsk9. **(C)** Detection of *mdx* exon 23 skipping of mCherry-DMD$_{Ex23}$ mRNA by RT-PCR. Total RNA was extracted from cells 3 days after treatment with Cas9 polyplexes formed with LAF 1611 at N/P 18 (10 nM sgDMD$_{Ex23}$ or 10 nM sgPcsk9). The sequence surrounding *mdx* exon23 in mCherry-DMDEx23 was amplified by RT-PCR. The band resulting from *mdx* exon 23 skipping is shown (~280 bp) and exon 23 skipping was confirmed by Sanger sequencing. RNA extraction and evaluation was performed by Anna-Lina Lessl as part of her PhD study at Pharmaceutical Biotechnology, LMU, Munich. **(D)** CLSM images of HeLa mCherry-DMD$_{Ex23}$ cells 72 h after transfection with 1611 polyplexes (N/P 18) containing either Cas9 mRNA and sgDMD$_{Ex23}$ (weight ratio 1:1) or Cas9 mRNA and sgPcsk9 (weight ratio 1:1) resulting in a concentration of 10 nM sgRNA. Nuclei were stained with DAPI (blue), cytoskeleton was stained with rhodamine phalloidin (green) and mCherry is shown in red. Scale bar represents 50 µm. RNP: ribonucleoprotein; CLSM: confocal laser scanning microscopy. Complete gels of B) and C) are provided in **Figure 21**. Nitrogen Catwalk of LAF-Stp carriers with U1 topology (left) or B2 topology (right), comparing editing efficiencies in HeLa GFPd2 and HeLa mCherry-DMDex23 reporter cell lines. For details see **Figure 14** and **Figure 15**. Graphics of part A and B were created using Biorender.com.

It enabled efficient *in vitro* screening of the antisense activity of phosphorodiamidate morpholino oligomers (PMOs) and their conjugate formulations. The specific PMO(Ex_{23}) sequence blocks a splice site of dystrophin pre-mRNA and prompts the skipping of mutated dystrophin exon 23. Such an exon skipping has been therapeutically applied in the well-established murine DMD *mdx* model. Notably, this specific genetic sequence can also trigger exon skipping of the healthy dystrophin in wild-type mice. To ensure the effective use of the same PMO(Ex_{23}) sequence in both the *in vitro* reporter system and *in vivo* experiments, the donor splice site of the intron downstream of *mdx* exon 23 was designed based on the physiological donor splice site sequence of dystrophin intron 23. We now selected a sgRNA ($sgDMD_{Ex23}$) [159, 171] targeting the same specific donor splice site and evaluated the feasability of a Cas9-based single-cut gene editing approach on this positive read-out reporter model to test the efficiency of Cas9 mRNA/$sgDMD_{Ex23}$ polyplexes. According to reports, precise genetic modification is not necessary for the correction of DMD defects via exon skipping. Rather, any indels introduced by NHEJ disrupting a splice donor or acceptor sequence in a mutant exon can lead to exon skipping [159]. By the $sgDMD_{Ex23}$ a double strand break (DSB) in the proximity of the donor splice site of the targeted dystrophin exon 23 is generated. INDELs introduced in the target locus after NHEJ repair lead to the correction of the reporter gene open reading frame (ORF) resulting in observable functional mCherry expression through fluorescence detection (**Figure 20A**). The ORF can be restored by: (i) exon skipping if the INDELs disrupt the splice consensus site of the targeted exon, or (ii) exon reframing if the right number of INDELs is generated in the exonic region [176]. To confirm the specificity of the $sgDMD_{EX23}$ to the target sequence in the reporter construct, we performed an *in vitro* cleavage assay (**Figure 20B, Figure 21B**). The reporter plasmid DNA construct was linearized and then exposed to ribonucleoprotein complexes (RNPs) containing either $sgDMD_{Ex23}$, sgGFP, or sgPcsk9. Only incubation with the Cas9/$sgDMD_{Ex23}$ complex induced cleavage of the reporter DNA resulting in two bands on the agarose gel (**Figure 20B**).

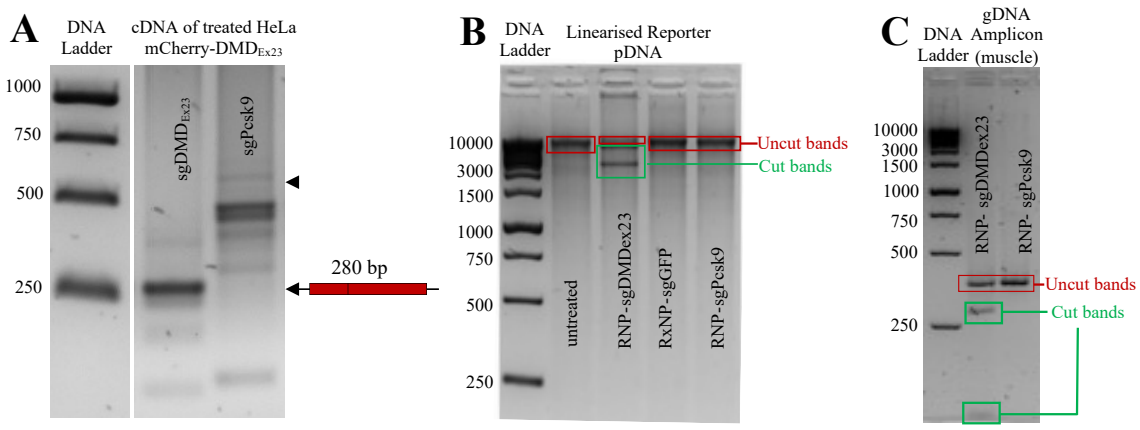

Figure 21. Gel electrophoresis (A) Detection of mdx exon 23 skipping of mCherry-DMD$_{Ex23}$ mRNA by RT-PCR. Total RNA was extracted from cells 3 days after treatment with Cas9 polyplexes formed with LAF 1611 at N/P 18 (10 nM sgDMD$_{Ex23}$ or 10nM sgPcsk9). A sequence surrounding mdx exon 23 in mCherry-DMD$_{Ex23}$ was amplified by RT-PCR. The band resulting from mdx exon 23 skipping is shown (~280 bp). RNA extraction and evaluation were performed by Anna-Lina Lessl as part of her PhD study at Pharmaceutical Biotechnology, LMU, Munich. **(B)** Results from an in vitro cleavage assay to confirm the specificity of the cleavage of the reporter gene by the RNP complex formed with sgDMD$_{Ex23}$ compared to no cleavage by RNP complex formed with other sgRNAs. Representative analysis of the initially linearized mCherry plasmid containing the sgDMD$_{Ex23}$ target site followed by a second cleavage due to incubation with precomplexed RNP visualized on a 1.5 % agarose gel containing Gel Red. DNA cleavage products of the second digest after incubation with sgRNA precomplexed with Cas9 protein. **(C)** Results from an in vitro cleavage assay to confirm the specificity of the cleavage of the genomic donor splice site downstream exon 23 by the RNP complex formed with sgDMD$_{Ex23}$ compared to no cleavage by RNP complex formed with other sgRNAs. Representative analysis of PCR amplified genomic sequence containing the sgDMD$_{Ex23}$ target site followed by a cleavage due to incubation with precomplexed RNP visualized on a 1.5 % agarose gel containing Gel Red. DNA cleavage products of the second digest after incubation with sgRNA precomplexed with Cas9 protein.

The reporter cell line HeLa mCherry-DMD$_{Ex23}$ was treated with 1611 polyplexes (N/P 18) containing either Cas9 mRNA/sgDMD$_{Ex23}$ (weight ratio 1:1) or Cas9 mRNA/sgPcsk9 (weight ratio 1:1). Three days post treatment, total RNA was extracted from treated cells and reverse transcribed into cDNA. The splicing product leading to functional mCherry expression was amplified and analyzed via gel electrophoresis. The band resulting from mdx exon 23 skipping (~280 bp) was only detected in cells treated with sgDMD$_{Ex23}$, and exon 23 skipping was confirmed by Sanger sequencing (**Figure 20C, Figure 21A**). Additionally, the presence of mCherry protein was further determined by confocal laser scanning microscopy (CLSM) images of HeLa mCherry-DMD$_{Ex23}$ cells 72 h after transfection with 1611 polyplexes (N/P 18) containing either Cas9 mRNA and sgDMD$_{Ex23}$ or sgPcsk9 (**Figure 20D**). mCherry fluorescence was detectable solely in cells treated with sgDMD$_{Ex23}$. For genomic evaluation of the Cas9 induced edits on the mCherry-DMD$_{Ex23}$ reporter, total genomic DNA was isolated from HeLa mCherry-DMD$_{Ex23}$ cells 2 weeks after treatment with either 1611 (N/P 18) or 1752 (N/P 24) polyplexes containing Cas9 mRNA and either sgPcsk9 or sgDMD$_{Ex23}$ (**Figure 22**). In groups treated with Cas9 mRNA/sgPcsk9, gel electrophoresis of the PCR products revealed only one band with the expected length (841 bp) of the complete unedited sequence. Additional bands of approximately 450 bp were observed in all groups treated with Cas9 mRNA/sgDMD$_{Ex23}$, indicating large genomic deletions (**Figure 22A**). Sanger sequencing of the isolated bands confirmed the full sequence of the unedited 841 bp band and a 388 bp long deletion,

surrounding the Cas9 cut side, for the shorter band (**Figure 22D**). The untypical large deletion after Cas9 induced double strand break might be caused by locus specific properties of the artificial construct surrounding the *mdx*-DMD$_{Ex23}$ sequence [177, 178]. Nevertheless, the specificity of the reporter for the testing of sgDMD$_{Ex23}$ containing Cas9 formulations was proven by the comparison to sgPcsk9 containing formulations as stated above. Additionally, gene editing results on HeLa mCherry-DMD$_{Ex23}$ cells evaluated by flow cytometry strongly correlate with the GFP knock out data on the HeLa GFPd2 cell line confirming the suitability of this reporter model for library screening (**Figure 20**, **Figure 14,** and **Figure 15**).

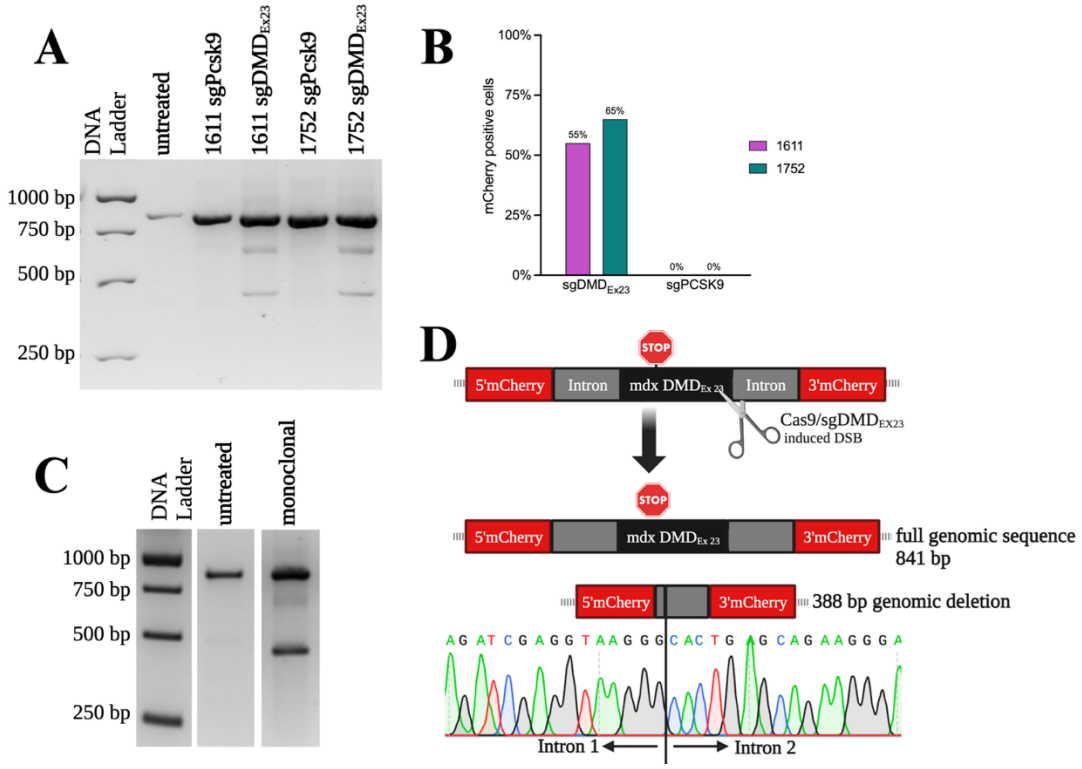

Figure 22. Genomic evaluation of mCherry-DMD$_{Ex23}$ reporter after treatment with Cas9 polyplexes (A) Gel electrophoresis of PCR products. Genomic DNA was extracted from HeLa mCherry-DMD$_{Ex23}$ cells 2 weeks after treatment with either 1611 (N/P 18) or 1752 (N/P 24) polyplexes containing Cas9 mRNA and either sgPcsk9 or sgDMD$_{Ex23}$. The mCherry-DMD$_{Ex23}$ reporter region was amplified by PCR. Both polyplex groups containing Cas9 mRNA/sgDMD$_{Ex23}$ revealed additional bands, indicating big genomic deletions whilst the Cas9 mRNA/sgPcsk9 and the untreated control groups only show the expected band of the unedited sequence (841 bp) with no additional bands. **(B)** Flow cytometric evaluation of HeLa mCherry-DMD$_{Ex23}$ treated with LAF polyplexes as shown in **A**. Only treatment with Cas9 mRNA/sgDMD$_{Ex23}$ resulted in mCherry positive cells. **(C)** By limiting dilution, a monoclonal mCherry positive cell line was generated from 1752 (N/P 24) polyplexes containing Cas9 mRNA/sgDMD$_{Ex23}$ treated cells as shown in **A**. Genomic DNA was isolated and the mCherry-DMD$_{Ex23}$ reporter region was amplified by PCR. Resulting bands of approximately 841 bp and 450 bp indicating unedited sequence and genomic deletion, respectively, were extracted and purified. **(D)** Sanger sequencing of purified samples confirmed the unedited full genomic reporter sequence with a size of 841 bp. The lower band revealed a 388 bp genomic deletion spanning including most of the intron upstream and a short sequence of the intron downstream (until 18 bp downstream of expected cut side) of the *mdx* DMD$_{Ex23}$ reporter.

4.4. Characterization of top performing polyplexes for in vivo application

While it was evident that 1611 proved to be the optimal carrier for the U-shaped LAF-Stp topology, the trends associated with various B2-shaped carriers were less distinct. Consequently, the subsequent analysis focused on 1611 alongside three promising representatives of B2-shaped carrier candidates, specifically 1621, 1752, and 1762, at a further reduced dosage. As pathways and routes differ between various cell types, also efficiency ranking of different carriers can be at variance, as demonstrated in **Figure 23** for Hepa and HeLa. The *Pcsk9* knock out after treatment with a dose range from 0.25 nM to 15 nM sgPcsk9 was evaluated on Hepa 1-6 *Pcsk9*^{tdTomato} cells and compared to Lipofectamine^{TM} Messenger MAX^{TM} lipoplexes, resulting in sgPCSK9 concentrations of 5 nM, 10 nM, and 15 nM as positive control. All LAF-Stp carriers achieved 2-5-fold higher knock out efficiencies than the positive control at corresponding concentrations. Carrier 1611 showed an EC_{50} (defined as the concentration of delivered sgRNA required to provoke 50 % gene edited cells) of ~1 nM sgRNA whilst all B2 carriers resulted in $EC_{50} \geq 4.0$ nM sgRNA (**Figure 23A, Table S3**).

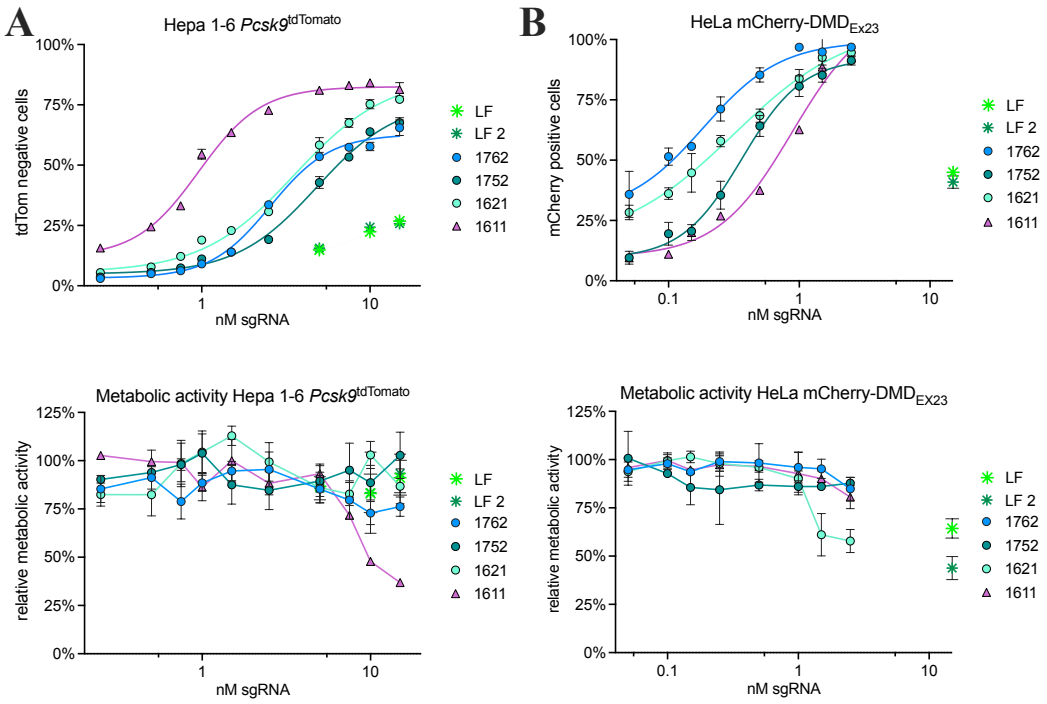

Figure 23. Dose titration of best performing LAF-Stp carriers forming Cas9 polyplexes containing Cas9 mRNA and sgRNA at weight ratio 1:1. N/P ratio of bundle and U1 carriers was 24 and 18, respectively. **(A)** Top: *In vitro Pcsk9* knock out in Hepa 1-6 *Pcsk9*^{tdTomato} cells treated with 0.25 nM-15 nM sgPcsk9. Positive controls were presented by Lipofectamine^{TM} Messenger MAX^{TM} lipoplexes (LF, LF 2) used for transfection of Cas9 mRNA and sgRNA according to both manufacturer's protocol options resulting in a concentration of 5 nM, 10 nM, and 15 nM sgPcsk9. Bottom: Metabolic activity of cells transfected with Cas9 polyplexes in relation to HBG buffer treated control cells determined via MTT assay at 24 h after transfection. **(B)** Top: *In vitro* exon skipping evaluation on HeLa mCherry-DMD$_{EX23}$ cells treated with 50 pM – 2.5 nM sgDMD$_{Ex23}$. Positive controls were presented by Lipofectamine^{TM} Messenger MAX^{TM} lipoplexes used for transfection of Cas9 mRNA and sgRNA according to both manufacturer's protocol options resulting in a concentration of 15 nM sgRNA. Bottom: Metabolic activity of cells transfected with Cas9 polyplexes in relation to HBG buffer treated control cells determined via MTT assay at 24 h after transfection.

Given the previously shown high efficiency of LAF-Stp carriers on HeLa cells, we chose an ultra-low dose range from 50 pM to 2.5 nM sgRNA for the evaluation on HeLa mCherry-DMD_{Ex23}. Interestingly, a strong benefit of the B2 topology could be observed in this cell line resulting in more than 10-fold lower EC_{50} values (0.1 nM to 0.4 nM $sgDMD_{Ex23}$) compared to the EC_{50} in Hepa 1-6 *Pcsk9*^{tdTomato}. Gene editing of 1611 polyplexes (EC_{50}: 0.7 nM $sgDMD_{Ex23}$), on the other hand, was comparable to the results on Hepa 1-6 *Pcsk9*^{tdTomato} cells (**Figure 23B**). Consistent with prior research, a connection between increased potency and toxicity at elevated doses was evident. Notably, while amongst all the evaluated carriers only compound 1611 reduced the metabolic activity of Hepa 1-6 *Pcsk9*^{tdTomato} cells at higher doses, the metabolic activity of HeLa cells was only reduced by higher doses of the B2 carrier 1621 (**Figure 23**). There is a significant disparity between the *in vitro* conditions in cell culture and those in animal models (*in vivo*). Upon intravenous administration of nanoparticles, their interaction with blood components may critically influence on their performance [179, 180]. Hence, transfection efficiency was evaluated after pre-incubation of the polyplexes in full (≥ 90 % v/v) serum at 37 °C for 2 h (**Figure 24**).

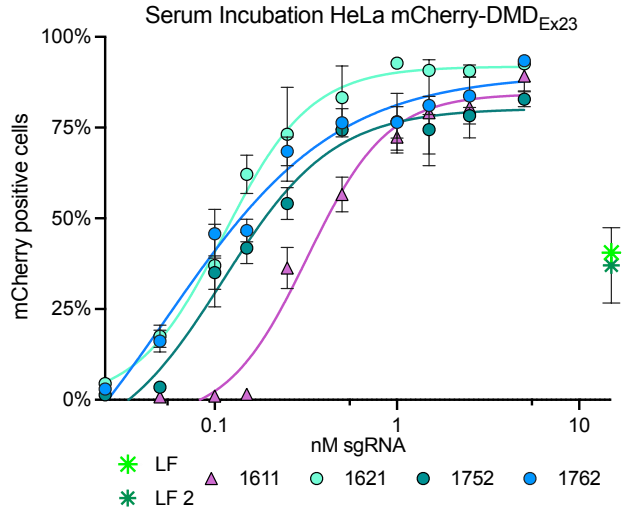

Figure 24. *In vitro* performance of LAF polyplexes in presence of full serum. Dose titration of best performing LAF-Stp carriers forming Cas9 polyplexes containing Cas9 mRNA and sgRNA at weight ratio 1:1. N/P ratio of bundle and U1 carriers was 24 and 18, respectively. Samples were diluted in full serum (25 pM– 0.5 nM $sgDMD_{Ex23}$, 98 % serum; 1-2.5 nM, 90 % serum) and transfected at indicated low doses on HeLa mCherry-DMD_{Ex23}. Positive controls were presented by Lipofectamine™ Messenger MAX™ lipoplexes used for transfection of Cas9 mRNA and sgRNA according to both manufacturer's protocol options resulting in a concentration of 15 nM sgRNA without any serum addition. (n=3, mean ± SD)

Notably, despite full serum incubation efficacies of top carriers were not reduced, with sub-nanomolar EC_{50} values of as low as 0.4 nM $sgDMD_{Ex23}$ for carrier 1611 and 0.1 nM $sgDMD_{Ex23}$ for carrier 1762. Consequently, carrier 1611 at N/P 18 and carrier 1762 at N/P 24 emerged as the most suitable candidates for *in vivo* evaluation of U1 and B2 topologies, respectively. Concentrated formulations intended for *in vivo* application underwent testing for their physicochemical properties, demonstrating resistance toward full serum, long-term stability upon storage at 4 °C for up to 127 days, and high transfection efficiency after 14 days storage at 4 °C (**Table S4, Figure 25, Figure 26**).

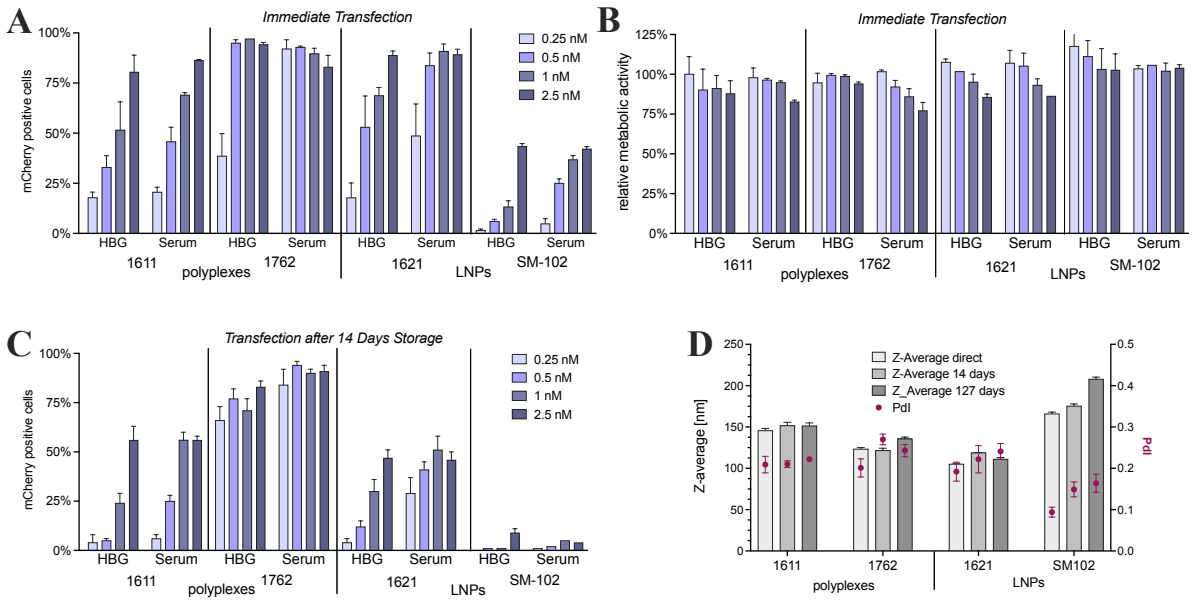

Figure 25. Long term stability of Cas9mRNA/sgDMD$_{Ex23}$ formulations at high concentration. Nanoparticles were formed with different LAF carriers at indicated N/P ratios resulting in a total RNA concentration of 200 ng µL^{-1} for 1611 polyplexes and 60 ng µL^{-1} for all other formulations (Cas9 mRNA and sgDMD$_{Ex23}$ at weight ratio 1:1). All formulations were stored at 4 °C until indicated evaluation time points. HeLa mCherry-DMD$_{Ex23}$ cells were treated with Cas9 polyplexes immediately after dilution of the nanoparticles in either HBG or full serum (≥90 % serum). **(A)** Directly after formulation of the nanoparticles were diluted in HBG or serum and immediately transfected at indicated concentrations of sgDMD$_{Ex23}$. Exon skipping efficiency was evaluated by flow cytometry 3 days after treatment of HeLa mCherry-DMD$_{Ex23}$ cells with Cas9 polyplexes or Cas9 LNPs. **(B)** Metabolic activity of cells 24 h post treatment with nanoparticle formulations as in (A). **(C)** Following 14 day storage at 4 °C, the formulations were diluted in HBG or serum and immediately transfected at indicated concentrations of sgDMD$_{Ex23}$. Exon skipping efficiency was evaluated by flow cytometry 3 days after treatment of HeLa mCherry-DMD$_{Ex23}$ cells with Cas9 polyplexes or Cas9 LNPs. **(D)** At indicated time points, nanoparticles were diluted to a total RNA concentration of 12.5 ng µL^{-1} for DLS and ELS measurement.

These results further confirm the feasibility of using these structures for *in vivo* testing. Successful delivery of nanocarriers into specific tissues is often facilitated by their surface interactions with distinct serum proteins and subsequent binding to their cognate receptors [63, 181] and succeeding productive intracellular routing. Therefore, the transfection efficiency of the nanocarriers was assessed subsequent to dilution of the concentrated formulations in full serum **Figure 25**.

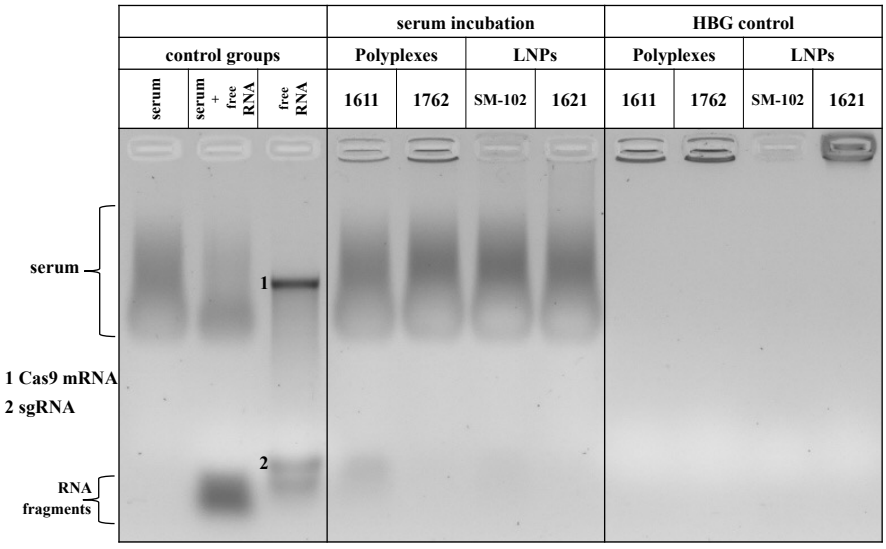

Figure 26. Stability of Cas9mRNA / sgDMD$_{Ex23}$ formulations at high concentration in presence of full serum. Nanoparticles were formed with different LAF carriers at indicated N/P ratios resulting in a total RNA concentration of 200 ng µL^{-1} for 1611 polyplexes and 60 ng µL^{-1} for all other formulations (Cas9 mRNA and sgRNA at weight ratio 1:1). Nanoparticles were diluted 1:10 (v/v) in either HBG or full serum (90 % serum). An agarose gel shift assay was performed after incubation for 2 h at 37 °C. Only a very slight release of RNA can be observed after serum incubation of 1611 polyplexes. All other formulations exhibit full protection and no release of the RNA cargo.

4.5. In Vivo Editing of Dystrophin Gene

Optimized LAF-Stp carriers formulated with mRNA either as polyplexes [163] or as cationizable component in LNPs [172] were found to efficiently deliver luciferase mRNA at low 1–10 µg mRNA/mouse doses upon intravenous application in A/J mice. Combined with the current *in vitro* findings, we selected the promising carriers 1611 and 1762 for polyplex formulation well as a 1621-based LNP formulation for Cas9 mRNA/sgRNA delivery *in vivo*. Biophysical characterization of 1621 LNPs is presented in **Tables S5, S6**; **and Figure 27**.

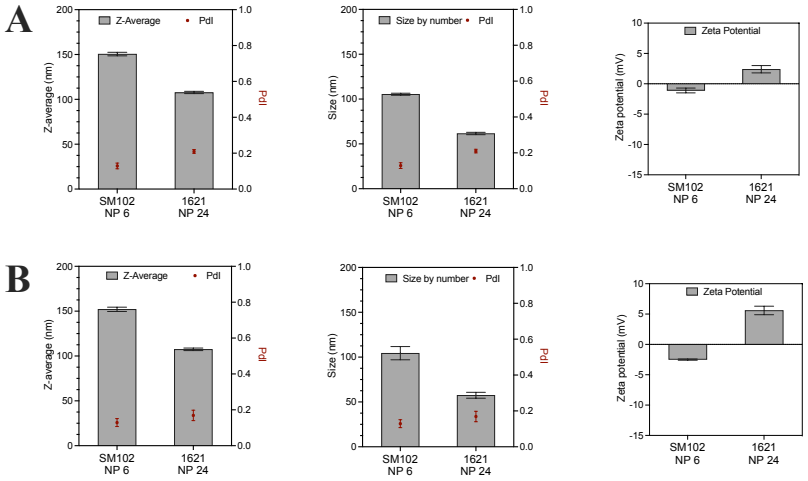

Figure 27. Physicochemical characterization different lipid compositions of LNP formed with B2 structure 1621 as ionizable lipid at 24. LNP containing SM-102 at N/P 6 were evaluated as positive control group. **(A)** DLS and ELS of LNP containing 6.7 ng µL-[1] luciferase mRNA. Left: particle size (Z-Ave), polydispersity index (PdI); middle: particle size by number, polydispersity index (PdI); right: zeta potential. **(B)** DLS and ELS of LNP containing Cas9 mRNA and sgRNA at weight ratio 1:1 and a total RNA concentration of 6.7 ng µL-[1]. Left: particle size (Z-Ave), polydispersity index (PdI); middle: particle size by number, polydispersity index (PdI); right: zeta potential. Data are presented as mean ± SD (n=3).

Similar to the polyplexes, the selected LAF-Stp LNP formulations exhibited remarkable long-term stability (storage at 4° C for 127 days). In contrast to parallel tested gold standard SM-102-containing LNP, they still induced gene editing upon transfection following 14 days of storage at 4 °C (**Figure 25**). For Cas9-induced dystrophin gene editing in healthy mice *in vivo*, the same $sgDMD_{Ex23}$ sgRNA sequence can be applied as in the positive read-out reporter model described in section 4.3and originally designed for assessment of splice-switching oligonucleotides by Lessl et al. (**Figure 20C**). Using PMO(Ex_{23}) conjugates of related sequence-defined xenopeptides, Lessl et al. could demonstrate *in vivo* dystrophin exon 23 skipping in several organs. By Cas9 mediated genomic disruption of the donor splice site, the efficiency of gene editing can be assessed by: (i) examining the genomic sequence in the vicinity of the specific cleavage site, and (ii) analyzing exon skipping at the mRNA level. Genome editing and mRNA splicing modulation after intravenous injection with Cas9 polyplexes and Cas9 LNPs in BALB/c mice is displayed in **Figure 28**.

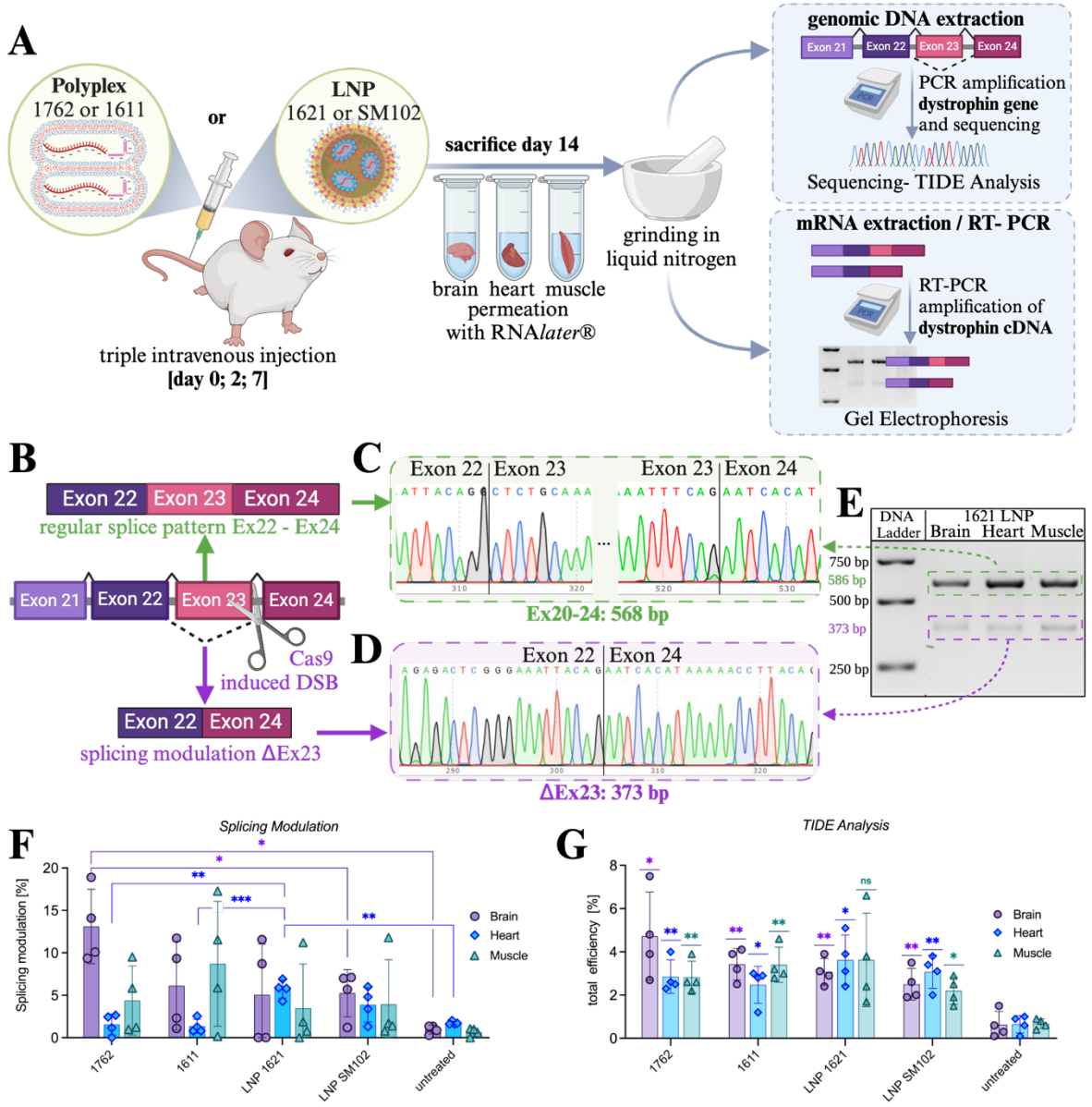

Figure 28. ***In vivo*** **genome editing and mRNA splicing modulation in BALB/c mice after intravenous injection with Cas9 polyplexes and Cas9 LNPs.** Dystrophin gene editing and mRNA splicing modulation and in different organs of BALB/C mice after triple injections Cas9 polyplexes or Cas LNP solution containing Cas9 mRNA and sgDMD$_{Ex23}$ at weight ratio 1:1. All LAF-Stp formulations were compared to LNPs containing SM-102 at N/P 6 as gold standard. **(A)** Treatment scheme: triple intravenous injection of 150 µL polyplex or LNP solution containing either 3 µg total RNA in 1762 polyplexes, LNP 1621 and LNP SM-102 or 10 µg total RNA in 1611 polyplexes. Euthanasia at 7 days post last injection, sample preparation and evaluation. Total RNA and genomic DNA was extracted from homogenized dystrophin expressing organs (brain, heart, muscle tissue) at 7 days after last injection. For the evaluation of splicing modulation, a nested RT-PCR was conducted to amplify dystrophin exon 20-24. The RT-PCR product was analyzed on a 2 % agarose gel and ratios of splicing modulation were determined using ImageJ Software. For the analysis of the gene editing efficiency a PCR was performed to amplify the region surrounding exon 23. PCR products were purified and sequenced via Sanger sequencing. The sequencing results were evaluated using the TIDE (Tracking of Indels by Decomposition) analysis tool. **(B)** Scheme of splicing modulation after of Cas9 induced DSB at donor splice site downstream dystrophin exon 23 **(C)** Sanger sequencing of gel extracted bands corresponding to ~568 bp (complete DMD Ex20-24) **(D)** Sanger sequencing of gel extracted bands corresponding to ~373 bp fragments for confirmation of exon 23 skipping. **(E)** Exemplary gel electrophoresis of RT-PCR products showing splicing modulation in brain, heart, and muscle of animal 1 after triple intravenous treatment with 1621 LNPs (N/P 24) containing 3 µg total RNA. **(F)** Evaluation of splicing modulation, as described above, after triple intravenous treatment with either 1762 (N/P 24) polyplexes, 1611 (N/P 18) polyplexes, 1621 (N/P 24) LNP or SM-102 (N/P 6) LNP as positive control.. Individual band intensities were quantified and put into relation to the band of full-length dystrophin exon 20-24 with a size of 568 bp by using the ImageJ software. The complete gel electrophoresis data are provided in **Figure 31**. **(G)** Evaluation of gene editing efficiency, as described above, after triple intravenous application of 1762 polyplexes, LNP 1621 and LNP SM-102 containing 3 µg total RNA and 1611 polyplexes containing 10 µg total RNA. Sanger-sequenced and evaluated by TIDE (Tracking of Indels by Decomposition) analysis. (n=4, mean ± SD). Asterisks indicate statistical significance between treated organ to untreated control. Statistical analysis was performed by unpaired Student's two-tailed t-test with Welch's correction; GraphPad Prism™ 10. * $p \leq 0.05$; ** $p \leq 0.01$; *** $p \leq 0.001$; ns, statistically not significant. Injections and harvesting of the organs were performed by Jana Pöhmerer and Ulrich Wilk as part of their veterinary MD studies at Pharmaceutical Biotechnology, LMU. DNA extraction was performed by Miriam Höhn (Pharmaceutical Biotechnology, LMU). Analysis of LNP SM-102 treated animals was performed by Eric Weidinger as part of his PhD studies at Pharmaceutical Biotechnology, LMU.

During a 7-day period, BALB/c mice were subjected to three intravenous injections, receiving either 1762 polyplexes or 1621 LNPs, both containing 3 µg total RNA (Cas9 mRNA and sgDMD$_{Ex23}$ at a weight ratio of 1:1). Well tolerable 1611 polyplexes contained 10 µg total RNA. Good biocompatibility of all formulations was demonstrated by standard plasma parameters (ALT, alanine transaminase; AST, aspartase aminotransferase; Crea, creatinine; BUN, blood urea nitrogen) and monitoring the body weight of animals (**Figure 29, Figure 30**).

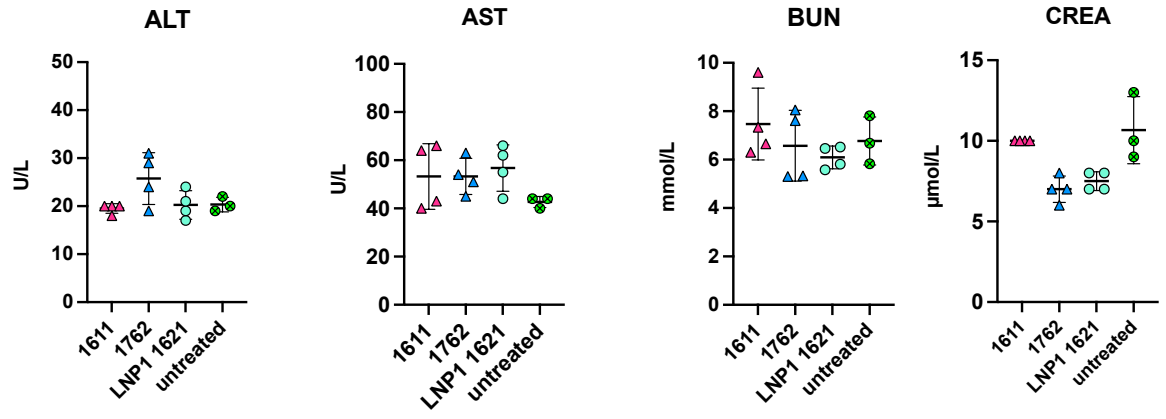

Figure 29. Evaluation of standard plasma parameters after intravenously applied Cas9 polyplexes and Cas9 LNPs. Blood samples were taken 7 days after ultimate of three injections with Cas9 polyplexes or Cas LNP containing Cas9 mRNA and sgDMD$_{Ex23}$ at weight ratio 1:1. 10 µg total RNA were applied with LAF 1611 containing Cas9 polyplexes (n=4), 3 µg total RNA was applied for all other Cas9 formulations (n=4), untreated (n=3). ALT, alanine transaminase; AST, aspartate aminotransferase; BUN, blood urea nitrogen; Crea, creatinine. Injections and analysis were performed by Jana Pöhmerer as part of their veterinary MD studies at Pharmaceutical Biotechnology, LMU.

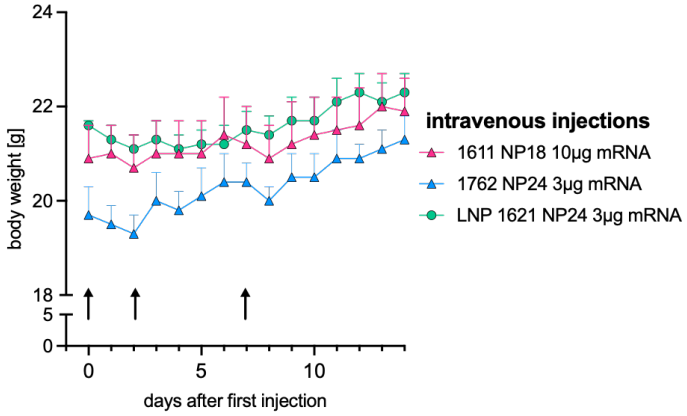

Figure 30. Body weight after of animals intravenously treated with Cas9 polyplexes and Cas9 LNPs. Triple administration of 150 µL nanocarrier solution containing 10 µg total RNA in 1611 polyplexes (N/P 18), 3 µg total RNA in 1762 polyplexes (N/P 24) and 3 µg total RNA in 1621 LNP (N/P 24); each animal's body weight was monitored until their sacrifice at day 14. Arrows indicate days of injection. (n=4, mean + SEM). Injections and monitoring of the animal's weight were performed by Jana Pöhmerer as part of their veterinary MD studies at Pharmaceutical Biotechnology, LMU.

The *ex vivo* assessment of dystrophin genome editing and mRNA exon 23 skipping was performed only with organs exhibiting high dystrophin expression [182], i.e. brain, heart, and biceps femoris muscle. We aimed to minimize other factors that might compromise gene editing efficiency i.e. chromatin modifications and DNA packaging that can block eukaryotic genome

editing [183]. Analysis was performed seven days after final intravenous administration and compared to results of untreated BALB/c mice. Confirmation of the desired exon 23 skipping in the physiological dystrophin mRNA was achieved by representative Sanger sequencing of the RT-PCR products isolated from an agarose gel (**Figure 28C, D**). RT-PCR products showed significant exon skipping in various groups (**Figure 28F, Figure 31**).

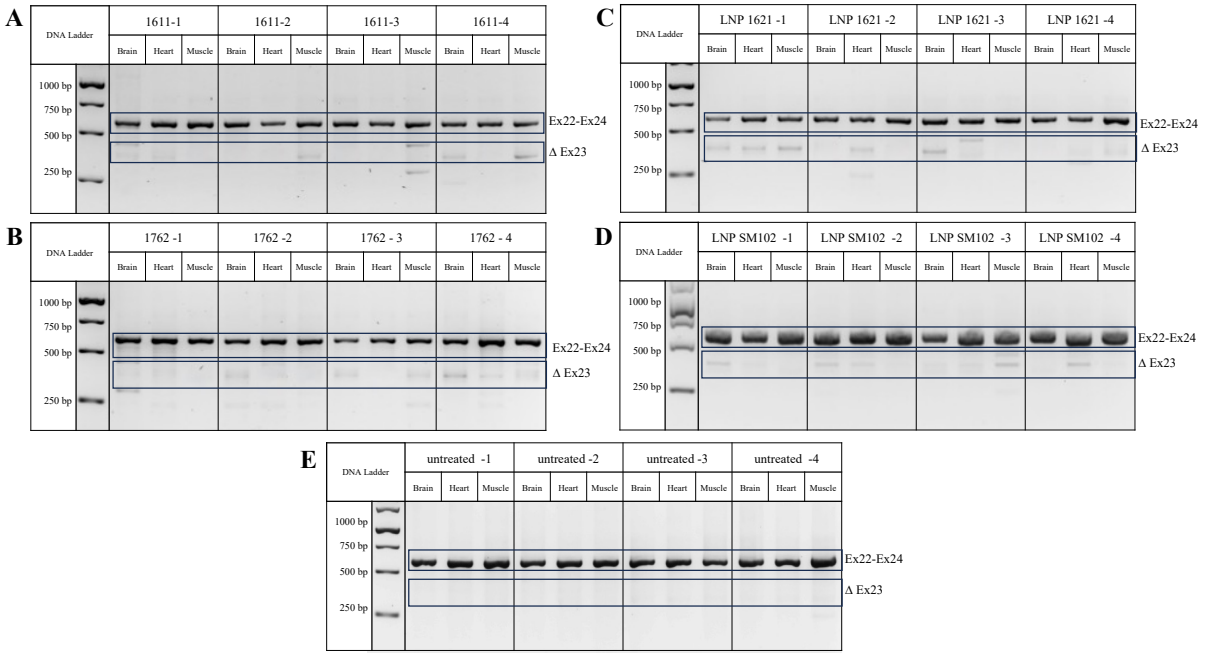

Figure 31. ***In vivo*** **mRNA splicing modulation in BALB/c mice after triple injection with Cas9 polyplexes and Cas9 LNPs.** All LAF-formulations were compared to LNP containing SM-102 at N/P 6 as gold standard. Total RNA was extracted from homogenized organs 7 days after last of triple intramuscular or intravenous injections with Cas9 polyplexes or Cas LNP containing Cas9 mRNA and $sgDMD_{Ex23}$ at weight ratio 1:1. 10 µg total RNA were applied with LAF 1611 containing Cas9 polyplexes, 3 µg total RNA was applied for all other Cas9 formulations. A nested RT-PCR was conducted to amplify dystrophin exon 20-24. The dystrophin expressing organs brain, heart and muscle tissue were analyzed after systemic application. Only the tissue of the injected muscle was analyzed after intramuscular application. **(A)** Systemic application of Cas9 polyplexes formed with LAF 1611 at N/P 18 (10 µg total RNA). **(B)** Systemic application Cas9 polyplexes formed with LAF 1762 at N/P 24 (3 µg total RNA). **(C)** Systemic application Cas9 LNP formed with LAF 1621 at N/P 24 (3 µg total RNA). **(D)** Systemic application Cas9 LNP formed with SM-102 at N/P 6 (3 µg total RNA) served as positive control. **(E)** Untreated treated animals (n=4) served as negative control. Total RNA was extracted from homogenized organs and nested RT-PCR was conducted to amplify dystrophin exon 20-24.

The 1621 containing LNP formulation resulted in significantly higher exon 23 skipping rates in heart tissue (5.7 % ± 1.1 %; mean ± SD) than both polyplex formulations. Splicing modulation in the brain was evident across all examined formulations. Especially, 1762 polyplexes elicited an high exon skipping rate of 13.1% ± 4.4% (mean ± SD) in brain tissue. Both the 1611 polyplex and the LNP 1621 group displayed considerable variability, with certain individual animals exhibiting higher splicing modulation compared to others. Considerable variability was similarly observed in skeletal muscle across all groups. High splicing modulation values of up to 17 %, stood in contrast to low levels of other individuals. Such differences in between the individual groups, tissues and individuals were not observed in the genomic evaluation of the gene sequence surrounding the expected cut site at the dystrophin exon 23. Using the TIDE analysis tool, total gene editing efficiencies of 2.5 % - 4.7 % were detected in organs of treated

animals compared to a background signal of < 0.7 % in untreated animals (**Figure 28G**). An exemplary TIDE plot is depicted in **Figure 32**.

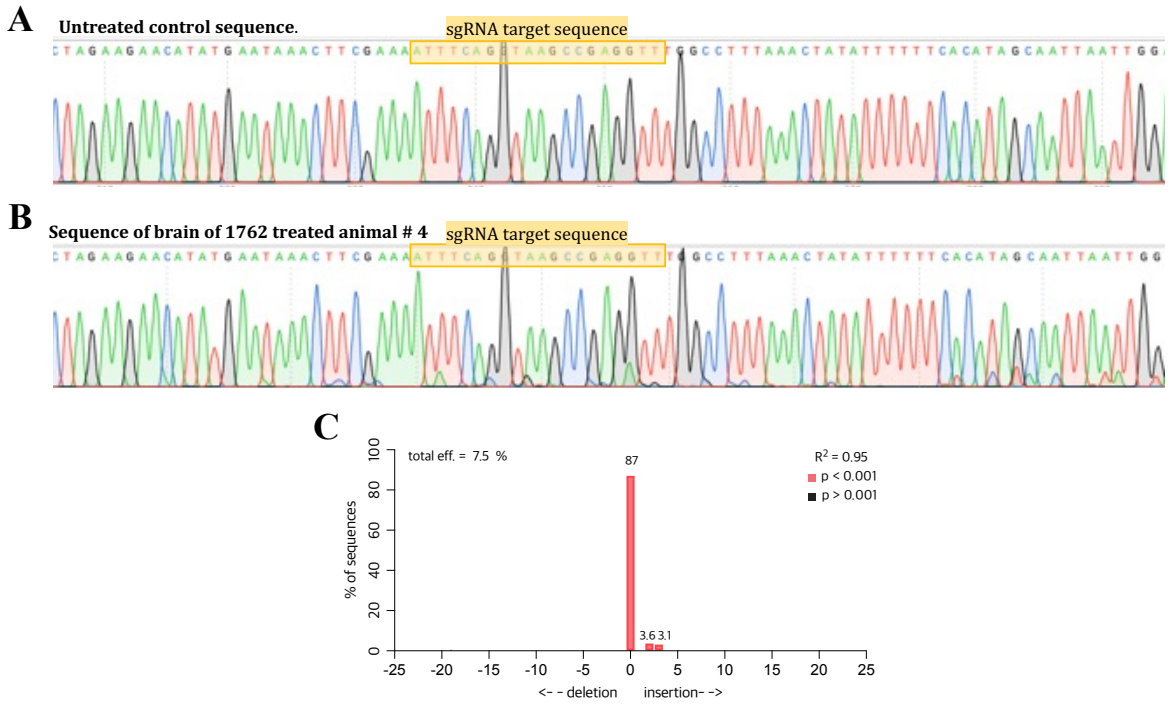

Even though significant gene editing values could be detected in most groups the editing values are lower than splicing modulation values in corresponding animals (**Table S8**). On the one hand it remains unclear which exact indel sequence causes a change in the splicing pattern of exon 23, on the other hand possible larger genomic deletions, as shown in the mCherry-DMDEx23 reporter model, would not be detectable by the TIDE analysis tool. The positive control SM-102 LNP mediated comparable genome editing efficiencies as 1621 LNP.

The next aim was to investigate genome editing and mRNA splicing modulation after local intramuscular injection with Cas9/sgRNA polyplexes and LNPs. As the i.m. administration of the novel class of carriers had not been studied in previous work, the efficiencies of polyplexes and LNPs were first analyzed by intramuscular application using luciferase reporter mRNA (**Table S7,Figure 33**). Within the class of mRNA polyplexes, all displayed a very high i.m. luciferase expression around 10^8-10^9 RLU/g muscle at 6 h post-injection; the bundle B2 carrier 1762 exhibited significantly higher luciferase expression levels in muscle tissue compared to all other tested polyplex formulations (**Figure 33**). Based on these results, the 1762 carrier, along with U1 carrier 1611, which displayed a more favorable toxicity profile [163], were

selected for the *in vivo* evaluation of polyplexes for Cas9-induced dystrophin modification. Additionally, luciferase mRNA LNP formulations containing either 1621 as cationizable component or, as gold standard, the well-established SM-102 lipid were included in the evaluation. Both luciferase mRNA LNPs showed comparable extremely high i.m. luciferase expression of $> 10^{10}$ RLU/g muscle, about 10– to 100-fold higher than the polyplex formulations (**Figure 33**). Notably, luciferase activity at the 6 h time point of investigation remained focused to the injected muscle (**Figure 33C**); activity in other organs of i.m. injected mice was several 100-fold to 1000-fold lower.

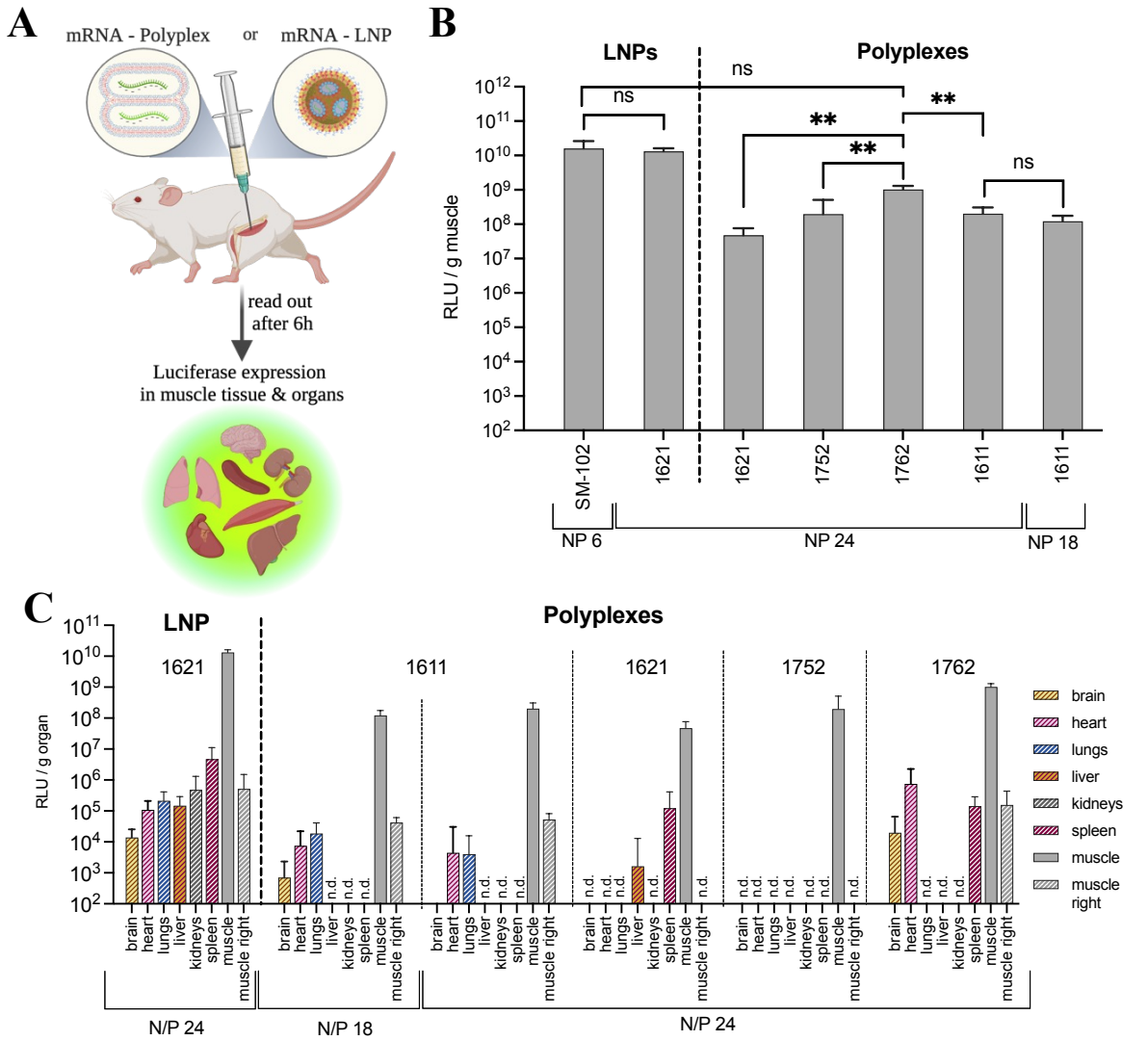

Figure 33. Luciferase expression in muscular tissue after intramuscular injection of LAF containing mRNA polyplexes and mRNA LNPs. All LAF-formulations were compared to LNP containing SM-102 at N/P 6 as gold standard. **(A)** Performance of 50 µL intramuscularly applied mRNA polyplexes or mRNA-LNP containing 60 ng μL^{-1} luciferase mRNA (3 µg) was evaluated six hours after injection into the left musculus biceps femoris via an ex vivo luciferase assay of the muscle tissue and organs of BALB/c mice. **(B)** Luciferase activity in RLU was determined ex vivo per gram (g) muscle at 6 h post injection (n=4; mean ± SD). LNP compositions see Experimental section. Statistical analysis was done by unpaired Student's two-tailed t-test with Welch's correction; GraphPad Prism™ 10. Significance between 1762 containing polyplexes and all other polyplexes: ** $p \leq 0.01$, Significance between 1762 containing polyplexes or LNP 1621 and SM-102: statistically not significant.* $p \leq 0.05$; ** $p \leq 0.01$; *** $p \leq 0.001$; **** $p \leq 0.0001$; ns, statistically not significant. **(C)** Performance of 1621 mRNA LNP. Performance of mRNA polyplexes with indicated N/P ratio 6 hours after intramuscular injection. (n=4; mean ± SD, n.d.: not detectable signal. Experiments were performed by Jana Pöhmerer and Ulrich Wilk as part of their veterinary MD studies at Pharmaceutical Biotechnology, LMU.

Genome editing and mRNA splicing modulation after single or triple intramuscular application of Cas9 polyplexes and Cas9-LNPs in BALB/c mice is displayed in **Figure 34**. Single treatment only yielded very low gene editing and splicing modulation. Triple application improved results for all tested formulations, with total gene editing efficiencies of 2.3 % - 3.4 %, triggering 6.0 % - 9.3 % splicing modulation (**Figure 34B, C, Figure 35**).

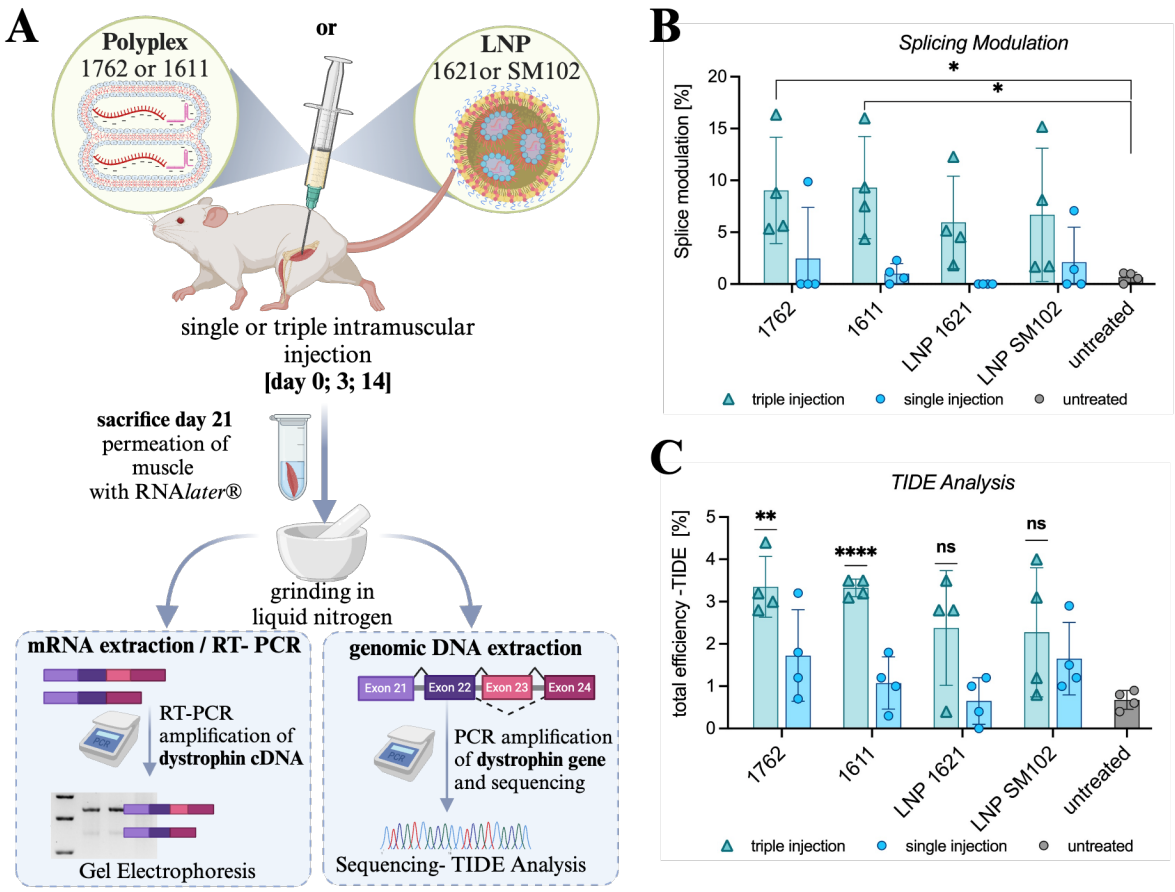

Figure 34. *In vivo* genome editing and mRNA splicing modulation in BALB/c mice (n=4) after intramuscular injection with Cas9 polyplexes and Cas9 LNPs. Comparison of dystrophin gene editing and mRNA splicing modulation in muscle tissue of BALB/C mice after single or triple intramuscular injections with polyplexes or Cas LNPs containing Cas9 mRNA and sgDMD$_{Ex23}$ at weight ratio 1:1 into the left musculus biceps femoris. Only the tissue of the injected muscle was analyzed after intramuscular application. **(A)** Injection scheme for single or triple intramuscular injection of 50 µL nanocarrier solution containing either 3 µg total RNA in1621 (N/P 24) containing LNP and 1762 polyplexes (N/P 24) or 10 µg total RNA in 1611 polyplexes (N/P 18). SM-102 LNP at N/P 6 containing 3 µg total RNA in 50 µL served as gold standard. **(B)** For the evaluation of splicing modulation, a nested RT-PCR was conducted to amplify dystrophin exon 20-24 . The RT-PCR product was analyzed on a 2% agarose gel and ratios of splicing modulation were determined using ImageJ Software. The complete gel electrophoresis data are provided in **Figure 35**. **(C)** Total genomic DNA was extracted from homogenized organs and PCR were conducted to amplify the genomic region surrounding the dystrophin exon 23. PCR products were purified, Sanger-sequenced and evaluated by TIDE (Tracking of Indels by Decomposition) analysis. (n=4, mean ± SD). Asterisks indicate statistical significance between treated organ to untreated control. Statistical analysis was done by unpaired Student's two-tailed t-test with Welch's correction; GraphPad Prism™ 10. * $p \leq 0.05$; ** $p \leq 0.01$; *** $p \leq 0.001$; **** $p \leq 0.0001$; ns, statistically not significant. Injections and harvesting of the organs were performed by Jana Pöhmerer, and Ulrich Wilk as part of their veterinary MD studies at Pharmaceutical Biotechnology, LMU. DNA extraction was performed by Miriam Höhn (pharmaceutical Biotechnology, LMU). RNA extraction, RNA and DNA evaluation of after single injections were performed by Anna-Lina Lessl as part of her PhD studies at Pharmaceutical Biotechnology, LMU.

Interestingly, genome editing and splice modulation efficiencies do not at all correlate with the relative expression levels of luciferase mRNA. Intramuscularly applied 1762 or 1611 polyplexes mediated slightly higher genome editing and splice modulating than 1621 or SM-102 LNPs, despite their far lower luciferase mRNA potency. Furthermore, comparing the higher

genome editing and splice modulation activity in muscle after intravenous administration with the lower activity in local intramuscular injection, an even higher discrepancy with the relative luciferase expression levels (>100-fold higher muscle luciferase expression upon local injection compared with analogous intravenous injection [163, 172]) is observed. Apparently, in the current case, efficient mRNA delivery does not present the bottleneck in the genome editing process in total. Additional hurdles, such as the intracellular assembly of sgRNA with the Cas9 protein to form the RNP complex, followed by their nuclear import, must be overcome after the mRNA is translated into Cas9 protein. Utilization of a non-optimized sgRNA sequence with a relatively low on-target activity score of 7.8 [184] might explain the discrepancy. Optimization of the sgRNA sequence or employing a double sgRNA double-cut approach to excise the genomic exon region, presents a potential option for optimizing genome editing.

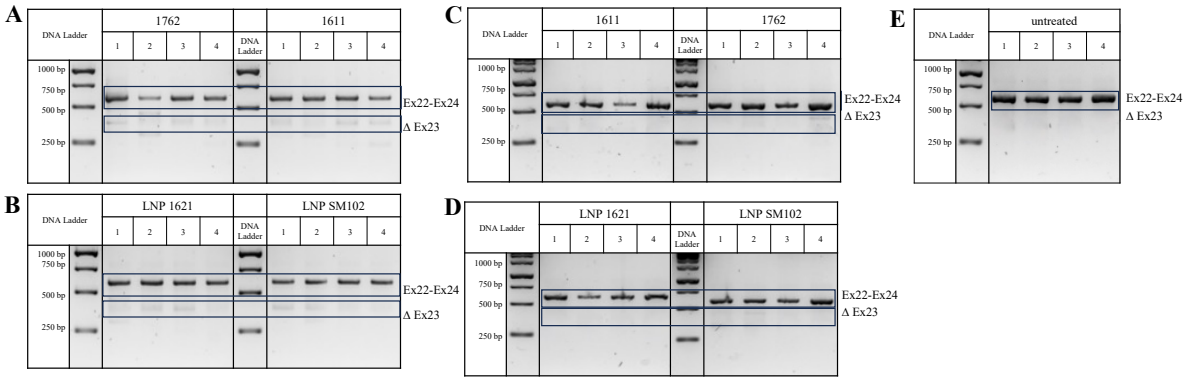

Figure 35. ***In vivo*** **mRNA splicing modulation in** ***muscle tissue*** **of BALB/c mice after intramuscular injection with Cas9 polyplexes and Cas9 LNPs.** Total RNA was extracted from homogenized muscle tissue 7 days after last of single or triple intramuscular injection with Cas9 polyplexes or Cas LNP containing Cas9 mRNA and $sgDMD_{Ex23}$ at weight ratio 1:1. 10 µg total RNA were applied with LAF 1611 containing Cas9 polyplexes, 3 µg total RNA was applied for all other Cas9 formulations. A nested RT-PCR was conducted to amplify dystrophin exon 20-24. Only the tissue of the injected muscle was analyzed after intramuscular application. **(A)** Triple intramuscular application Cas9 polyplexes formed with left: LAF 1762 at N/P 24 (3 µg total RNA) and right: LAF 1611 at N/P 18 (10 µg total RNA**). (B)** Triple intramuscular application Cas9 LNP formed with left: LAF 1621 at N/P 24 (3 µg total RNA) and right: Cas9 LNP formed with SM-102 as ionizable lipid as gold standard LNP formulation (3 µg total RNA). **(C)** Single intramuscular application Cas9 polyplexes formed with left: LAF 1611 at N/P 18 (10 µg total RNA), middle: LAF 1762 at N/P 24 (3 µg total RNA) and right: Cas9 LNP formed with LAF 1621 at N/P 24 (3 µg total RNA). **(D)** single intramuscular application Cas9 LNP formed with left: LAF 1621 at N/P 24 (3 µg total RNA) and right: Cas9 LNP formed with SM-102 as ionizable lipid as gold standard LNP formulation (3 µg total RNA). RNA extraction and evaluation after single injections were performed by Anna-Lina Lessl as part of her PhD studies at Pharmaceutical Biotechnology, LMU.

Controlling the biodistribution and delivering its nucleic acid payload into specific extrahepatic tissues and cell types remains a major hurdle for Cas9 mRNA/sgRNA nanocarriers. In this respect, the observed triggered alternative mRNA splicing with exon 23 skipping in brain tissue and in cardiac and skeletal muscle is noteworthy. Acknowledging the open questions raised by our present study and the utilized mouse model is paramount. Of note, physical delivery of Cas9 mRNA/sgRNA nanoparticles into tissues, which was not studied in the current study, may significantly differ from functional activity. The latter requires productive intracellular uptake, including endosomal escape, translation into Cas9 protein, assembly into sgRNA RNPs, nuclear delivery, and successful genome editing of target cells. Moreover, the uptake mechanisms,

including endocytosis, and cellular responses to nanoparticles, are known to vary among species, thereby influencing the efficacy of functional mRNA delivery [185]. Furthermore, while gene editing targeting the dystrophin 23 exon holds significance for the *mdx* mouse model, it is essential to recognize that a hot spot region of deletions in Duchenne muscular dystrophy is represented by exons 45 to 53. Notably, investigations involving relevant exon 50-deleted mouse and canine models [186, 187], alongside a humanized DMD mouse model [152], have been undertaken to assess editing strategies with enhanced translational potential to the human DMD condition.

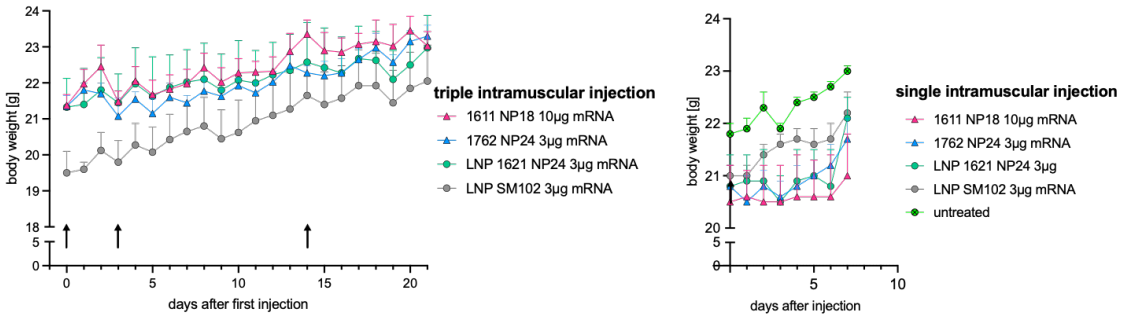

Figure 36. body weight after of animals intramuscularly treated with Cas9 polyplexes and Cas9 LNP. Triple (left) or single (right) administration of 50 µL nanocarrier solution containing 10 µg total RNA in 1611 polyplexes (N/P 18), 3 µg total RNA in 1762 polyplexes (N/P 24), in 1621 LNP (N/P 24) and in SM 102 LNP (N/P 6); each animal's body weight was monitored until their sacrifice at day 14. Arrows indicate days of injection. (n=4, mean + SEM). Injections and monitoring of the animal's weight was performed by Jana Pöhmerer as part of their veterinary MD studies at Pharmaceutical Biotechnology, LMU.

5. Summary

The Nobel Prize-winning CRISPR/Cas9 technology consisting of the RNA-guided endonuclease Cas9, a single guide RNA (sgRNA), and – optionally - donor DNA in case of homology-directed recombination repair (HDR) can be delivered with different non-viral formats [153, 188]. Constructs encoding the nuclease based on pDNA, on mRNA co-delivered with sgRNA, or direct delivery of the recombinant Cas9 protein with sgRNA as an RNP formulation have been utilized [189-191]. While transient mRNA expression may be perceived as a weakness in some applications, its short-term functionality offers clear advantages, particularly in terms of genetic safety and immunogenicity, for the CRISPR/Cas9 system [152]. The *in vivo* LNP therapy NTLA-2001, which transfers Cas9 mRNA/sgRNA into liver hepatocytes, just entered advanced clinical evaluation in global phase 3 studies [173]. Nevertheless, for applications beyond local administration or delivery into hepatocytes, efficient and safe delivery of the Cas9 system remains a challenge.

Starting point of this thesis was a novel design strategy of sequence-defined xenopeptide carrier libraries by chemical evolution [17, 87, 192, 193]. Notably, different nucleic acid cargos possess differing delivery demands, due to diverse physicochemical properties (lengths and type of nucleic acid) and diverging biological functions and locations such as the cytosol or nucleus [174, 194]. Previously optimized carriers for Cas9/sgRNA RNPs delivery with high efficiency at sub-nanomolar concentration [87, 192] display only moderate RNA delivery potential (our unpublished data). In this work, it was demonstrated that the potency of mRNA carriers and formulations may but need not necessarily be predictive for Cas9 mRNA/sgRNA delivery. Cas9mRNA (4.5kb) is more than twice as large as luciferase mRNA (1.9kb), and co-delivery with smaller sgRNA, and ideally also ssDNA for homology directed repair (HDR) makes it a more demanding cargo. To address this question, a library of recently reported double pH-responsive xenopeptide carriers containing succinoyl tetraethylene pentamine (Stp) and lipo amino fatty acids (LAFs) were evaluated for CRISPR/Cas9 based genome editing. Physicochemical nanoparticle properties of different carrier topologies, variations of LAF/Stp ratios and LAF types as Cas9 mRNA/sgRNA polyplexes were screened and functional biological characteristics in three different reporter cell lines using three different genomic targets (*Pcsk9*, eGFP, *mdx* exon 23) were evaluated. Xenopeptides 1611 (U-shape topology, Stp/LAF ratio 1:2) and 1762 (B2-topology, Stp/LAF 1:4) containing 12- and 10-aminooctanoic acid LAFs, respectively, were identified as best-performing carriers for Cas9 mRNA/sgRNA polyplexes. Remarkable *in vitro* gene editing potency of the top carriers were observed at sub-

nanomolar EC_{50} concentrations of 0.4 nM sgRNA and 0.1 nM sgRNA for the respective U-shape and B2 carriers, even after incubation in full (≥ 90 %) serum. Polyplexes formed with xenopeptide 1611 were identified as the most suitable carrier for the co-delivery of mRNA and DNA. Hence, the polyplexes' potency to co-deliver Cas9 mRNA/sgRNA with a single stranded DNA template for homology directed gene editing was assessed, resulting in up to 38 % conversion of eGFP to BFP in reporter cells. Additionally, a LNP formulation of B2 carrier 1621 was generated. Selected carrier formulations displayed physicochemical and functional stability upon storage at 4 °C and unaffected activity upon incubation in full serum. Importantly, after intravenous administration in mice, Cas9 mRNA/sgRNA formulations successfully demonstrated *in vivo* genome editing that targeted the dystrophin gene exon 23 splice site, thus also triggering alternative mRNA splicing with skipping of exon 23, as observed in cardiac and skeletal muscle and in brain tissue.

6. Appendix

6.1. Supporting Tables

Table S1. Particle characterization by dynamic and electrophoretic light scattering of Cas9 polyplexes.

ID	N/P	LAF	Stp:LAF ratio	Z-Average (nm)		PdI		ZP (mV)	
				mean	SD	mean	SD	mean	SD
Bundles B2									
1621	12	8Oc	1:4	7735.7	767.9	0.57	0.13	-4.0	0.8
	18			201.9	6.0	0.21	0.01	13.2	0.7
	24			134.5	4.0	0.10	0.01	15.9	1.6
1730	12	8Oc	2:4	120.3	4.1	0.22	0.02	7.2	1.1
	18			89.7	1.9	0.10	0.01	-5.4	1.2
	24			99.7	2.2	0.13	0.03	25.9	1.9
1613	24	12Oc	1:4	7180.7	765.5	0.62	0.15	-16.3	1.6
1752	24	12Bu	1:4	259.0	4.0	0.15	0.01	16.4	0.7
1753	24	16Bu	1:4	11409.0	1925.3	0.67	0.41	16.2	0.6
1754	24	12He	1:4	163.2	2.1	0.18	0.03	18.2	1.6
1755	24	14He	1:4	413.1	8.3	0.42	0.01	17.3	2.0
1762	24	10Oc	1:4	170.3	1.5	0.09	0.05	16.7	1.4
U1-shapes									
1611	12	12Oc	1:2	128.6	2.8	0.27	0.01	-1.5	1.4
	18			94.0	3.4	0.14	0.01	32.5	2.2
	24			126.4	3.7	0.35	0.03	34.8	0.8
1718	12	12Oc	1:4	143.9	4.0	0.19	0.01	10.8	2.2
	18			152.3	1.0	0.35	0.03	35.9	0.1
	24			143.9	2.8	0.36	0.04	37.9	0.4
1719	12	12Oc	2:4	100.2	6.5	0.24	0.05	8.4	0.9
	18			79.7	1.7	0.19	0.01	23.0	0.9
	24			75.5	1.9	0.13	0.01	28.5	2.4
1746	18	8Oc	1:2	80.87	1.29	0.159	0.014	17.97	2.02
1763	18	12Bu	1:2	116.07	3.79	0.248	0.01	30.93	1.19
1765	18	12He	1:2	98.14	4.76	0.252	0.023	21.97	0.92
1766	18	14He	1:2	125.17	9.54	0.312	0.018	28.83	1.37
1764	18	16Bu	1:2	129.23	6.89	0.328	0.01	27.07	1.63

U3-shapes									
1612	12		1:4	223.1	4.2	0.12	0.01	-40.0	2.9
	18			271.7	5.8	0.30	0.01	-27.0	1.2
	24			261.0	4.7	0.21	0.03	-20.0	1.4
1722	12		2:4	107.6	8.9	0.20	0.04	8.1	2.4
	18			86.9	2.0	0.14	0.00	11.4	1.7
	24			82.2	2.5	0.13	0.01	34.6	1.8
U4-shapes									
1716	12		1:4	4524.0	364.8	0.11	0.05	5.6	0.5
	18			1341.3	82.0	0.78	0.12	14.9	1.6
	24			250.3	6.9	0.16	0.03	18.4	1.3
1717	12		2:4	122.5	1.7	0.13	0.02	8.0	1.0
	18			86.7	2.1	0.12	0.02	25.3	0.4
	24			124.7	1.1	0.29	0.05	16.1	1.2

Polyplexes were formed with different LAF carriers at indicated N/P ratios resulting in a total RNA concentration of 12.5 ng µL-[1]. Data are presented as mean ± SD (n=3).

Table S2. Particle characterization by dynamic and electrophoretic light scattering of 1611 polyplexes for HDR.

ID	**sgRNA/ssDNA**	**Z-Average**		**Size by number**		**PdI**		**Zeta-potential**	
	ratio	**mean**	**SD**	**mean**	**SD**	**mean**	**SD**	**mean**	**SD**
1611 N/P 18	1:0	84.4	1.5	44.5	3.25	0.23	0.01	30.2	1.3
	1:0.5	86.5	0.1	42.8	1.39	0.29	0.02	26.3	1.9
	1:1	88.5	1.2	38.0	1.58	0.35	0.01	25.7	1.0
	1:2	80.0	0.8	32.1	3.72	0.33	0.00	29.3	1.1

1611 polyplexes at N/P 18 formed with Cas9 mRNA and sgGFP at weight ratio 1:1 and the single stranded DNA template (ssDNA) at indicated ratios of sgRNA:ssDNA. Data are presented as mean ± SD (n=3).

Table S3. Half maximal effective concentration (EC_{50}) of Cas9 mRNA/sgDMD$_{Ex23}$ polyplexes.

	1611 N/P 18	**1621 N/P 24**	**1752 N/P 24**	**1762 N/P 24**
Hepa	1.1 nM sgPcsk9	4.0 nM sgPcsk9	6.5 nM sgPcsk9	4.4 nM sgPcsk9
HeLa	0.7 nM sgDMD$_{Ex23}$	0.2 nM sgDMD$_{Ex23}$	0.4 nM sgDMD$_{Ex23}$	0.1 nM sgDMD$_{Ex23}$
HeLa (serum)	0.4 nM sgDMD$_{Ex23}$	0.1 nM sgDMD$_{Ex23}$	0.2 nM sgDMD$_{Ex23}$	0.1 nM sgDMD$_{Ex23}$

Half maximal effective concentration (EC_{50}), defined as sgRNA concentration resulting in 50 % gene edited cells after treatment with best performing Cas9 polyplexes in in vitro experiments as shown in Figure 5. The first row of the table shows EC_{50} for *Pcsk9* knock out of all treated Hepa 1-6 *Pcsk9*^{tdTomato}. Second and third row show EC_{50} on HeLa mCherry-DMD$_{Ex23}$ cells with carriers without and with dilution in full serum (≥ 90% serum), respectively.

Table S4. Long time stability and particle characterization by dynamic and electrophoretic light scattering of Cas9 mRNA/sgDMD$_{Ex23}$ polyplexes and LNP

ID	Type	N/P	TP	Z-Average (nm)		Size by number (nm)		PdI		Zeta-potential (mV)		EE
			Day	mean	SD	mean	SD	mean	SD	mean	SD	%
1611	Polyplex	18	0	145.7	2.5	73.1	15.0	0.21	0.02	28.1	0.8	96.2
			14	151.7	4.0	57.7	27.3	0.21	0.01	25.6	0.0	96.4
			127	151.4	3.5	52.3	36.2	0.22	0.00	21.8	0.8	NE
1762	Polyplex	24	0	123.4	1.7	55.5	6.5	0.20	0.02	23.1	0.9	95.9
			14	121.7	2.6	47.2	2.8	0.27	0.01	16.5	1.1	99.1
			127	135.7	2.1	63.1	20.3	0.24	0.002	-5.4	1.5	NE
1621	LNP	24	0	105.2	0.9	64.3	7.8	0.19	0.02	4.8	0.4	91.7
			14	118.9	0.2	64.5	12.3	0.22	0.03	3.3	0.1	98.2
			127	111.1	1.9	58.1	6.2	0.24	0.002	1.3	0.7	NE
SM102	LNP	6	0	165.9	2.1	124.4	5.5	0.09	0.01	-0.9	0.0	86.6
			14	175.4	2.4	136.1	9.4	0.15	0.02	-3.9	2.5	96.3
			127	143.2	1.7	90.4	2.7	0.15	0.00	-1.8	0.4	NE

Nanoparticles were formed with different LAF carriers at indicated N/P ratios resulting in a total RNA concentration of 200 ng μL^{-1} for 1611 polyplexes and 60 ng μL^{-1} for all other formulations. All formulations were stored at 4 °C until determined time points and were diluted with HBG to a total RNA concentration of 12.5 ng μL^{-1} for size and zeta potential measurements. LNP compositions see Experimental part section 2.6. (n=3, mean ± SD). NE: not evaluated; EE: encapsulation efficiency

Table S5. Particle characterization by dynamic and electrophoretic light scattering of luciferase mRNA LNP.

ID	N/P	Z-Average (nm)		Size by number (nm)		PdI		Zeta-potential (mV)	
		mean	SD	mean	SD	mean	SD	mean	SD
SM102	6	150.5	2.0	105.4	1.1	0.13	0.02	-1.1	0.4
1621	18	115.7	2.7	51.5	0.2	0.23	0.01	2.5	1.0
	24	107.7	1.3	61.6	1.3	0.21	0.01	2.4	0.6

Nanoparticles were formed with different LAF carriers at indicated N/P ratios resulting in a mRNA concentration of 6.7 ng μL^{-1}. LNP compositions see Experimental section. Data are presented as mean ± SD (n=3).

Table S6. Particle characterization by dynamic and electrophoretic light scattering of Cas9 mRNA/sgDMD$_{Ex23}$ LNP

ID	N/P	Z-Average (nm)		Size by number (nm)		PdI		Zeta-potential (mV)	
		mean	SD	mean	SD	mean	SD	mean	SD
SM102	6	152.1	2.4	104.4	7.4	0.15	0.01	-2.5	0.1
1621	18	110.3	0.9	77.3	3.9	0.15	0.02	4.5	0.8
	24	107.5	1.4	57.5	3.3	0.17	0.03	5.6	0.7

Nanoparticles were formed with different LAF carriers at indicated N/P ratios resulting in a mRNA concentration of 6.7 ng μL^{-1}. LNP compositions see Experimental part section 2.6. Data are presented as mean ± SD (n=3).

Table S7. Particle characterization by dynamic and electrophoretic light scattering of luciferase mRNA polyplexes and LNP for intramuscular injections.

ID	Type	N/P	Z-Average (nm)		Size by number (nm)		PdI		Zeta-potential (mV)		EE
			mean	SD	mean	SD	mean	SD	mean	SD	%
SM102	LNP	6	226.6	4.9	181.0	6.3	0.11	0.00	-1.09	0.67	89.1
1621	LNP	24	107.9	1.2	65.4	6.9	0.16	0.04	6.04	0.80	90.3
1611	Polyplex	18	145.7	3.5	58.8	25.0	0.24	0.00	29.63	1.10	NE
		24	156.5	2.5	62.0	15.0	0.24	0.01	28.43	0.67	NE
1621	Polyplex	24	122.7	0.7	65.12	7.0	0.24	0.01	25.67	0.90	NE
1752	Polyplex	24	144.2	1.8	51.3	29.4	0.18	0.01	15.93	0.57	NE
1762	Polyplex	24	105.7	2.2	40.9	14.6	0.21	0.02	26.20	0.95	NE

Nanoparticles were formed with different LAF carriers at indicated N/P ratios resulting in a mRNA concentration of 60 ng µL-^{1}. All formulations were diluted with HBG to a mRNA concentration of 12.5 ng µL^{-1} for size and zeta potential measurements. LNP compositions see Experimental section 2.6. Data are presented as mean ± SD (n=3). NE: not evaluated.

Table S8. *in vivo* editing of dystrophin gene after intravenous application

ID		Splicing modulation		Genomic evaluation		Splicing modulation		Genomic evaluation		Splicing modulation		Genomic evaluation	
	No	(%)	mean ± SD	(%)	mean ± SD	(%)	mean ± SD	(%)	mean ± SD	(%)	mean ± SD	(%)	mean ± SD
		brain				heart				muscle			
1762	#1	9.4	13.1 ± 4.4	2.7	4.7 ± 2.0	1.1	1.6 ± 1.2	2.3	2.9 ± 0.8	8.8	9.0 ± 5.1	2.6	2.8 ± 0.7
	#2	14.1		4.8		2.6		2.5		16.4		2.2	
	#3	10.1		3.9		0.0		2.6		5.6		2.6	
	#4	18.9		7.5		2.4		4.0		5.4		3.9	
1611	#1	11.7	6.1 ± 5.2	4.1	3.4 ± 0.7	2.6	1.4 ± 0.8	2.8	2.5 ± 0.9	0.2	8.7 ±7.4	2.8	3.4 ± 0.8
	#2	2.3		3.9		0.8		2.9		5.9		4.6	
	#3	1.1		2.5		1.3		1.2		17.3		3.2	
	#4	9.3		3.2		0.8		3.0		11.6		3.0	
1621- LNP	#1	11.6	5.1 ± 6.0	3.1	3.1 ± 0.6	5.9	5.7 ± 1.1	5.1	3.6 ± 1.2	11.2	3.5 ±5.2	6.6	3.6 ±2.2
	#2	0.0		2.4		5.8		3.1		0.8		2.4	
	#3	8.7		3.9		6.9		2.4		0.0		1.7	
	#4	0.0		2.9		4.3		3.9		1.9		3.8	
untreated	#1	1.3	1.0 ± 0.5	0.3	0.6 ± 0.6	1.6	1.7 ± 0.2	0.1	0.7 ± 0.4	1.1	0.7 ± 0.5	0.4	0.7 ± 0.2
	#2	0.3		0.6		1.7		1.0		0.6		0.8	
	#3	1.3		1.5		2.0		0.6		0.0		0.9	
	#4	0.9		0.1		1.6		0.9		1.0		0.6	

In vivo mRNA splicing modulation and genome editing in BALB/c mice after intravenous injection with Cas9 polyplexes and Cas9 LNP as shown in **Fig. 6**. Splicing modulation was determined using ImageJ Software. Genomic evaluation was performed by Sanger sequencing and subsequent evaluation of total editing efficiency with the TIDE analysis tool (https://tide.nki.nl/). All data are presented in percent for individual animals and mean ± SD (n=4).

Table S9. *in vivo* editing of dystrophin gene after intramuscular application

ID		Splicing modulation		Genomic evaluation		Splicing modulation		Genomic evaluation	
	No	(%)	mean ± SD	(%)	mean ± SD	(%)	mean ± SD	(%)	mean ± SD
		triple application				single application			
1762	#1	8.8	9.0 ± 5.1	4.4	3.4 ± 0.7	0.0	2.5 ± 4.9	1.2	1.7 ± 0.8
	#2	16.4		3.2		0.0		0.7	
	#3	5.6		2.8		0.0		1.8	
	#4	5.4		3.0		9.9		3.2	
1611	#1	7.5	9.3 ± 4.9	3.2	3.3 ± 0.2	1.2	1.0 ± 1.0	0.3	1.1 ± 0.6
	#2	4.4		3.1		0.6		1.8	
	#3	9.3		3.5		2.3		1.0	
	#4	16.0		3.5		0.0		1.2	
1621- LNP	#1	4.5	6.0 ± 4.5	2.8	2.4 ± 1.4	0.0	0.0 ± 0.0	0.0	0.7 ± 0.6
	#2	5.2		2.8		0.0		1.2	
	#3	12.3		3.5		0.0		1.0	
	#4	1.8		0.4		0.0		0.4	
SM-102 -LNP	#1	15.2	6.7 ± 6.4	4.0	2.3 ± 1.5	1.4	2.1 ± 3.4	1.2	1.7 ± 0.9
	#2	8.1		3.1		7.1		2.9	
	#3	1.7		1.2		0.0		1.0	
	#4	1.7		0.8		0.0		1.5	

In vivo mRNA splicing modulation and genome editing in BALB/c mice after triple and single intramuscular injection with Cas9 polyplexes and Cas9 LNP as shown in **Fig. 7**. Splicing modulation was determined using ImageJ Software. Genomic evaluation was performed by Sanger sequencing and subsequent evaluation of total editing efficiency with the TIDE analysis tool (https://tide.nki.nl/). All data are presented in percent for individual animals and mean ± SD (n=4).

6.2. Abbreviations

Abbreviation	
° C	degree Celsius
µg, µL	microgram(s), microliter(s)
ALT	alanine aminotransferase
ASO	antisense oligonucleotide
AST	aspartate aminotransferase
ATP	adenosine triphosphate
BUN	blood urea nitrogen
bp	base pairs
Cas 9	CRISPR (Clustered Regularly Interspaced Short Palindromic Repeats) associated protein 9
CAR T cell	Chimeric antigen receptor T cell
cDNA	complementary DNA
CLSM	confocal laser scanning microscope
CPP	cell penetrating peptide
Crea	creatinine
cSNP	coding single-nucleotide polymorphisms
Ctrl	control
DAPI	4′,6-diamidino-2-phenylindole
DBCO-NHS	dibenzocyclooctyne-N-hydroxysuccinimidyl
DMD	Duchenne Muscular Dystrophy
DMDEx23	Duchenne Muscular Dystrophy exon 23
DMEM	Dulbecco’s Modified Eagle’s Medium
DMSO	dimethyl sulfoxide
DNA	deoxyribonucleic acid
dsRNA	double-stranded RNA
EDTA	ethylenediaminetetraacetic acid
e.g.	exempli gratia (for example)
eGFP	enhanced green fluorescent protein
EMA	European Medicine Agency
EtOH	ethanol
Ex23	exon 23

FACS	fluorescence-activated cell sorting
FBS	fetal bovine serum
FDA	Food and Drug Administration- U.S. federal agency of the department of health and human services
fwd	forward
GFPd2	destabilized green fluorescent protein
HBG	HEPES-buffered glucose
HCl	hydrochloric acid solution
HEPES	N-(2-hydroxethyl) piperazine-N‘-(2-ethansulfonic acid)
i.e.	id est (that is)
i.m.	intramuscular(ly)
i.v.	Intravenous(ly)
kDa	kilodalton
KO	knock out
LAF	lipo amino fatty acid
LAR buffer	Luciferase Asssay Reagent buffer
Luc	luciferase
mg, mm	milligram(s), millimeter(s)
miRNA	microRNA
mRNA	messenger RNA
MTBE	methyl tert-butyl ether
MTT	3-(4,5-dimethylthiazol-2-yl)-2,5-diphenyltetrazolium bromide
n	number of samples
N/P	carrier nitrogen to nucleic acid phosphate ratio
NA	nucleic acid
nM	nanomolar
OAA	oligoamidoamide
PBS	phosphate-buffered saline
PCR	polymerase chain reaction
pDNA	plasmid deoxyribonucleic acid
PEG	polyethylene gycol
PFA	paraformaldehyde
Ph.D.	Doctor of Philosophy

PMO	phosphorodiamidate morpholino oligomer
pre-mRNA	precursor-mRNA
rev	reverse
RNA	ribonucleic acid
RNAi	RNA interference
RNP	ribonucleoprotein
rpm	revolutions per minute
RT	room temperature
SD	standard deviation
sec	second
sgRNA	single guide RNA
siRNA	short interfering RNA
succPEI	succinyl polethylenimine
SPPS	solid-phase peptide synthesis
SSO	splice switching oligonucleotide
Stp	succinyl-tetraethylene pentamine
TE	trypsin/EDTA
TIDE	tracking of indels by decomposition
TLR	Toll-like receptors
w/w	weight to weight ratio
wt	wild type

6.3. Plasmid Maps and Reporter Gene Sequence

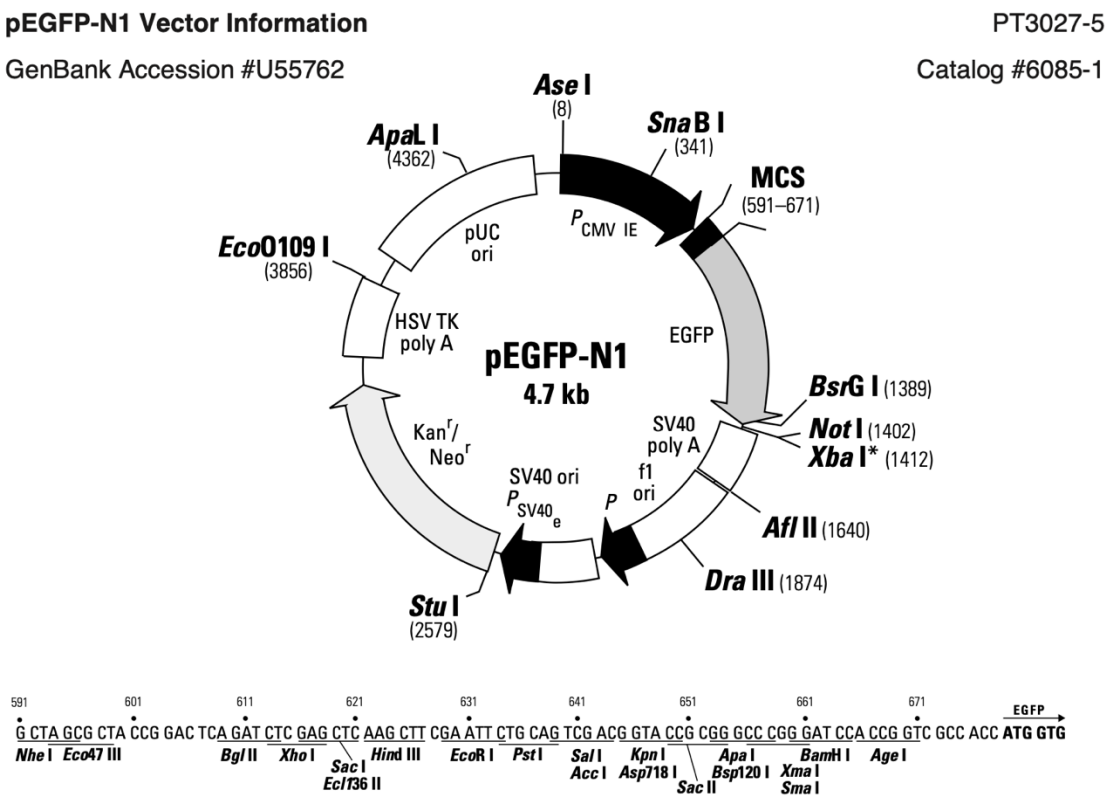

Figure 37 Plasmid map of pEGFP-N1.

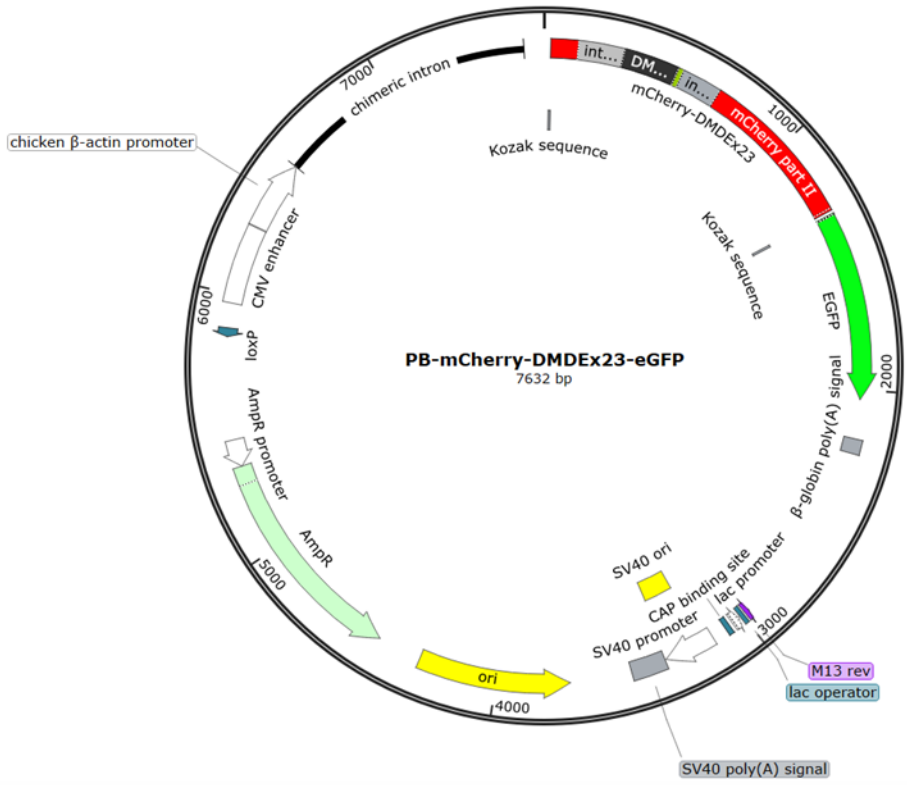

Figure 38 Plasmid map of PB-mCherry-DMDEx23-eGFP. Deposited at Addgene (#211366).

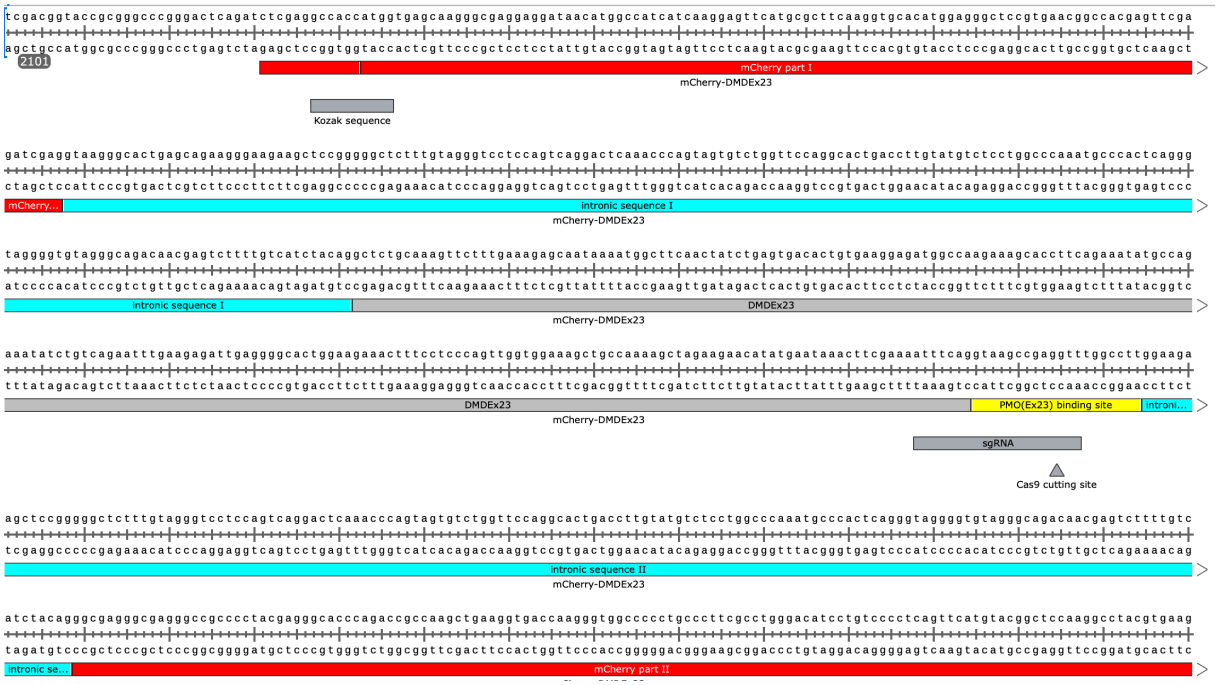

Figure 39 Sequence of the reporter gene mCherry-DMDEx23 with separate section labels and PMO(Ex23) binding site.

7. References

[1] B. Arjmand, B. Larijani, M. Sheikh Hosseini, M. Payab, K. Gilany, P. Goodarzi, P. Parhizkar Roudsari, M. Amanollahi Baharvand, N.s. Hoseini Mohammadi, The horizon of gene therapy in modern medicine: advances and challenges, Cell Biology and Translational Medicine, Volume 8: Stem Cells in Regenerative Medicine, (2020) 33-64.
[2] H.L. Malech, E.K. Garabedian, M.M. Hsieh, Evolution of Gene Therapy, Historical Perspective, Hematology/Oncology Clinics, 36 (2022) 627-645.
[3] J.A. Wolff, J. Lederberg, An early history of gene transfer and therapy, Human Gene Therapy, 5 (1994) 469-480.
[4] R.M. Blaese, Development of gene therapy for immunodeficiency: adenosine deaminase deficiency, Pediatric research, 33 (1993) S49-S55.
[5] ASGCT Gene, Cell, & RNA Therapy Landscape Report, in, 2023.
[6] K. Bulaklak, C.A. Gersbach, The once and future gene therapy, Nature Communications, 11 (2020) 5820.
[7] E.S. Lander, L.M. Linton, B. Birren, C. Nusbaum, M.C. Zody, J. Baldwin, K. Devon, K. Dewar, M. Doyle, W. FitzHugh, et al., Initial sequencing and analysis of the human genome, Nature, 409 (2001) 860-921.
[8] I.H.G.S. Consortium, Initial sequencing and analysis of the human genome, nature, 409 (2001) 860-921.
[9] J.-P. Gillet, B. Macadangdang, R.L. Fathke, M.M. Gottesman, C. Kimchi-Sarfaty, The development of gene therapy: from monogenic recessive disorders to complex diseases such as cancer, Gene Therapy of Cancer: Methods and Protocols, (2009) 5-54.
[10] U. Lächelt, E. Wagner, Nucleic Acid Therapeutics Using Polyplexes: A Journey of 50 Years (and Beyond), Chemical Reviews, 115 (2015) 11043-11078.
[11] M.L. Maeder, C.A. Gersbach, Genome-editing technologies for gene and cell therapy, Molecular Therapy, 24 (2016) 430-446.
[12] J.A. Doudna, E. Charpentier, The new frontier of genome engineering with CRISPR-Cas9, Science, 346 (2014) 1258096.
[13] M.K.K. Azhagiri, P. Babu, V. Venkatesan, S. Thangavel, Homology-directed gene-editing approaches for hematopoietic stem and progenitor cell gene therapy, Stem Cell Research & Therapy, 12 (2021) 1-12.
[14] J.T. Bulcha, Y. Wang, H. Ma, P.W. Tai, G. Gao, Viral vector platforms within the gene therapy landscape, Signal transduction and targeted therapy, 6 (2021) 53.
[15] C.E. Thomas, A. Ehrhardt, M.A. Kay, Progress and problems with the use of viral vectors for gene therapy, Nature Reviews Genetics, 4 (2003) 346-358.
[16] B.B. Mendes, J. Conniot, A. Avital, D. Yao, X. Jiang, X. Zhou, N. Sharf-Pauker, Y. Xiao, O. Adir, H. Liang, Nanodelivery of nucleic acids, Nature Reviews Methods Primers, 2 (2022) 24.
[17] F. Freitag, E. Wagner, Optimizing synthetic nucleic acid and protein nanocarriers: The chemical evolution approach, Advanced Drug Delivery Reviews, 168 (2021) 30-54.
[18] P.R. Cullis, M.J. Hope, Lipid Nanoparticle Systems for Enabling Gene Therapies, Mol Ther, 25 (2017) 1467-1475.
[19] U. Sahin, K. Karikó, Ö. Türeci, mRNA-based therapeutics—developing a new class of drugs, Nature reviews Drug discovery, 13 (2014) 759-780.
[20] H. Büning, Gene therapy enters the pharma market: the short story of a long journey, EMBO molecular medicine, 5 (2013) 1-3.
[21] S. Russell, J. Bennett, J.A. Wellman, D.C. Chung, Z.-F. Yu, A. Tillman, J. Wittes, J. Pappas, O. Elci, S. McCague, Efficacy and safety of voretigene neparvovec (AAV2-hRPE65v2) in patients with RPE65-mediated inherited retinal dystrophy: a randomised, controlled, open-label, phase 3 trial, The Lancet, 390 (2017) 849-860.
[22] S.M. Hoy, Onasemnogene abeparvovec: first global approval, Drugs, 79 (2019) 1255-1262.
[23] T. Asmamaw Dejenie, M. Tiruneh G/Medhin, G. Dessie Terefe, F. Tadele Admasu, W. Wale Tesega, E. Chekol Abebe, Current updates on generations, approvals, and clinical trials of CAR T-cell therapy, Human Vaccines & Immunotherapeutics, 18 (2022) 2114254.
[24] L. Schoenmaker, D. Witzigmann, J.A. Kulkarni, R. Verbeke, G. Kersten, W. Jiskoot, D.J.A. Crommelin, mRNA-lipid nanoparticle COVID-19 vaccines: Structure and stability, Int J Pharm, 601 (2021) 120586.
[25] S.S. Cargill, A. Eidsvik, M. Lamm, Updating the ethical guidance for gene and cell therapy research participation, Molecular Therapy, 29 (2021) 2394-2395.
[26] D. Drago, B. Foss-Campbell, K. Wonnacott, D. Barrett, A. Ndu, Global regulatory progress in delivering on the promise of gene therapies for unmet medical needs, Molecular Therapy-Methods & Clinical Development, 21 (2021) 524-529.
[27] A.W.T. Muigai, Expanding global access to genetic therapies, Nature Biotechnology, 40 (2022) 20-21.
[28] M.R. Cring, V.C. Sheffield, Gene therapy and gene correction: targets, progress, and challenges for treating human diseases, Gene therapy, 29 (2022) 3-12.

[29] W. Sun, Q. Shi, H. Zhang, K. Yang, Y. Ke, Y. Wang, L. Qiao, Advances in the techniques and methodologies of cancer gene therapy, Discov Med, 27 (2019) 45-55.
[30] A.J. Hinrich, F.M. Jodelka, J.L. Chang, D. Brutman, A.M. Bruno, C.A. Briggs, B.D. James, G.E. Stutzmann, D.A. Bennett, S.A. Miller, F. Rigo, R.A. Marr, M.L. Hastings, Therapeutic correction of ApoER2 splicing in Alzheimer's disease mice using antisense oligonucleotides, EMBO Molecular Medicine, 8 (2016) 328-345.
[31] C. Seymour, Cancer Vaccine mRNA-4157 Improves Recurrence-Free Survival for Patients With High-Risk Melanoma.
[32] N. Jain, U. Nagaich, M. Pandey, D.K. Chellappan, K. Dua, Predictive genomic tools in disease stratification and targeted prevention: a recent update in personalized therapy advancements, EPMA Journal, 13 (2022) 561-580.
[33] S. Grabbe, H. Haas, M. Diken, L.M. Kranz, P. Langguth, U. Sahin, Translating nanoparticulate-personalized cancer vaccines into clinical applications: case study with RNA-lipoplexes for the treatment of melanoma, Nanomedicine, 11 (2016) 2723-2734.
[34] T. Wei, Q. Cheng, L. Farbiak, D.G. Anderson, R. Langer, D.J. Siegwart, Delivery of tissue-targeted scalpels: opportunities and challenges for in vivo CRISPR/Cas-based genome editing, ACS nano, 14 (2020) 9243-9262.
[35] S. Deng, H. Liang, P. Chen, Y. Li, Z. Li, S. Fan, K. Wu, X. Li, W. Chen, Y. Qin, Viral vector vaccine development and application during the COVID-19 pandemic, Microorganisms, 10 (2022) 1450.
[36] T.M. Allen, P.R. Cullis, Drug delivery systems: entering the mainstream, Science, 303 (2004) 1818-1822.
[37] S. Mitragotri, J. Lahann, Materials for drug delivery: innovative solutions to address complex biological hurdles, (2012).
[38] U. Lächelt, E. Wagner, Nucleic Acid Therapeutics Using Polyplexes: A Journey of 50 Years (and Beyond), Chemical reviews, 115 (2015) 11043-11078.
[39] M. Chamundeeswari, J. Jeslin, M.L. Verma, Nanocarriers for drug delivery applications, Environmental Chemistry Letters, 17 (2019) 849-865.
[40] R. Dewey, G. Morrissey, C. Cowsill, D. Stone, F. Bolognani, N. Dodd, T. Southgate, D. Klatzmann, H. Lassmann, M. Castro, Chronic brain inflammation and persistent herpes simplex virus 1 thymidine kinase expression in survivors of syngeneic glioma treated by adenovirus-mediated gene therapy: implications for clinical trials, Nature medicine, 5 (1999) 1256-1263.
[41] H. Xu, Z. Li, J. Si, Nanocarriers in gene therapy: a review, Journal of biomedical nanotechnology, 10 (2014) 3483-3507.
[42] H. Yin, R.L. Kanasty, A.A. Eltoukhy, A.J. Vegas, J.R. Dorkin, D.G. Anderson, Non-viral vectors for gene-based therapy, Nature Reviews Genetics, 15 (2014) 541-555.
[43] A. Srivastava, In vivo tissue-tropism of adeno-associated viral vectors, Current opinion in virology, 21 (2016) 75-80.
[44] R. Waehler, S.J. Russell, D.T. Curiel, Engineering targeted viral vectors for gene therapy, Nature reviews genetics, 8 (2007) 573-587.
[45] M. Cavazzana-Calvo, A. Thrasher, F. Mavilio, The future of gene therapy, Nature, 427 (2004) 779-781.
[46] L. Smith, J.F. Byers, Gene therapy in the post-Gelsinger era, JONA'S healthcare law, ethics and regulation, 4 (2002) 104-110.
[47] S. Hager, E. Wagner, Bioresponsive polyplexes - chemically programmed for nucleic acid delivery, Expert Opin Drug Deliv, 15 (2018) 1067-1083.
[48] T. Luo, H. Liang, R. Jin, Y. Nie, Virus-inspired and mimetic designs in non-viral gene delivery, The journal of gene medicine, 21 (2019) e3090.
[49] Y. Cheng, R.C. Yumul, S.H. Pun, Virus-Inspired Polymer for Efficient In Vitro and In Vivo Gene Delivery, Angew Chem Int Ed Engl, 55 (2016) 12013-12017.
[50] D.P. Feldmann, Y. Cheng, R. Kandil, Y. Xie, M. Mohammadi, H. Harz, A. Sharma, D.J. Peeler, A. Moszczynska, H. Leonhardt, S.H. Pun, O.M. Merkel, In vitro and in vivo delivery of siRNA via VIPER polymer system to lung cells, Journal of controlled release : official journal of the Controlled Release Society, 276 (2018) 50-58.
[51] A.-M. Caminade, C.-O. Turrin, Dendrimers for drug delivery, Journal of Materials Chemistry B, 2 (2014) 4055-4066.
[52] C. Jiang, J. Chen, Z. Li, Z. Wang, W. Zhang, J. Liu, Recent advances in the development of polyethylenimine-based gene vectors for safe and efficient gene delivery, Expert Opinion on Drug Delivery, 16 (2019) 363-376.
[53] A. Zintchenko, A. Philipp, A. Dehshahri, E. Wagner, Simple Modifications of Branched PEI Lead to Highly Efficient siRNA Carriers with Low Toxicity, Bioconjugate Chemistry, 19 (2008) 1448-1455.
[54] M. Prabaharan, J. Mano, Chitosan-based particles as controlled drug delivery systems, Drug delivery, 12 (2004) 41-57.
[55] N.S. Templeton, D.D. Lasic, New directions in liposome gene delivery, Molecular biotechnology, 11 (1999) 175-180.
[56] S. Siddique, J.C. Chow, Gold nanoparticles for drug delivery and cancer therapy, Applied Sciences, 10 (2020) 3824.

[57] Y. Zhou, G. Quan, Q. Wu, X. Zhang, B. Niu, B. Wu, Y. Huang, X. Pan, C. Wu, Mesoporous silica nanoparticles for drug and gene delivery, Acta pharmaceutica sinica B, 8 (2018) 165-177.
[58] Y. Zhao, L. Huang, Lipid nanoparticles for gene delivery, Advances in genetics, 88 (2014) 13-36.
[59] M. Karimi, N. Solati, A. Ghasemi, M.A. Estiar, M. Hashemkhani, P. Kiani, E. Mohamed, A. Saeidi, M. Taheri, P. Avci, Carbon nanotubes part II: a remarkable carrier for drug and gene delivery, Expert opinion on drug delivery, 12 (2015) 1089-1105.
[60] S. Ren, M. Wang, C. Wang, Y. Wang, C. Sun, Z. Zeng, H. Cui, X. Zhao, Application of non-viral vectors in drug delivery and gene therapy, Polymers, 13 (2021) 3307.
[61] D. Adams, A. Gonzalez-Duarte, W.D. O'Riordan, C.-C. Yang, M. Ueda, A.V. Kristen, I. Tournev, H.H. Schmidt, T. Coelho, J.L. Berk, Patisiran, an RNAi therapeutic, for hereditary transthyretin amyloidosis, New england journal of medicine, 379 (2018) 11-21.
[62] P.S. Kowalski, A. Rudra, L. Miao, D.G. Anderson, Delivering the Messenger: Advances in Technologies for Therapeutic mRNA Delivery, Mol Ther, 27 (2019) 710-728.
[63] Q. Cheng, T. Wei, L. Farbiak, L.T. Johnson, S.A. Dilliard, D.J. Siegwart, Selective organ targeting (SORT) nanoparticles for tissue-specific mRNA delivery and CRISPR–Cas gene editing, Nature nanotechnology, 15 (2020) 313-320.
[64] J.C. Kaczmarek, K.J. Kauffman, O.S. Fenton, K. Sadtler, A.K. Patel, M.W. Heartlein, F. DeRosa, D.G. Anderson, Optimization of a Degradable Polymer-Lipid Nanoparticle for Potent Systemic Delivery of mRNA to the Lung Endothelium and Immune Cells, Nano letters, 18 (2018) 6449-6454.
[65] P.R. Cullis, M.J. Hope, Lipid nanoparticle systems for enabling gene therapies, Molecular Therapy, 25 (2017) 1467-1475.
[66] S.-D. Li, L. Huang, Pharmacokinetics and Biodistribution of Nanoparticles, Molecular Pharmaceutics, 5 (2008) 496-504.
[67] P.L. Felgner, Y. Barenholz, J.P. Behr, S.H. Cheng, P. Cullis, L. Huang, J.A. Jessee, L. Seymour, F. Szoka, A.R. Thierry, E. Wagner, G. Wu, Nomenclature for synthetic gene delivery systems, Hum Gene Ther, 8 (1997) 511-512.
[68] N. Yoshinaga, S. Uchida, A. Dirisala, M. Naito, K. Osada, H. Cabral, K. Kataoka, mRNA loading into ATP-responsive polyplex micelles with optimal density of phenylboronate ester crosslinking to balance robustness in the biological milieu and intracellular translational efficiency, Journal of Controlled Release, 330 (2021) 317-328.
[69] A.S. Piotrowski-Daspit, A.C. Kauffman, L.G. Bracaglia, W.M. Saltzman, Polymeric vehicles for nucleic acid delivery, Advanced drug delivery reviews, 156 (2020) 119-132.
[70] A.K. Blakney, G. Yilmaz, P.F. McKay, C.R. Becer, R.J. Shattock, One Size Does Not Fit All: The Effect of Chain Length and Charge Density of Poly(ethylene imine) Based Copolymers on Delivery of pDNA, mRNA, and RepRNA Polyplexes, Biomacromolecules, 19 (2018) 2870-2879.
[71] A.C. Kauffman, A.S. Piotrowski-Daspit, K.H. Nakazawa, Y. Jiang, A. Datye, W.M. Saltzman, Tunability of Biodegradable Poly(amine- co-ester) Polymers for Customized Nucleic Acid Delivery and Other Biomedical Applications, Biomacromolecules, 19 (2018) 3861-3873.
[72] L. Peng, E. Wagner, Polymeric Carriers for Nucleic Acid Delivery: Current Designs and Future Directions, Biomacromolecules, 20 (2019) 3613-3626.
[73] J. Germer, E. Wagner, Polymer-Based Nonviral Nucleic Acid Delivery and Genome Editing, in: Molecular Analyses, CRC Press, 2022, pp. 165-182.
[74] R. Kircheis, L. Wightman, A. Schreiber, B. Robitza, V. Rössler, M. Kursa, E. Wagner, Polyethylenimine/DNA complexes shielded by transferrin target gene expression to tumors after systemic application, Gene Ther, 8 (2001) 28-40.
[75] Y. Xie, N.H. Kim, V. Nadithe, D. Schalk, A. Thakur, A. Kılıç, L.G. Lum, D.J. Bassett, O.M. Merkel, Targeted delivery of siRNA to activated T cells via transferrin-polyethylenimine (Tf-PEI) as a potential therapy of asthma, Journal of Controlled Release, 229 (2016) 120-129.
[76] S. Abbasi, S. Uchida, K. Toh, T.A. Tockary, A. Dirisala, K. Hayashi, S. Fukushima, K. Kataoka, Co-encapsulation of Cas9 mRNA and guide RNA in polyplex micelles enables genome editing in mouse brain, Journal of Controlled Release, 332 (2021) 260-268.
[77] D. Schaffert, N. Badgujar, E. Wagner, Novel Fmoc-Polyamino Acids for Solid-Phase Synthesis of Defined Polyamidoamines, Organic Letters, 13 (2011) 1586-1589.
[78] D. Schaffert, C. Troiber, E.E. Salcher, T. Fröhlich, I. Martin, N. Badgujar, C. Dohmen, D. Edinger, R. Kläger, G. Maiwald, Solid-phase synthesis of sequence-defined T-, i-, and U-shape polymers for pDNA and siRNA delivery, Angewandte Chemie International Edition, 50 (2011) 8986-8989.
[79] A.K. Levačić, S. Berger, J. Müller, A. Wegner, U. Lächelt, C. Dohmen, C. Rudolph, E. Wagner, Dynamic mRNA polyplexes benefit from bioreducible cleavage sites for in vitro and in vivo transfer, Journal of Controlled Release, 339 (2021) 27-40.
[80] C. Scholz, E. Wagner, Therapeutic plasmid DNA versus siRNA delivery: common and different tasks for synthetic carriers, Journal of controlled release, 161 (2012) 554-565.
[81] P. Kos, U. Lächelt, A. Herrmann, F.M. Mickler, M. Döblinger, D. He, A.K. Levačić, S. Morys, C. Bräuchle, E. Wagner, Histidine-rich stabilized polyplexes for cMet-directed tumor-targeted gene transfer, Nanoscale, 7 (2015) 5350-5362.

[82] S. Wang, S. Reinhard, C. Li, M. Qian, H. Jiang, Y. Du, U. Lächelt, W. Lu, E. Wagner, R. Huang, Antitumoral cascade-targeting ligand for IL-6 receptor-mediated gene delivery to glioma, Molecular Therapy, 25 (2017) 1556-1566.
[83] C. Troiber, D. Edinger, P. Kos, L. Schreiner, R. Klager, A. Herrmann, E. Wagner, Stabilizing effect of tyrosine trimers on pDNA and siRNA polyplexes, Biomaterials, 34 (2013) 1624-1633.
[84] J. Luo, J. Schmaus, M. Cui, E. Hörterer, U. Wilk, M. Höhn, M. Däther, S. Berger, T. Benli-Hoppe, L. Peng, Hyaluronate siRNA nanoparticles with positive charge display rapid attachment to tumor endothelium and penetration into tumors, Journal of Controlled Release, 329 (2021) 919-933.
[85] J. Kuhn, Y. Lin, A. Krhac Levacic, N. Al Danaf, L. Peng, M. Hohn, D.C. Lamb, E. Wagner, U. Lachelt, Delivery of Cas9/sgRNA Ribonucleoprotein Complexes via Hydroxystearyl Oligoamino Amides, Bioconjug Chem, 31 (2020) 729-742.
[86] Y. Lin, X. Luo, T. Burghardt, S. Dorrer, M. Höhn, E. Wagner, U. Lächelt, Chemical Evolution of Amphiphilic Xenopeptides for Potentiated Cas9 Ribonucleoprotein Delivery, Journal of the American Chemical Society, (2023).
[87] Y. Lin, U. Wilk, J. Pöhmerer, E. Hörterer, M. Höhn, X. Luo, H. Mai, E. Wagner, U. Lächelt, Folate Receptor-Mediated Delivery of Cas9 RNP for Enhanced Immune Checkpoint Disruption in Cancer Cells, Small, 19 (2023) 2205318.
[88] S. Thalmayr, M. Grau, L. Peng, J. Pöhmerer, U. Wilk, P. Folda, M. Yazdi, E. Weidinger, T. Burghardt, M. Höhn, Molecular Chameleon Carriers for Nucleic Acid Delivery: The Sweet Spot Between Lipoplexes and Polyplexes, Advanced Materials, 2211105.
[89] F. Haase, J. Pöhmerer, M. Yazdi, M. Grau, Y. Zeyn, U. Wilk, T. Burghardt, M. Höhn, C. Hieber, M. Bros, Lipoamino bundle LNPs for efficient mRNA transfection of dendritic cells and macrophages show high spleen selectivity, European Journal of Pharmaceutics and Biopharmaceutics, (2023).
[90] D.H. Martínez-Puente, J.J. Pérez-Trujillo, L.M. Zavala-Flores, A. García-García, A. Villanueva-Olivo, H. Rodríguez-Rocha, J. Valdés, O. Saucedo-Cárdenas, R. Montes de Oca-Luna, M.J. Loera-Arias, Plasmid DNA for Therapeutic Applications in Cancer, Pharmaceutics, 14 (2022).
[91] C.L. Hardee, L.M. Arévalo-Soliz, B.D. Hornstein, L. Zechiedrich, Advances in Non-Viral DNA Vectors for Gene Therapy, Genes (Basel), 8 (2017).
[92] L.K. Nyberg, S. Quaderi, G. Emilsson, N. Karami, E. Lagerstedt, V. Müller, C. Noble, S. Hammarberg, A.N. Nilsson, F. Sjöberg, J. Fritzsche, E. Kristiansson, L. Sandegren, T. Ambjörnsson, F. Westerlund, Rapid identification of intact bacterial resistance plasmids via optical mapping of single DNA molecules, Scientific Reports, 6 (2016) 30410.
[93] H. Schreier, The new frontier: gene and oligonucleotide therapy, Pharmaceutica Acta Helvetiae, 68 (1994) 145-159.
[94] M. Schleef, Minicircle and miniplasmid dna vectors: the future of non-viral and viral gene transfer, John Wiley & Sons, 2013.
[95] M. Wilke, E. Fortunati, M. Van Den Broek, A. Hoogeveen, B. Scholte, Efficacy of a peptide-based gene delivery system depends on mitotic activity, Gene therapy, 3 (1996) 1133-1142.
[96] M. Sadelain, Insertional oncogenesis in gene therapy: how much of a risk?, Gene Therapy, 11 (2004) 569.
[97] H. Zhao, H. Hemmi, S. Akira, S.H. Cheng, R.K. Scheule, N.S. Yew, Contribution of Toll-like receptor 9 signaling to the acute inflammatory response to nonviral vectors, Molecular Therapy, 9 (2004) 241-248.
[98] S. Tahmasebi, N. Sonenberg, J.W.B. Hershey, M.B. Mathews, Protein Synthesis and Translational Control: A Historical Perspective, Cold Spring Harbor Perspectives in Biology, 11 (2019).
[99] S. Hocine, R.H. Singer, D. Grünwald, RNA processing and export, Cold Spring Harbor Perspectives in Biology, 2 (2010) a000752.
[100] S. Shuman, Structure, mechanism, and evolution of the mRNA capping apparatus, Progress in Nucleic Acid Research and Molecular Biology, 66 (2001) 1-40.
[101] C.L. Hsu, A. Stevens, Yeast cells lacking 5'-->3' exoribonuclease 1 contain mRNA species that are poly(A) deficient and partially lack the 5' cap structure, Molecular and Cellular Biology, 13 (1993) 4826-4835.
[102] D.D. Licatalosi, R.B. Darnell, RNA processing and its regulation: global insights into biological networks, Nature Reviews Genetics, 11 (2010) 75-87.
[103] D.R. Drummond, J. Armstrong, A. Colman, The effect of capping and polyadenylation on the stability, movement and translation of synthetic messenger RNAs in Xenopus oocytes, Nucleic Acids Research, 13 (1985) 7375-7394.
[104] H. Lodish, A. Berk, S.L. Zipursky, P. Matsudaira, D. Baltimore, J. Darnell, Structure of nucleic acids, in: Molecular Cell Biology. 4th edition, WH Freeman, 2000.
[105] H. Kwon, M. Kim, Y. Seo, Y.S. Moon, H.J. Lee, K. Lee, H. Lee, Emergence of synthetic mRNA: In vitro synthesis of mRNA and its applications in regenerative medicine, Biomaterials, 156 (2018) 172-193.
[106] D. Kawaguchi, A. Kodama, N. Abe, K. Takebuchi, F. Hashiya, F. Tomoike, K. Nakamoto, Y. Kimura, Y. Shimizu, H. Abe, Phosphorothioate modification of mRNA accelerates the rate of translation initiation to provide more efficient protein synthesis, Angewandte Chemie International Edition, 59 (2020) 17403-17407.

[107] J. Devoldere, H. Dewitte, S.C. De Smedt, K. Remaut, Evading innate immunity in nonviral mRNA delivery: don't shoot the messenger, Drug discovery today, 21 (2016) 11-25.
[108] K. Karikó, H. Ni, J. Capodici, M. Lamphier, D. Weissman, mRNA is an endogenous ligand for Toll-like receptor 3, Journal of Biological Chemistry, 279 (2004) 12542-12550.
[109] K.J. Kauffman, F.F. Mir, S. Jhunjhunwala, J.C. Kaczmarek, J.E. Hurtado, J.H. Yang, M.J. Webber, P.S. Kowalski, M.W. Heartlein, F. DeRosa, Efficacy and immunogenicity of unmodified and pseudouridine-modified mRNA delivered systemically with lipid nanoparticles in vivo, Biomaterials, 109 (2016) 78-87.
[110] K. Karikó, H. Muramatsu, F.A. Welsh, J. Ludwig, H. Kato, S. Akira, D. Weissman, Incorporation of pseudouridine into mRNA yields superior nonimmunogenic vector with increased translational capacity and biological stability, Molecular therapy, 16 (2008) 1833-1840.
[111] L. Warren, P.D. Manos, T. Ahfeldt, Y.-H. Loh, H. Li, F. Lau, W. Ebina, P.K. Mandal, Z.D. Smith, A. Meissner, Highly efficient reprogramming to pluripotency and directed differentiation of human cells with synthetic modified mRNA, Cell stem cell, 7 (2010) 618-630.
[112] A. Thess, S. Grund, B.L. Mui, M.J. Hope, P. Baumhof, M. Fotin-Mleczek, T. Schlake, Sequence-engineered mRNA without chemical nucleoside modifications enables an effective protein therapy in large animals, Molecular Therapy, 23 (2015) 1456-1464.
[113] E. Giuliani, C. Piovan, S. Bossi, S. Corna, C. Scavullo, M. Pema, T. Di Tomaso, P. Genovese, A. Lombardo, L. Naldini, 130. Purification of Large Scale mRNA Encoding ZFN Nucleases by dHPLC Technology, Molecular Therapy, 24 (2016) S53-S54.
[114] M. Alberer, U. Gnad-Vogt, H.S. Hong, K.T. Mehr, L. Backert, G. Finak, R. Gottardo, M.A. Bica, A. Garofano, S.D. Koch, Safety and immunogenicity of a mRNA rabies vaccine in healthy adults: an open-label, non-randomised, prospective, first-in-human phase 1 clinical trial, The Lancet, 390 (2017) 1511-1520.
[115] A.O. Aliprantis, C.A. Shaw, P. Griffin, N. Farinola, R.A. Railkar, X. Cao, W. Liu, J.R. Sachs, C.J. Swenson, H. Lee, A phase 1, randomized, placebo-controlled study to evaluate the safety and immunogenicity of an mRNA-based RSV prefusion F protein vaccine in healthy younger and older adults, Human vaccines & immunotherapeutics, 17 (2021) 1248-1261.
[116] H. Kübler, B. Scheel, U. Gnad-Vogt, K. Miller, W. Schultze-Seemann, F. Vom Dorp, G. Parmiani, C. Hampel, S. Wedel, L. Trojan, Self-adjuvanted mRNA vaccination in advanced prostate cancer patients: a first-in-man phase I/IIa study, Journal for immunotherapy of cancer, 3 (2015) 1-14.
[117] M. Sebastian, A. Schröder, B. Scheel, H.S. Hong, A. Muth, L. von Boehmer, A. Zippelius, F. Mayer, M. Reck, D. Atanackovic, A phase I/IIa study of the mRNA-based cancer immunotherapy CV9201 in patients with stage IIIB/IV non-small cell lung cancer, Cancer Immunology, Immunotherapy, 68 (2019) 799-812.
[118] A. Khattak, M. Carlino, T. Meniawy, G. Ansstas, T. Medina, M.H. Taylor, K.B. Kim, M. McKean, G.V. Long, R.J. Sullivan, Abstract CT001: A personalized cancer vaccine, mRNA-4157, combined with pembrolizumab versus pembrolizumab in patients with resected high-risk melanoma: Efficacy and safety results from the randomized, open-label Phase 2 mRNA-4157-P201/Keynote-942 trial, Cancer Research, 83 (2023) CT001-CT001.
[119] N. Dagan, N. Barda, E. Kepten, O. Miron, S. Perchik, M.A. Katz, M.A. Hernán, M. Lipsitch, B. Reis, R.D. Balicer, BNT162b2 mRNA Covid-19 vaccine in a nationwide mass vaccination setting, New England Journal of Medicine, 384 (2021) 1412-1423.
[120] D. Di Fusco, V. Dinallo, I. Marafini, M.M. Figliuzzi, B. Romano, G. Monteleone, Antisense Oligonucleotide: Basic Concepts and Therapeutic Application in Inflammatory Bowel Disease, Frontiers in Pharmacology, 10 (2019) 305.
[121] C. Rinaldi, M.J.A. Wood, Antisense oligonucleotides: the next frontier for treatment of neurological disorders, Nature Reviews Neurology, 14 (2018) 9-21.
[122] M.A. Havens, M.L. Hastings, Splice-switching antisense oligonucleotides as therapeutic drugs, Nucleic Acids Research, 44 (2016) 6549-6563.
[123] M.A. Behlke, Chemical modification of siRNAs for in vivo use, Oligonucleotides, 18 (2008) 305-320.
[124] G.F. Deleavey, M.J. Damha, Designing chemically modified oligonucleotides for targeted gene silencing, Chemistry & biology, 19 (2012) 937-954.
[125] H. Yin, C.-Q. Song, S. Suresh, Q. Wu, S. Walsh, L.H. Rhym, E. Mintzer, M.F. Bolukbasi, L.J. Zhu, K. Kauffman, H. Mou, A. Oberholzer, J. Ding, S.-Y. Kwan, R.L. Bogorad, T. Zatsepin, V. Koteliansky, S.A. Wolfe, W. Xue, R. Langer, D.G. Anderson, Structure-guided chemical modification of guide RNA enables potent non-viral in vivo genome editing, Nature Biotechnology, 35 (2017) 1179-1187.
[126] M. Jinek, K. Chylinski, I. Fonfara, M. Hauer, J.A. Doudna, E. Charpentier, A programmable dual-RNA–guided DNA endonuclease in adaptive bacterial immunity, science, 337 (2012) 816-821.
[127] W. Mu, N. Tang, C. Cheng, W. Sun, X. Wei, H. Wang, In vitro transcribed sgRNA causes cell death by inducing interferon release, Protein & Cell, 10 (2019) 461-465.
[128] B. Wienert, J. Shin, E. Zelin, K. Pestal, J.E. Corn, In vitro–transcribed guide RNAs trigger an innate immune response via the RIG-I pathway, PLoS biology, 16 (2018) e2005840.
[129] Q. Chen, Y. Zhang, H. Yin, Recent advances in chemical modifications of guide RNA, mRNA and donor template for CRISPR-mediated genome editing, Advanced Drug Delivery Reviews, 168 (2021) 246-258.

[130] J.D. Finn, A.R. Smith, M.C. Patel, L. Shaw, M.R. Youniss, J. van Heteren, T. Dirstine, C. Ciullo, R. Lescarbeau, J. Seitzer, R.R. Shah, A. Shah, D. Ling, J. Growe, M. Pink, E. Rohde, K.M. Wood, W.E. Salomon, W.F. Harrington, C. Dombrowski, W.R. Strapps, Y. Chang, D.V. Morrissey, A Single Administration of CRISPR/Cas9 Lipid Nanoparticles Achieves Robust and Persistent In Vivo Genome Editing, Cell Reports, 22 (2018) 2227-2235.
[131] A. Mir, J.F. Alterman, M.R. Hassler, A.J. Debacker, E. Hudgens, D. Echeverria, M.H. Brodsky, A. Khvorova, J.K. Watts, E.J. Sontheimer, Heavily and fully modified RNAs guide efficient SpyCas9-mediated genome editing, Nature Communications, 9 (2018) 2641.
[132] D.E. Ryan, D. Taussig, I. Steinfeld, S.M. Phadnis, B.D. Lunstad, M. Singh, X. Vuong, K.D. Okochi, R. McCaffrey, M. Olesiak, Improving CRISPR–Cas specificity with chemical modifications in single-guide RNAs, Nucleic acids research, 46 (2018) 792-803.
[133] M. Rahdar, M.A. McMahon, T.P. Prakash, E.E. Swayze, C.F. Bennett, D.W. Cleveland, Synthetic CRISPR RNA-Cas9–guided genome editing in human cells, Proceedings of the National Academy of Sciences, 112 (2015) E7110-E7117.
[134] T. Nie, Y.-A. Heo, M. Shirley, Vutrisiran: A Review in Polyneuropathy of Hereditary Transthyretin-Mediated Amyloidosis, Drugs, 83 (2023) 1425-1432.
[135] T. Coelho, W. Marques, N.R. Dasgupta, C.-C. Chao, Y. Parman, M.C. França, Y.-C. Guo, J. Wixner, L.-S. Ro, C.R. Calandra, Eplontersen for hereditary transthyretin amyloidosis with polyneuropathy, Jama, 330 (2023) 1448-1458.
[136] M. Egli, M. Manoharan, Chemistry, structure and function of approved oligonucleotide therapeutics, Nucleic Acids Research, 51 (2023) 2529-2573.
[137] C. Wong, UK first to approve CRISPR treatment for diseases: what you need to know, Nature, (2023).
[138] H. Frangoul, D. Altshuler, M.D. Cappellini, Y.-S. Chen, J. Domm, B.K. Eustace, J. Foell, J. de la Fuente, S. Grupp, R. Handgretinger, CRISPR-Cas9 gene editing for sickle cell disease and β-thalassemia, New England Journal of Medicine, 384 (2021) 252-260.
[139] B. Leader, Q.J. Baca, D.E. Golan, Protein therapeutics: a summary and pharmacological classification, Nature reviews Drug discovery, 7 (2008) 21-39.
[140] C.M. Dobson, Protein misfolding, evolution and disease, Trends in biochemical sciences, 24 (1999) 329-332.
[141] A.M. Cuervo, E.S. Wong, M. Martinez-Vicente, Protein degradation, aggregation, and misfolding, Movement Disorders, 25 (2010) S49-S54.
[142] A. Krisko, M. Radman, Protein damage, ageing and age-related diseases, Open biology, 9 (2019) 180249.
[143] E.K. Sims, A.L. Carr, R.A. Oram, L.A. DiMeglio, C. Evans-Molina, 100 years of insulin: celebrating the past, present and future of diabetes therapy, Nature medicine, 27 (2021) 1154-1164.
[144] D.S. Dimitrov, Therapeutic proteins, Therapeutic Proteins: Methods and Protocols, (2012) 1-26.
[145] S.S. Usmani, G. Bedi, J.S. Samuel, S. Singh, S. Kalra, P. Kumar, A.A. Ahuja, M. Sharma, A. Gautam, G.P. Raghava, THPdb: Database of FDA-approved peptide and protein therapeutics, PloS one, 12 (2017) e0181748.
[146] P.M. Klein, E. Wagner, Bioreducible polycations as shuttles for therapeutic nucleic acid and protein transfection, Antioxidants & redox signaling, 21 (2014) 804-817.
[147] Y.-W. Lee, D.C. Luther, J.A. Kretzmann, A. Burden, T. Jeon, S. Zhai, V.M. Rotello, Protein delivery into the cell cytosol using non-viral nanocarriers, Theranostics, 9 (2019) 3280.
[148] T. Gaj, C.A. Gersbach, C.F. Barbas, ZFN, TALEN, and CRISPR/Cas-based methods for genome engineering, Trends in biotechnology, 31 (2013) 397-405.
[149] J.A. Doudna, E. Charpentier, Genome editing. The new frontier of genome engineering with CRISPR-Cas9, Science, 346 (2014) 1258096.
[150] E. Charpentier, J.A. Doudna, Rewriting a genome, Nature, 495 (2013) 50-51.
[151] J.D. Sander, J.K. Joung, CRISPR-Cas systems for editing, regulating and targeting genomes, Nature biotechnology, 32 (2014) 347-355.
[152] E. Kenjo, H. Hozumi, Y. Makita, K.A. Iwabuchi, N. Fujimoto, S. Matsumoto, M. Kimura, Y. Amano, M. Ifuku, Y. Naoe, Low immunogenicity of LNP allows repeated administrations of CRISPR-Cas9 mRNA into skeletal muscle in mice, Nature communications, 12 (2021) 7101.
[153] Y. Lin, E. Wagner, U. Lächelt, Non-viral delivery of the CRISPR/Cas system: DNA versus RNA versus RNP, Biomaterials Science, 10 (2022) 1166-1192.
[154] X. Liang, J. Potter, S. Kumar, Y. Zou, R. Quintanilla, M. Sridharan, J. Carte, W. Chen, N. Roark, S. Ranganathan, Rapid and highly efficient mammalian cell engineering via Cas9 protein transfection, Journal of biotechnology, 208 (2015) 44-53.
[155] C.T. Charlesworth, P.S. Deshpande, D.P. Dever, J. Camarena, V.T. Lemgart, M.K. Cromer, C.A. Vakulskas, M.A. Collingwood, L. Zhang, N.M. Bode, Identification of preexisting adaptive immunity to Cas9 proteins in humans, Nature medicine, 25 (2019) 249-254.
[156] V.L. Simhadri, J. McGill, S. McMahon, J. Wang, H. Jiang, Z.E. Sauna, Prevalence of pre-existing antibodies to CRISPR-associated nuclease Cas9 in the USA population, Molecular Therapy-Methods & Clinical Development, 10 (2018) 105-112.

[157] H. Yin, C.-Q. Song, S. Suresh, Q. Wu, S. Walsh, L.H. Rhym, E. Mintzer, M.F. Bolukbasi, L.J. Zhu, K. Kauffman, Structure-guided chemical modification of guide RNA enables potent non-viral in vivo genome editing, Nature biotechnology, 35 (2017) 1179-1187.
[158] M.A. Cappelluti, V. Mollica Poeta, S. Valsoni, P. Quarato, S. Merlin, I. Merelli, A. Lombardo, Durable and efficient gene silencing in vivo by hit-and-run epigenome editing, Nature, (2024) 1-8.
[159] C. Long, L. Amoasii, A.A. Mireault, J.R. McAnally, H. Li, E. Sanchez-Ortiz, S. Bhattacharyya, J.M. Shelton, R. Bassel-Duby, E.N. Olson, Postnatal genome editing partially restores dystrophin expression in a mouse model of muscular dystrophy, Science, 351 (2016) 400-403.
[160] S.M. Hammond, G. McClorey, J.Z. Nordin, C. Godfrey, S. Stenler, K.A. Lennox, C.I. Smith, A.M. Jacobi, M.A. Varela, Y. Lee, M.A. Behlke, M.J. Wood, S.E. Andaloussi, Correlating In Vitro Splice Switching Activity With Systemic In Vivo Delivery Using Novel ZEN-modified Oligonucleotides, Mol Ther Nucleic Acids, 3 (2014) e212.
[161] P. Gee, M.S.Y. Lung, Y. Okuzaki, N. Sasakawa, T. Iguchi, Y. Makita, H. Hozumi, Y. Miura, L.F. Yang, M. Iwasaki, X.H. Wang, M.A. Waller, N. Shirai, Y.O. Abe, Y. Fujita, K. Watanabe, A. Kagita, K.A. Iwabuchi, M. Yasuda, H. Xu, T. Noda, J. Komano, H. Sakurai, N. Inukai, A. Hotta, Extracellular nanovesicles for packaging of CRISPR-Cas9 protein and sgRNA to induce therapeutic exon skipping, Nature communications, 11 (2020) 1334.
[162] H. Yin, H.M. Moulton, Y. Seow, C. Boyd, J. Boutilier, P. Iverson, M.J. Wood, Cell-penetrating peptide-conjugated antisense oligonucleotides restore systemic muscle and cardiac dystrophin expression and function, Hum Mol Genet, 17 (2008) 3909-3918.
[163] S. Thalmayr, M. Grau, L. Peng, J. Pöhmerer, U. Wilk, P. Folda, M. Yazdi, E. Weidinger, T. Burghardt, M. Höhn, E. Wagner, Molecular Chameleon Carriers for Nucleic Acid Delivery: The Sweet Spot Between Lipoplexes and Polyplexes, Advanced Materials, (2023) 2211105.
[164] Q. Cheng, T. Wei, Y. Jia, L. Farbiak, K. Zhou, S. Zhang, Y. Wei, H. Zhu, D.J. Siegwart, Dendrimer-based lipid nanoparticles deliver therapeutic FAH mRNA to normalize liver function and extend survival in a mouse model of hepatorenal tyrosinemia type I, Advanced materials, 30 (2018) 1805308.
[165] A. Lombardo, D. Cesana, P. Genovese, B. Di Stefano, E. Provasi, D.F. Colombo, M. Neri, Z. Magnani, A. Cantore, P.L. Riso, Site-specific integration and tailoring of cassette design for sustainable gene transfer, Nature methods, 8 (2011) 861-869.
[166] A.-L. Lessl, J. Pöhmerer, Y. Lin, U. Wilk, M. Höhn, E. Hörterer, E. Wagner, U. Lächelt, mCherry on Top: A Positive Read-Out Cellular Platform for Screening DMD Exon Skipping Xenopeptide–PMO Conjugates, Bioconjugate Chemistry, (2023).
[167] D. Schaffert, M. Kiss, W. Rödl, A. Shir, A. Levitzki, M. Ogris, E. Wagner, Poly(I:C)-Mediated Tumor Growth Suppression in EGF-Receptor Overexpressing Tumors Using EGF-Polyethylene Glycol-Linear Polyethylenimine as Carrier, Pharmaceutical Research, 28 (2011) 731-741.
[168] L. Farbiak, Q. Cheng, T. Wei, E. Álvarez-Benedicto, L.T. Johnson, S. Lee, D.J. Siegwart, All-in-one dendrimer-based lipid nanoparticles enable precise HDR-mediated gene editing in vivo, Advanced Materials, 33 (2021) 2006619.
[169] E.K. Brinkman, T. Chen, M. Amendola, B. Van Steensel, Easy quantitative assessment of genome editing by sequence trace decomposition, Nucleic acids research, 42 (2014) e168-e168.
[170] E.K. Brinkman, B. van Steensel, Rapid Quantitative Evaluation of CRISPR Genome Editing by TIDE and TIDER, in: Y. Luo (Ed.) CRISPR Gene Editing: Methods and Protocols, Springer New York, New York, NY, 2019, pp. 29-44.
[171] P. Gee, M.S. Lung, Y. Okuzaki, N. Sasakawa, T. Iguchi, Y. Makita, H. Hozumi, Y. Miura, L.F. Yang, M. Iwasaki, Extracellular nanovesicles for packaging of CRISPR-Cas9 protein and sgRNA to induce therapeutic exon skipping, Nature communications, 11 (2020) 1334.
[172] F. Haase, J. Pöhmerer, M. Yazdi, M. Grau, Y. Zeyn, U. Wilk, T. Burghardt, M. Höhn, C. Hieber, M. Bros, E. Wagner, S. Berger, Lipoamino bundle LNPs for efficient mRNA transfection of dendritic cells and macrophages show high spleen selectivity, European Journal of Pharmaceutics and Biopharmaceutics, (2023).
[173] J.D. Gillmore, E. Gane, J. Taubel, J. Kao, M. Fontana, M.L. Maitland, J. Seitzer, D. O'Connell, K.R. Walsh, K. Wood, CRISPR-Cas9 in vivo gene editing for transthyretin amyloidosis, New England Journal of Medicine, 385 (2021) 493-502.
[174] B. Winkeljann, D.C. Keul, O.M. Merkel, Engineering poly- and micelleplexes for nucleic acid delivery - A reflection on their endosomal escape, J Control Release, 353 (2023) 518-534.
[175] K. Von Gersdorff, N.N. Sanders, R. Vandenbroucke, S.C. De Smedt, E. Wagner, M. Ogris, The internalization route resulting in successful gene expression depends on both cell line and polyethylenimine polyplex type, Molecular therapy, 14 (2006) 745-753.
[176] F. Chemello, E.N. Olson, R. Bassel-Duby, CRISPR-editing therapy for Duchenne muscular dystrophy, Human gene therapy, 34 (2023) 379-387.
[177] M. Kosicki, F. Allen, F. Steward, K. Tomberg, Y. Pan, A. Bradley, Cas9-induced large deletions and small indels are controlled in a convergent fashion, Nature communications, 13 (2022) 3422.
[178] M. Kosicki, K. Tomberg, A. Bradley, Repair of double-strand breaks induced by CRISPR–Cas9 leads to large deletions and complex rearrangements, Nature biotechnology, 36 (2018) 765-771.

[179] S. Berger, M. Berger, C. Bantz, M. Maskos, E. Wagner, Performance of nanoparticles for biomedical applications: The in vitro/in vivo discrepancy, Biophysics Reviews, 3 (2022).
[180] K. Paunovska, C.D. Sago, C.M. Monaco, W.H. Hudson, M.G. Castro, T.G. Rudoltz, S. Kalathoor, D.A. Vanover, P.J. Santangelo, R. Ahmed, A direct comparison of in vitro and in vivo nucleic acid delivery mediated by hundreds of nanoparticles reveals a weak correlation, Nano letters, 18 (2018) 2148-2157.
[181] S.A. Dilliard, Q. Cheng, D.J. Siegwart, On the mechanism of tissue-specific mRNA delivery by selective organ targeting nanoparticles, Proc Natl Acad Sci U S A, 118 (2021).
[182] M.V. Petkova, S. Morales-Gonzales, K. Relizani, E. Gill, F. Seifert, J. Radke, W. Stenzel, L. Garcia, H. Amthor, M. Schuelke, Characterization of a Dmd EGFP reporter mouse as a tool to investigate dystrophin expression, Skeletal muscle, 6 (2016) 1-16.
[183] R.M. Daer, J.P. Cutts, D.A. Brafman, K.A. Haynes, The impact of chromatin dynamics on Cas9-mediated genome editing in human cells, ACS synthetic biology, 6 (2017) 428-438.
[184] J.G. Doench, E. Hartenian, D.B. Graham, Z. Tothova, M. Hegde, I. Smith, M. Sullender, B.L. Ebert, R.J. Xavier, D.E. Root, Rational design of highly active sgRNAs for CRISPR-Cas9–mediated gene inactivation, Nature Biotechnology, 32 (2014) 1262-1267.
[185] M.Z. Hatit, M.P. Lokugamage, C.N. Dobrowolski, K. Paunovska, H. Ni, K. Zhao, D. Vanover, J. Beyersdorf, H.E. Peck, D. Loughrey, Species-dependent in vivo mRNA delivery and cellular responses to nanoparticles, Nature nanotechnology, 17 (2022) 310-318.
[186] L. Amoasii, C. Long, H. Li, A.A. Mireault, J.M. Shelton, E. Sanchez-Ortiz, J.R. McAnally, S. Bhattacharyya, F. Schmidt, D. Grimm, Single-cut genome editing restores dystrophin expression in a new mouse model of muscular dystrophy, Science translational medicine, 9 (2017) eaan8081.
[187] L. Amoasii, J.C. Hildyard, H. Li, E. Sanchez-Ortiz, A. Mireault, D. Caballero, R. Harron, T.-R. Stathopoulou, C. Massey, J.M. Shelton, Gene editing restores dystrophin expression in a canine model of Duchenne muscular dystrophy, Science, 362 (2018) 86-91.
[188] C.A. Tsuchida, K.M. Wasko, J.R. Hamilton, J.A. Doudna, Targeted nonviral delivery of genome editors in vivo, Proc Natl Acad Sci U S A, 121 (2024) e2307796121.
[189] J. Walther, D. Porenta, D. Wilbie, C. Seinen, N. Benne, Q. Yang, O.G. de Jong, Z. Lei, E. Mastrobattista, Comparative analysis of lipid Nanoparticle-Mediated delivery of CRISPR-Cas9 RNP versus mRNA/sgRNA for gene editing in vitro and in vivo, Eur J Pharm Biopharm, 196 (2024) 114207.
[190] L. Farbiak, Q. Cheng, T. Wei, E. Álvarez-Benedicto, L.T. Johnson, S. Lee, D.J. Siegwart, All-In-One Dendrimer-Based Lipid Nanoparticles Enable Precise HDR-Mediated Gene Editing In Vivo, Adv Mater, 33 (2021) e2006619.
[191] T. Wei, Q. Cheng, Y.L. Min, E.N. Olson, D.J. Siegwart, Systemic nanoparticle delivery of CRISPR-Cas9 ribonucleoproteins for effective tissue specific genome editing, Nat Commun, 11 (2020) 3232.
[192] Y. Lin, X. Luo, T. Burghardt, S. Dorrer, M. Höhn, E. Wagner, U. Lächelt, Chemical Evolution of Amphiphilic Xenopeptides for Potentiated Cas9 Ribonucleoprotein Delivery, J Am Chem Soc, 145 (2023) 15171-15179.
[193] S. Thalmayr, M. Grau, L. Peng, J. Pöhmerer, U. Wilk, P. Folda, M. Yazdi, E. Weidinger, T. Burghardt, M. Höhn, E. Wagner, S. Berger, Molecular Chameleon Carriers for Nucleic Acid Delivery: The Sweet Spot between Lipoplexes and Polyplexes, Adv Mater, 35 (2023) e2211105.
[194] C. Scholz, E. Wagner, Therapeutic plasmid DNA versus siRNA delivery: common and different tasks for synthetic carriers, J Control Release, 161 (2012) 554-565.

8. Publications

8.1. Original Article and Review

Germer J, Lessl AL, Pöhmerer J, Grau M, Weidinger E, Höhn M, Yazdi M, Cappelluti M, Lombardo A, Lächelt U, Wagner E, *Lipo-Xenopeptide Polyplexes for CRISPR/Cas9 Based Gene Editing at Ultra-Low Dose*. Journal of Controlled Release. DOI:10.1016/j.jconrel.2024.04.037

Germer J, Wagner E, *Polymer-Based Nonviral Nucleic Acid Delivery and Genome Editing*. Molecular Analyses, CRC Press, 2022, pp. 165-182. DOI:10.1201/9781003247432-18

8.2. Patent Application

Prof. Dr. Ernst Wagner, Lun Peng, Simone Berger, Sophie Thalmayr, Paul Folda, Franziska Haase, Melina Grau, **Janin Germer**, Mina Yazdi, Eric Weidinger, Tobias Burghardt, Johanna Seidl, Ricarda Steffens, *Novel carriers for nucleic acid and/or protein delivery* PCT application number: 118699P1272EP

9. Acknowledgements

I am deeply appreciative of the steadfast support and guidance provided by my supervisor, Professor Dr. Ernst Wagner, throughout the duration of this thesis. His enthusiasm for formulation technology and chemistry served as an invaluable source of inspiration, motivating me to explore unanswered questions. It has been a privilege to be a member of his research group and to have had the opportunity to collaborate with like-minded individuals who share a passion for problem-solving.

Furthermore, I wish to extend my sincere appreciation to Prof. Dr. Ulrich Lächelt for his guidance and support. I am grateful for every kind word of appreciation and encouragement, particularly during most challenging times.

I want to thank all Cas9-Taskforce group members i.e. Dr. Yi Lin, Dr. Franziska Haase, Xianjin Luo and Eric Weidinger for our monthly UPGRADE meetings. Regardless of the numerous last-minute slides stressfully prepared on Wednesday night for these meetings, it was still the most productive and inspiring time of the month. Despite experiencing some bumps along the way, I'd like to express gratitude to Eric for joining me as the collaborator I've longed for in the Cas9 mRNA team, and, more significantly, for becoming a cherished friend. Finally, I no longer felt lonely working on the Cas9 topic.

I'd like to express my gratitude to all those who directly contributed to this work: Dr. Ulrich Wilk, Jana Pöhmerer and Mina Yazdi who performed the animal experiments; Melina Grau who synthesized all used LAF-carriers; Miriam Höhn for performing CLSM and DNA extractions and helping my desperate attempt to troubleshoot failed PCR experiments; Wolfgang Rödl for keeping the lab from falling apart, for making sure I would always receive all needed materials in time, for joining my rants about failed experiments, messy laboratories and all the instruments and materials that magically kept disappearing—you always cheered me up.

I'd like to thank numerous members of our and collaborating groups who greatly contributed to my experience: Fengrong, Johanna, Paul, Ricarda, Sophie, Simone, Tobi, Vicky, Ben, Philipp, Max, Minh, Jan Felber und Jan Vietor.

Anni— thank you for having been my friend, my ally, my room mate, my partner in crime, for popcorn at our screen campfire, for knowing when I needed a snack, for jumping out of a plane with me — for everything. I already miss seeing you every single day!

I extend special thanks to Dr. Ines Truebenbach and Dr. Jasmin Hotz for introducing me to this laboratory. You both serve as my inspiration for empowered women in the field of science. I deeply admire your resilience, determination, and the supportive friendship you've shown me during both bright and colourful but also very dark times.

My most unexpected discoveries during my PhD studies were found during my teaching duties. In the OTS group I discovered the best group of people I have ever met. Dr. Adrian Müller-Deku, Dr. Li Gao, and Dr. Alex Sailer truly turned the challenging period of lockdown into unexpectedly pleasant times. Many of my fondest memories are from that period. Since the departure of the three of you from the campus, it has never quite felt the same.

Finally, I want to express my gratitude to my family. My siblings, who have been the only constant in my life, providing me with a profound sense of belonging. My parents, whose unwavering support has always bolstered my decisions. My grandfather, whose wise words taught me that regrets stem from missed opportunities, not daring to venture. My brother Dr. Jan Germer, my lifelong inspiration and role model. I thank Dr. Sajad Saeedinaeeni, whose calming presence helps me to keep my chill during moments of overwhelming stress. I've made it this far solely because of the love and support you've given me.